Evaluation of the Effect of Microporous Sublayer Design and Fabrication on Performance and Adhesion in PEM Fuel Cell Assemblies

Kenneth Reed Henderson Jr.

Thesis submitted to the faculty of Virginia Polytechnic Institute and State University in partial fulfillment of the requirements for the degree of

Master of Science
In
Mechanical Engineering

Committee Members:

Dr. Michael W. Ellis – Chair, ME
Dr. Douglas J. Nelson – ME
Dr. David A. Dillard – ESM

September 16, 2005
Blacksburg, Virginia

Keywords: Fuel Cell, PEMFC, Microporous Sublayer, Water Management Layer, Catalyst Support Layer

Evaluation of the Effect of Microporous Sublayer Design and Fabrication on Performance and Adhesion in PEM Fuel Cell Assemblies

Kenneth Reed Henderson Jr.

Abstract

The typical architecture of the proton exchange membrane fuel cell (PEMFC) contains a layer called the microporous sublayer (MSL). The MSL is a mixture of carbon black and polytetrafluoroethylene (PTFE), which is typically applied to the gas diffusion layer (GDL). The composition (wt.% PTFE) and loading (mg/cm^2) can be varied to optimize the electrochemical performance of the PEMFC and the overall adhesion of the layers within the PEMFC. This research establishes correlations that characterize the performance and adhesion of the layers within the PEMFC based on composition, loading, fabrication pressure, and fabrication time. MSL loading was varied from 1.5-4 mg/cm^2, composition was varied from 10-50 wt.% PTFE, fabrication pressure was varied from 3.45-10.34 MPa, and fabrication time was varied from 2-8 minutes. Using these four factors, correlations were created, and optimal solutions for each response were identified. The adhesion correlation identifies a low MSL loading, mid-range MSL composition, high fabrication pressure, and high fabrication time as desirable factors. The performance correlation suggests that the PEMFC performance is enhanced with low MSL loadings, low MSL PTFE content, and a low fabrication pressure and does not find fabrication time to be a significant factor in the correlation.

Acknowledgements

I would like to thank a few special people that contributed to this research, and supported me. I would like to thank Dr. Michael Ellis, my advisor and committee chairman, for his constant support and encouragement. Without his time and financial commitments, this research would have never been possible. I would also like to thank my other two committee members, Dr. David Dillard and Dr. Doug Nelson, for their time and support. I'd like to thank fellow lab members Josh Sole and Michael Christopher for their willingness to help, and for always making the laboratory a fun place to be.

I would like to thank Father John Whallen and Ken Henderson Sr., former board members of Power Systems Inc., for introducing me to fuel cell technology, and supporting my education. I would like to thank Michael and Jennifer Christopher for their constant support and contributions made towards this research. I would like to thank Chris Williams, Shaun Grahe, and Lincoln Tran for their constant moral support. Finally, I would like to thank Ashley Perkins for her dedication and support of the past year and a half.

Dedication

To my mother and father, Andee and Kenneth Henderson, and Ashley Perkins for their constant love and support.

Table of Contents

List of Figures

List of Tables

List of Equations

1 Introduction

1.1 Background of the Proton Exchange Membrane Fuel Cell

The Proton Exchange Membrane Fuel Cell (PEMFC) "was first developed by General Electric in the United States in the 1960s for use by NASA on their first manned space vehicles." [15] The PEMFC is a device that is capable of producing power with no harmful emissions. The reactants for a PEMFC are hydrogen and air, and the only byproduct is hot water. The electrical efficiency of a PEMFC is better than a gasoline generator, and when used in a cogeneration system, the overall efficiency can reach 80%. Furthermore, "small systems can be just as efficient as large ones" [15], which allows for a wide range of applications for a fuel cell. Another advantage of the PEMFC is that it is as silent as the fans needed to cool it.

With the turmoil in the Middle East, and long-term threat of oil depletion, PEMFC's and similar fuel cell technologies, are attracting considerable attention. Fuel cells could be suitable power supplies for many applications including stationary, portable power, and transportation. Companies such as Plug Power, Hydrogenics, United Technologies, and others have focused their efforts on the residential and light commercial market, using fuel cells as both a back-up and primary electricity supply. Due to the numerous combat applications for which a silent portable power generation device could be of use, PEMFC's are also of interest to the Army and Navy.

Recently, the growing population, increased desire to travel, and rising petroleum prices, have encouraged the search for an alternative to our petroleum fueled automobiles. Today, most of the major car companies, General Motors, Honda, Ford, and DaimlerCrysler, just to name a few, are pursuing the development of fuel cell powered vehicles. The automotive market has the potential to be the largest market for fuel cell systems. There are many reasons why fuel cells are attractive for the automotive market. First, there is the need for car companies to comply with increasingly restrictive emission laws. Another reason is the need for an alternative to petroleum. Petroleum, although it

has been a very plentiful resource in the past, will not be available forever. The fuel cell will operate on hydrogen, which can be produced from a variety of feedstocks. Some of these feedstocks include fossil fuels (e.g. gas, oil, coal), renewable fuels (e.g. biofuels and waste), nuclear, and electricity generated by renewable energy (e.g. solar, wind, wave) [15]. Another attractive, and somewhat more near-term, application for fuel cells is the back-up/portable power market. These systems, as currently being demonstrated by Plug Power and Hydrogenics, can be used as an alternative to current internal combustion back-up systems, as well as being a remote application power supply.

1.2 Anatomy of Proton Exchange Membrane Fuel Cell

The PEMFC is composed of many layers, each serving a unique and critical function. The structure of a mono-polar PEMFC is illustrated in *Figure 1-1*. The outside components of the PEMFC, as depicted in *Figure 1-1*, are the collector plates, which in this case are considered mono-polar plates. Moving inward, the next layer is the gas diffusion layer (GDL). The next two layers, on both sides of the membrane, are the microporous sublayer (MSL) and catalyst layer respectively. At the center of the PEMFC is the membrane.

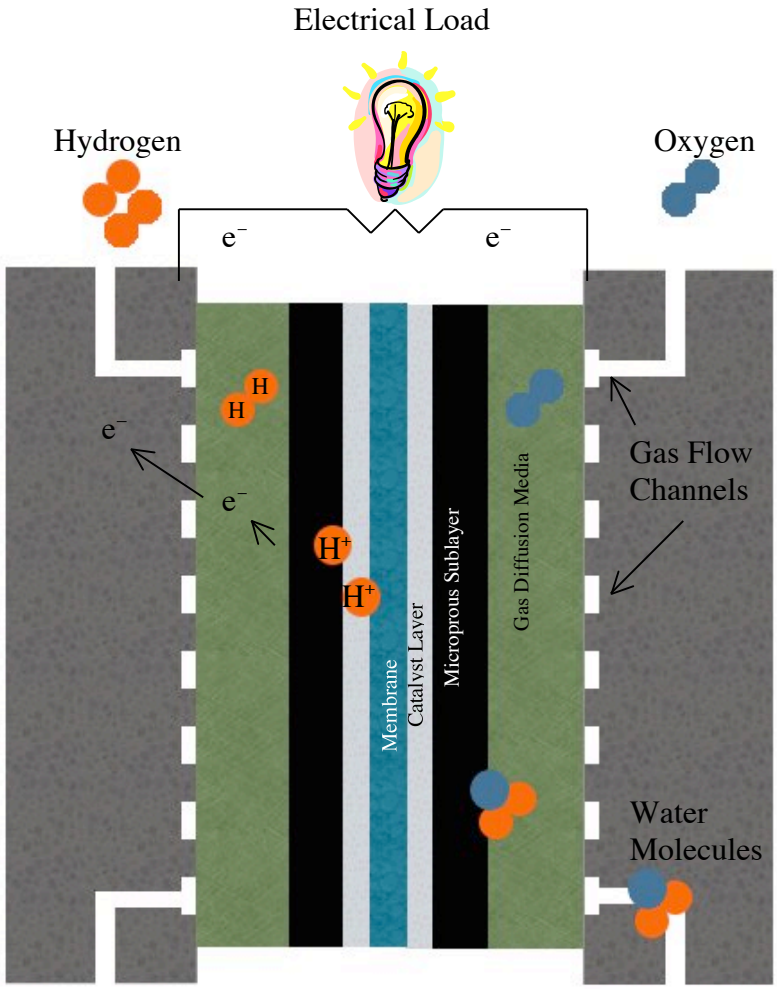

Figure 1-1. Basic anatomy of the PEMFC

The basic operation of a PEMFC begins with the flow of gas through the collector plates into the GDL. Hydrogen (H_2) is supplied on the anode side, and either air or pure oxygen (O_2) is supplied on the cathode side. The GDL disperses the gas evenly across the MSL, and the MSL further disperses the gas across the catalyst layer. The primary function of the catalyst layer, as discussed in further detail later in this section, is to encourage the anode and cathode half reactions. The half reactions (see *Equation 1-1&1-2*) of the PEMFC, are illustrated in *Figure 1-1*.

Anode:	$2H_2 \text{ ---> } 4H^+ + 4e^-$	(1-1)
Cathode:	$O_2 + 4e^- + 4H^+ \text{ ---> } 2H_20$	(1-2)

The protons formed at the anode are able to pass through the membrane, hence the name proton exchange membrane, however the electrons are unable to pass through

the membrane. The electrons are conducted through the collector plate and then through the external circuit that connects the two collector plates to the load. In the case of the fuel cell, the cathode is considered the positive terminal and the anode is considered the negative terminal.

In most applications one single fuel cell will not be able to produce enough power to satisfy the load. PEMFC's can be connected in series to form what is most widely identified as a "stack" of these cells. When a stack is formed, the collector plate from one cell is located back to back with the collector plate from another cell. In this situation the collector plate is considered a bipolar plate, because for one cell it is the anode and for the other cell it is the cathode. *Figure 1-2* is an illustration of the typical fuel cell stack architecture. The following sections discuss each of the PEMFC components in more detail.

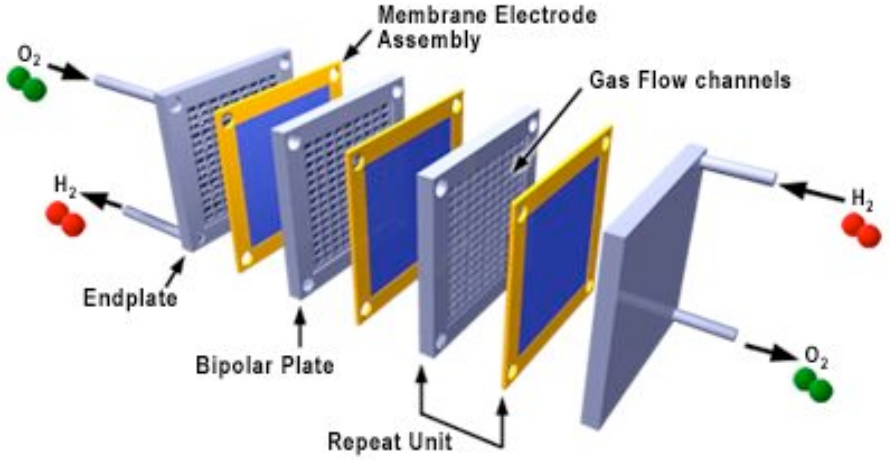

Figure 1-2. Example of a fuel cell stack [24]

1.2.1 Collector Plates. Collector plates are designed to distribute gas to the surface of the GDL and to provide an electrical connection to the external circuit. The dispersion of gas over the GDL's can be accomplished in many different ways, as displayed by the variety of flow field designs displayed in *Figure 1-3*. Because of its high conductivity and corrosion resistance, most of these collector plates are made of graphite. The drawback behind using graphite is that the flow fields must be machined into the

graphite plate. The machining of collector plate flow paths can be very expensive and time consuming. Alternatives such as stamping these flow fields into various forms of composite materials is a current area of interest. [19] In addition to distributing reactant gas, collector plates must readily conduct electrons, provide good contact at the interface with the GDL, and provide structural support for the fuel cell assembly.

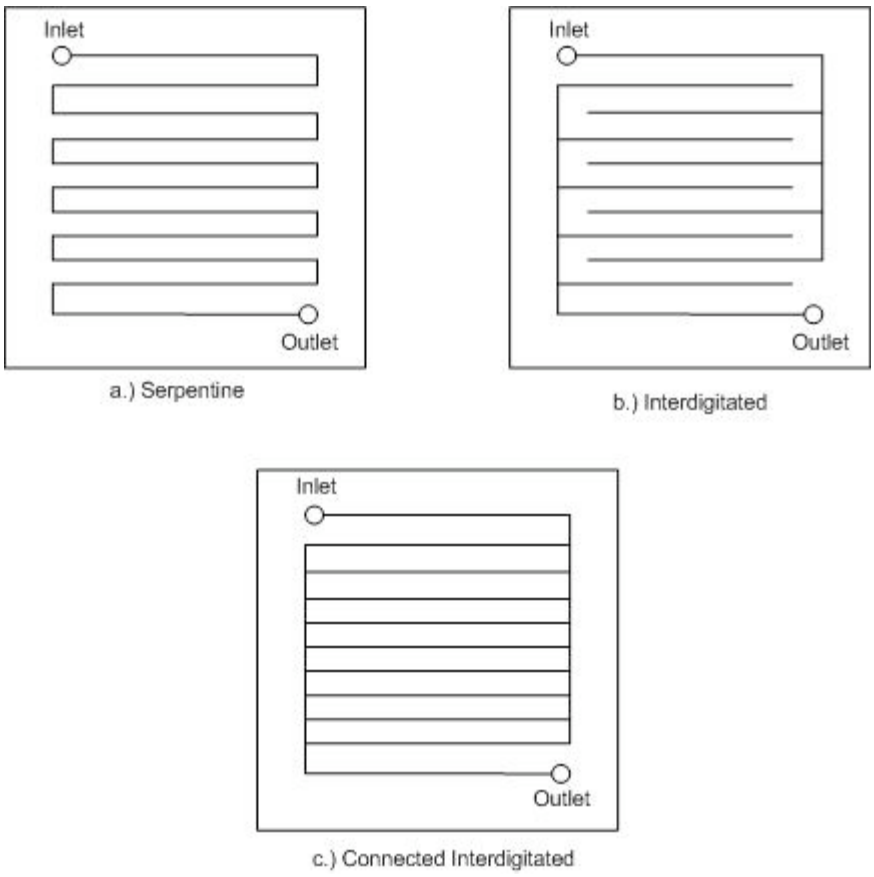

Figure 1-3. Example of a collector plate flow fields

1.2.2 Gas Diffusion Layer. The primary function of the gas diffusion layer is, just as the name says, to diffuse the reactant gas as effectively as possible. If there was no gas diffusion layer, the gas coming out of the flow channels in the collector plates would only contact the part of the catalyst layer that is exposed to the flow channel. This would not be a very efficient design since the flow channels usually cover only about 50% of the

total MEA area. Furthermore, without the GDL, there would be no electrical path from the MEA to the area exposed to the flow channel.

A GDL can be constructed using many different methods and materials. The most common materials used are carbon fibers, because they are conductive and corrosion resistant. To form a carbon "paper", the carbon fibers are chopped, "impregnated with carbonizable thermoset resin", and baked at a high temperature with a high amount of compression [21]. To form a carbon cloth/weave, the fibers are bundled and woven together. Although carbon paper is less expensive to produce, it seems as though the research community is divided with regard to whether carbon paper or carbon cloth is the best choice. There are many characteristics of both carbon paper and carbon cloth that can be controlled to affect the properties, including the carbon fiber size, quantity, and number of strands per bundle for the weave. Changing characteristics such as these will affect the overall performance of the GDL, and in turn the overall performance of the PEMFC. For example, changing the size of the carbon fibers will affect the porosity of the GDL, which can in turn affect its ability to evenly disperse the gas over the catalyst layer.

The GDL must also be able to convey the water produced by the PEMFC and provided by the humidification of the feed gases. The GDL is typically treated to make it hydrophobic to help maintain open flow paths for liquid water. This is accomplished by soaking the GDL in a fluoropolymer, such as polytetrafluoroethylene (PTFE), and baking it at 350ºC to sinter the PTFE to the carbon.

1.2.3 Microporous Sublayer. The microporous sublayer (MSL) is a more recent addition to the anatomy of the PEMFC. This layer is composed of very small carbon particles and a fluoroploymer, such as PTFE. The MSL, as displayed in *Figure 1-1*, is placed between the catalyst layer and the GDL. Varying the MSL loading (thickness) and composition (PTFE content) within the MSL can drastically change the characteristics of the MSL, and in turn affect the performance of the PEMFC as a whole. The MSL is the

focus of the research, and more information regarding the functions and design of the MSL is given in *Section 1.3*.

1.2.4 Catalyst Layer. The main role of the catalyst layer is to facilitate the half reactions at the anode and cathode. The most common catalyst for PEMFC's is platinum. Some of the first fuel cells utilized a catalyst loading that was approximately 28 mg/cm^2 of platinum. [15] The high cost of platinum made these cells prohibitively expensive. Over the past 30 years, researchers have made great strides reducing the platinum requirement. One of the more significant developments was the ability to support tiny platinum particles (~2.2 nm) on larger carbon particles (~30 nm). This carbon-supporting technique provides maximum platinum surface area with minimum platinum usage. Another major advancement was achieved by Ticianelli [16] (working at Las Alamos National Laboratory) who used supported catalysts in a Nafion impregnated catalyst layer to lower the catalyst loading from around 4 mg/cm^2 to around 0.35 mg/cm^2 of platinum. Current catalyst loadings are approximately 0.14 mg-Pt/cm^2 to 0.4 mg-Pt/cm^2 (see *Appendix A*).

1.2.5 Membrane. As depicted in *Figure 1-1,* the membrane is at the center of the fuel cell assembly. The membrane is formed from an ion-conducting polymer that provides a path for H^+ ions while preventing the flow of gas and electrons. Although there are currently several manufacturers for these ion-conducting polymers, one of the more common materials is Nafion. Preparation of the polymer begins with a process called "perfluorination". Perfluorination is the process of modifying a basic polymer (e.g. ethylene) by substituting fluorine for hydrogen within its structure. [15] One of the more common polymers is polytetrafluoroethylene (PTFE). By nature, PTFE is a very hydrophobic substance, meaning it does not attract water. The next step in constructing an ionic polymer is to "sulphonate" the perflourinated polymer. This sulphonation is accomplished by adding a side chain, ending with a sulphonic acid (HSO_3), to the polymer backbone. [15] It is interesting to note that sulphonic acid is very hydrophilic, meaning it will want to attract water, as noted by Larminie [15]. Nafion can also absorb large quantities of water, which can increase its weight by up to 50% [15].

1.2.6 Fabrication of a Fuel Cell. Typical fabrication of the PEMFC begins with the preparation of the membrane electrode assembly (MEA). The MEA is the combination of the membrane and the catalyst layer. One of the more successful and common methods of fabricating the MEA, for laboratory use, is the decal method. This method utilizes decals (usually small pieces of fabric coated with Teflon®) onto which the catalyst layer is painted and dried. Once the decals are dry, they are pressed, under a substantial amount of pressure and at a high temperature, onto the membrane. Once the MEA is completed, the next step is to prepare the GDL.

The GDL is typically prepared by adding a hydrophobic substance (e.g. PTFE) to improve the transport of water. Once this process is completed, the MSL is then applied to the GDL, and baked at 350ºC to sinter the layers together. Once the MSL is applied to the GDL, the fuel cell is ready to be assembled. In a conventional fuel cell the GDL is placed on both sides of the MEA (MSL side of GDL against the catalyst layer), and the collector plates hold the entire structure together with a prescribed amount of compression. To assist in adhesion and reduction of contact resistance, the procedures followed in this research consist of hot pressing the MSL coated GDL's to the MEA (MSL side of GDL against the catalyst layer) before further compressing the structure with the collector plates.

1.3 Essential Functions of the Microporous Sublayer

The MSL, which is the focus of this research, is summarized here and described in more detail in the literature review. The MSL has four basic functions. As noted previously, the MSL enhances water transport and reactant diffusion. The MSL also serves as a catalyst support that stabilizes the catalyst layer. The term catalyst support is derived from the point of view that if you were to consider a PEMFC without the MSL, the catalyst layer would be adjacent to the GDL during assembly. Since most GDL's do not have a perfectly uniform surface for the catalyst layer to contact, the catalyst layer can be forced into the interstices of the GDL. Over time, the catalyst layer can further

migrate into the GDL. The migration of the catalyst layer away from the membrane reduces the number of reaction sites in contact with the electrolyte, and in turn will decrease the performance of the fuel cell.

The final critical function of the MSL is to decrease electrical contact resistance between the GDL and catalyst layer. The technique of MEA construction described previously provides very good adhesion between the catalyst layer and the membrane (being pressed under high pressure and temperature). The catalyst layer and the membrane both contain a very uniform surface, which provides a tight connection between them. Due to non-uniformities found in most GDL's, this tight connection will most likely not be achieved at the interface between the GDL and catalyst layer. There is a greater possibility that small voids will be formed between these layers. These small voids will cause an increase in the contact resistance that occurs at the interface of the two materials. The MSL improves electrical contact by penetrating the pores of the GDL and providing a smooth surface at the catalyst interface. To further bond the MSL to the GDL, a process called sintering is used. This process involves simply heating the GDL, with applied MSL, to a temperature of approximately 350°C and maintaining this temperature for approximately 30 min. This allows the PTFE in the GDL (used for hydrophobicizing) to bond with the PTFE found in the MSL. As discussed in further detail in the literature review, the research community has explored many methods of applying the MSL. Some of the more common methods include; application by brushing, rolling, spraying, casting, and screen-printing.

As outlined above, the MSL performs several critical functions. The design and fabrication of the MSL affects its performance and in turn affect the overall performance of the fuel cell. This research will review past and current work relating to the MSL, identify opportunities to build upon this research, and describe results and conclusions from a series of experiments that were conducted to investigate the MSL's effect on fuel cell performance and adhesion. The following chapter will highlight fundamental concepts and current research trends related to the MSL.

2 Literature Review

The fuel cell research community is working towards a better understanding of PEMFC's as a whole, and towards improvements in the individual layers that comprise the PEMFC. The following review presents results and information related specifically to the MSL that have been reported by a variety of researchers. This review will organize the findings related to the MSL into four categories – fundamental functions; composition; loading; and application. Much of the prior research reports on the performance obtained using the MSL's with specific characteristics. Comparing results across different studies is often challenging. For example, when an optimal value for the composition of the MSL is reported based on a polarization curve, the cell operating temperature, relative humidity of each feed gas, stoichiometry, and perhaps the catalyst loading should be reported as well. These are just a few of the critical design and operating parameters of a PEMFC that can drastically affect the performance, and that must all be identified to accurately evaluate the performance of a fuel cell component. In the following sections of this literature review, only the most significant aspects of each reference are reviewed. Additional details of each work are included in *Appendix A*.

2.1 Fundamental Functions

The MSL is thought to have certain fundamental functions within the PEMFC. Some of these suggested functions are as follows: support the catalyst layer, assist water transport, enhance diffusion of reactant gases, and reduce contact resistance between the catalyst layer and the GDL. The following table, *Table 2-1*, identifies references that address each of these functions.

Table 2-1. MSL Fundamental Functions Summary

Author	Catalyst Support	Water Transport	Reactant Diffusion	Reduce Electrical Resistance
Qi [1]	■	■		
Song [2]	■	■	■	
Nam[5]		■		
Passaogullari [6]		■		
Lim [8]	■	■		■
Passalacqua[14]	■	■	■	

Song [2] claims that the major roles of the MSL are to act as a catalyst support layer (as depicted in figure 2-1), maintain proper water balance at the GDL and polymer electrolyte interface, and enhance diffusion of the reacting species. They also claim "Elimination of the supporting layer should allow part of the catalyst region to penetrate deep inside the backings thus, that region becoming inaccessible to the gas or the proton."

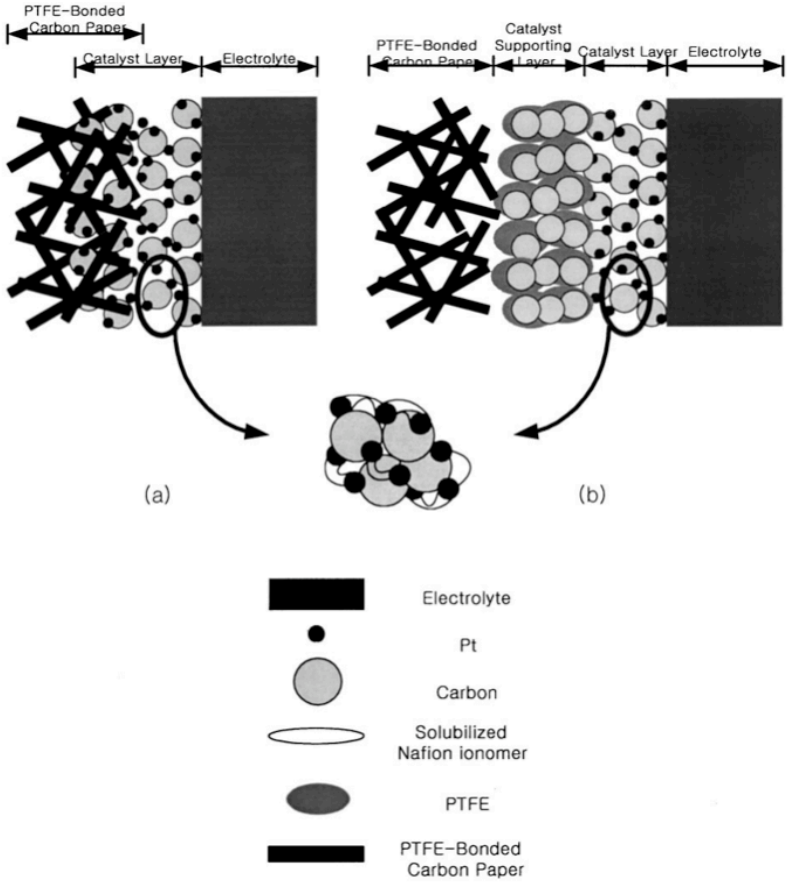

Figure 2-1. Diagram to display catalyst layer support [2]

Qi [1] claim that the MSL, when applied to carbon paper from various companies or batches from the same company, could "diminish the differences" observed in performance. In their view, once the MSL is applied, the choice of carbon paper becomes less critical. The carbon paper is simply a support for the MSL. They also claimed that the MSL assists with water management within the MEA; stating, "Such a layer was extremely helpful where the carbon paper was prone to flooding." This article supports the claim that the MSL acts as a catalyst support, and in turn may also increase fuel cell performance.

Lim [8] claim that the MSL "is intended to provide wicking of liquid water into the GDL, minimize electric contact resistance with the adjacent catalyst layer ink, and furthermore prevent the catalyst layer ink from leaking into the GDL, thereby increasing the catalyst utilization and reducing the tendency of electrode flooding". Their observation does not reflect their own results, but is rather their interpretation of the opinions of the research community.

Nam [5] and Passaogullari [6] present analytical studies that utilize computer simulations to focus on the water removal/transport aspect of the MSL. Both these articles claim that the water transport function of the MSL originates from the physical differences between the GDL and MSL. Nam [5] describe the GDL as a course fiber layer and the MSL as a fine fiber layer. The difference in density and pore volume allows for a jump in liquid water saturation across the interface of the two layers. If the MSL thickness is optimized properly, this jump in saturation can be used to lower the liquid water saturation within the MSL, and in turn against the catalyst layer. The common theme of both of these articles, is that if the MSL is designed properly it can improve water transport and in turn the overall fuel cell performance.

Passalacqua [14], one of the earlier references to explore the MSL, claim that the MSL serves as a catalyst layer support. They explored different layer arrangements within the MEA, some with and some without the MSL. They provided an Energy Dispersive X-Ray (EDX) analysis on the MEA's without the MSL to show the existence

of platinum in the pores of the GDL after operation. The MEA's that contained the MSL exhibited a much better performance, based on *i-v* curves. The MEA with MSL produced 279.5 mW/cm^2, whereas the MEA without the MSL could only produce 178.5 mW/cm^2. These power densities where recorded at 0.5 A/cm^2 and with hydrogen and air as the feed gases. They also claim that the MSL can be thought of as a microporous carbon structure, whereas the carbon paper to which it is applied is more of a macroporous carbon structure. This means that the "…. produced water at the cathode will be reduced in small droplet decreasing the gas diffusion barrier." In other words, the MSL will assist with water transport and species diffusion throughout the MEA.

2.2 Composition

The MSL is typically composed of carbon black and PTFE, although in some cases alternative materials have been suggested for both. By nature PTFE is very hydrophobic, so finding an agent in which to suspend the PTFE/carbon black to form a homogeneous mixture can be a challenge. The use of a variety of solvents including isopropanol (IPA), cyclohexane, and deionized water are reported in the literature. Another consideration is the ratio of carbon black to PTFE. *Table 2-2* provides a summary of compositions explored in prior research.

Table 2-2. Composition Findings Summary

Author	Loading (mg/cm^2)	Compositions Tested (wt% PTFE)	Optimal Composition (wt% PTFE)
Qi [1]	2	24,35,45	35
Song [2]	3.5	10,20,30,40	30
Paganin [11]	50um GDL+MSL	10,15,20,30,40	15
Giorgi [13]	2	10,20,40,60	10

Qi [1] constructed their MSL of carbon black (Vulcan XC-72) and PTFE. They reported testing compositions of 24, 35, and 45 wt.% PTFE. Their optimization of composition was done in conjunction with an optimization of loading (or thickness) of

the MSL. In other words, they tested various loadings at various compositions. They then performed an independent composition optimization holding the MSL loading to around 2 mg/cm^2. They claim that 35 wt.% PTFE is the optimal composition ratio for the MSL. This optimum claim, of 35 wt.%, was based on current density as a function of voltage (*i-v)* performance.

Song [2] also constructed an MSL of carbon black (Vulcan XC-72) and PTFE (Teflon 30-J, Dupont). They report suspending the mixture in 2-propanol (IPA). They held the loading of the MSL constant, at 3.5 mg/cm^2, while adjusting the composition. The constant loading of 3.5 mg/cm^2 was chosen based on an independent loading optimization. They tested 10, 20, 30, and (+)40 wt.% PTFE. They report the optimal composition to be 30 wt.%. They chose the mid-range value claiming, "The water transport through the supporting layer should be impeded with increase in PTFE loading while the water generated in the cell cannot be effectively removed if the PTFE loading is too low." Their optimum claim, of 30 wt.%, was based on *i-v* performance and impedance spectroscopy.

Articles such as Lee [4], and Jordan [10] report optimal composition ratios, but do not support these ratios with an actual optimization. Lee [4] use a 30 wt.% PTFE and carbon black (Vulcan XC-72) mixture while investigating other aspects of the MSL. They suspend the PTFE/carbon black mixture in IPA. They report the use of a sonic mixer to provide a well-homogenized mixture.

Jordan [10] conducts an independent study on the difference between carbon black (Vulcan XC-72R) and acetylene black. Acetylene black has an overall lower pore volume of 10-100 μm range, thus making it less permeable to water. Their tests show that acetylene black will provide better *i-v* performance for the PEMFC. In constructing their MSL they suspend the mixture of acetylene black and PTFE in cyclohexane. In the design of their experiments they assume a constant composition of 10 wt.% PTFE. They report that this ratio was found to be the optimum ratio by Paganin [11].

Paganin [11] construct their MSL by suspending the PTFE (Teflon T-30, Dupont) and carbon black (Vulcan XC-72, Cabot) in water. It is interesting to note that in the preparation of their MSL they heat-treat the carbon black at 450°C, and then chemically treat it at 80°C for 1 hour with a "25% (v/v) nitric acid aqueous solution." In this article they explore a range of compositions (10, 15, 20, 30, 40 wt% PTFE) with a constant thickness (loading) of 50μm. They report thickness as the sum of the GDL and MSL, and as discussed in the application section of this review, their work was unique in that they apply their MSL to both sides of the GDL. With the constant thickness of 50μm, the *i-v* curves show nearly the same performance across all values of compositions, with 15 wt.% PTFE yielding slightly higher performance.

Giorgi [13] construct their MSL with PTFE (Hostaflon 5033, Hoechst) and carbon black (Vulcan XC-72). This article was among the first to claim the primary functions of PTFE in the MSL were "…binding the high surface carbon particles into a cohesive layer, and imparting some hydrophobic character." The MSL was prepared by mixing the solution in an ultrasonic bath. The experimental procedures consisted of holding the loading constant (2 mg/cm^2) while varying the composition of PTFE. Compositions of 10, 20, 40, and 60 wt.% PTFE were explored. This article explores variations in *i-v* performance, total porosity, impedance, and resistance, all as a function of the PTFE content within the MSL. It is found that as the amount of PTFE in the MSL increases, the total porosity decreases. It is also discovered that as the PTFE content in the MSL is increased the percent of macropores (pores >35 μm) is decreased. It is thought that when the macropores are decreased the MSL is better able to prevent migration of the catalyst layer into the MSL of GDL. Although, they state that the presence of macropores within the MSL, and the ability of the catalyst layer to penetrate deep into these pores will actually assist overall performance by increasing the catalyst's total active area. Physically, they claim that the MSL will contain more surface cracks as the amount of PTFE is increased. They discover that porosity in the range of 2-50μm has a minimum value at 20 wt.% PTFE. They claim, based on polarization data, that the total polarization loss will increase two-fold as the composition varies from 10-60 wt.% PTFE. The polarization loss they report is based on the sum of losses attributable to charge transfer

resistance, mass transfer losses, electrolyte resistance, and electrode resistance. At 0.5 Volts, a Nyquist plot reveals the same trend identified by the polarization data, the total polarization loss increases as the wt.% PTFE increases. They do not conclude by suggesting an overall optimal composition. Instead, they conclude by saying that the overall best performance will be found in the lower PTFE content, but you cannot lower the PTFE content too low, as some PTFE is needed to "bond the carbon particles" and avoid flooding of the electrode.

2.3 Loading / Thickness

Another major consideration in the optimization of the MSL is the loading (thickness) with which the MSL is applied. Some articles report the loading as mg/cm^2, and others report the loading as a thickness, or fraction of total diffusion layer thickness. The loading of the MSL is found to be a critical factor in the optimization of the MSL and the overall performance of the PEMFC. *Table 2-3* provides a summary of the studies of loading / thickness of the MSL.

Table 2-3. MSL Loading / Thickness Findings Summary

Corresponding Author (date)	Compositions (wt% PTFE)	Loading Tested (mg/cm^2)	Optimal Loading (mg/cm^2)
Qi [1](2002)	24	0.57, 0.97, 1.90, 3.28	3.28
Qi [1](2002)	35	0.0, 1.16, 2.33, 4.04	4.04 same as 2.33
Qi [1](2002)	45	1.09, 2.18, 3.21	2.18
Song [2] (2001)	30	1.5, 3.5, 10	3.5
Chen [3] (2004)	30	2.83, 373, 4.12, 5.55, 6.79	~4.12
Jordan [10] (2000)	10	0.7, 1.25, 1.9, 2.5	1.25
Paganin [11] (1996)	40	15,25,35,50,65 µm (MSL + GDL)	35 µm (MSL + GDL)

Qi [1] explored the optimal loading by running a variety of i-v performance based tests varying the loadings from 0-~4.0 mg/cm^2. As outlined above, their loading optimization was done in conjunction with a composition optimization. They ran four tests at 24 and 35 wt.% PTFE compositions and three tests at 45 wt.% PTFE, each test with a different loading. They claim "a carbon loading of 2.0 mg/cm^2 was sufficiently high to achieve maximum performance." They begin by optimizing the amount of PTFE

used to make the carbon paper hydrophobic. This optimization consistently yielded better *i-v* curve performance at higher (above 60°C) cell operating temperatures, which is consistent with what most of the PEMFC community reports. But while reporting the results of the PEMFC's with a MSL, they report using a much lower cell temperature (around 35°C). They do not give a reason for this inconsistency. Their results would be more useful if they would have conducted their tests at higher cell temperatures, at which their results suggest better fuel cell performance.

Song [2] held the composition of their MSL constant (at a value of 30 wt.% PTFE) while varying the loadings. They investigated 1.5, 3.5, and 10 mg/cm^2 loadings. Based on *i-v* curve performance, cyclic voltammogram, and AC impedance spectroscopy they concluded that 3.5 mg/cm^2 was the optimal value. Although they have done an excellent job in outlining their results, there are still a few unanswered areas of interest. Such as, what type of performance lies in the gap of 3.5 and 10 mg/cm^2. The difference of 6.5 mg/cm^2 is a large amount of MSL, and raises the question as to whether there is a more accurate result. As stated in the beginning of this paragraph, they perform the composition and loading optimizations separately, and do not address the interaction between these factors.

Lee [4] also held their composition of the MSL constant (at a value of 30 wt.% PTFE) while varying the loadings. They tested loadings of 2.83, 373, 4.12, 5.55, and 6.79 mg/cm^2, which correspond to a thickness of 90, 114, 123, 136, 196 μm respectively. They do not actually claim a certain optimal value for loading; they simply say that the best performance comes from an intermediate value. They use an *i-v* curve to evaluate the performance of each of the loadings.

Jordan [10] held the MSL composition at a constant value of 10 wt% PTFE. They explored 0.7, 1.25, 1.9, and 2.5 mg/cm^2 loadings. As previously noted their MSL was composed of acetylene black and PTFE. They concluded that a PEMFC running on air would find its optimal performance with a loading of 1.25 mg/cm^2, and a PEMFC

running on pure oxygen would find its optimal performance with a loading of 1.9 mg/cm^2. Their optimal values are derived from an *i-v* performance based test.

Nam [5] and Passaogullari [6] are analytical based articles that have formulated computer simulations to identify the optimal thickness of the MSL. Nam [5] produce a model in which they can relate uniform liquid flux to current density, from which they can predict the saturation within a two-layer diffusion medium. It is implied that this model is to be applied to both cathode and anode layers of the PEMFC. Their model predicts that the MSL should be less than 33% of the total thickness of the MSL and GDL.

Passaogullari [6] explore the unsaturated flow theory (UFT) model and the multi-phase mixture (M^2) model in an attempt to better understand one-dimensional two-phase transport within the MSL. The downside to the UFT model is that it assumes constant gas pressure across the GDL, where the M^2 model does not make this assumption. They show that this assumption causes the UFT model to greatly under predict saturation level within the two-layer diffusion. Within both models they assume that the catalyst layer is infinitely thin and that the oxygen reduction reaction (ORR) takes place at the GDL and membrane interface. Both models are also limited to the cathode side of the PEMFC, where the majority of mass transport limitations occur. The M^2 model claims that the MSL thickness should be between 30 and 45 μm, for a total MSL plus GDL thickness of 300 μm. In other words, the MSL should be 10 to 15% of the total GDL and MSL thickness. Along with optimizing the MSL loading/thickness, they also explore the porosity and wetting characteristics of the MSL. Claiming that a porosity of 0.6 and a contact angle of around 105^o are the optimum values.

Paganin [11] conduct an experiment at which they hold the composition constant at 40 wt.% PTFE and vary the thickness (loading) of the diffusion layer (MSL+GDL). As discussed above, they had a unique approach to the construction of their diffusion layers, applying the MSL to both sides of their GDL. Furthermore, the thickness they cite is the sum of the both MSL layer plus the GDL. They tested thicknesses of 15, 25, 35, 50, and

65 μm. The results form this test show that a diffusion layer thickness in the range of 35-65 μm will yield the best *i-v* performance. This analysis also concludes that the "charge transfer resistance of the hydrogen oxidation reaction (h.o.r.), the resistance of the electrolyte in the cell and the linear diffusion terms due to diffusion in the gas phase in the diffusion layer and /or in the thin film" will increase as the thickness of the MSL and GDL increase.

2.4 Application Techniques

Another major consideration in the optimization of the MSL is the method of application of the MSL. Different articles have reported very different methods to apply the MSL. The five methods observed in the research include tape casting, vacuum filtering, roller application using a paint roller, screen-printing, and spray application. *Table 2-4* summarizes the application techniques used in each experiment.

Table 2-4. MSL Application Methods Summary

Authors	Spray	Screen-Print	Brush	Rolling	Tape Casting	Vacuum Filtering
Lee [4] (2004)	■	■		■		
Lim [8] (2004)					■	
Jordan [10] (2000)			■			
Paganin [11] (1996)						■
Passalacqua [12] (2001)	■					
Giorgi [13] (1998)	■					
Passalacqua [14] (1998)		■				

Lee [4] explores the difference between roller application of the MSL using a paint roller, application using screen-printing apparatus, and application by spraying. This article claims that the main physical differences between the three methods are in the pore size. They claim that the screen-printing method is the best method of application. They claim the rolling method produces a flat and dense MSL, and that the distance between the particles is very short. "The total porosities of the rolling, spraying, and screen printing methods are 51, 57, 61%, respectively." Figure 1 displays the differences between the three methods, as seen under scanning electron microscope (SEM), *Figure 2-2* graphically displays the pore volume differences between the three

methods, and *Figure 2-3* displays the *i-v* performance differences between the three methods.

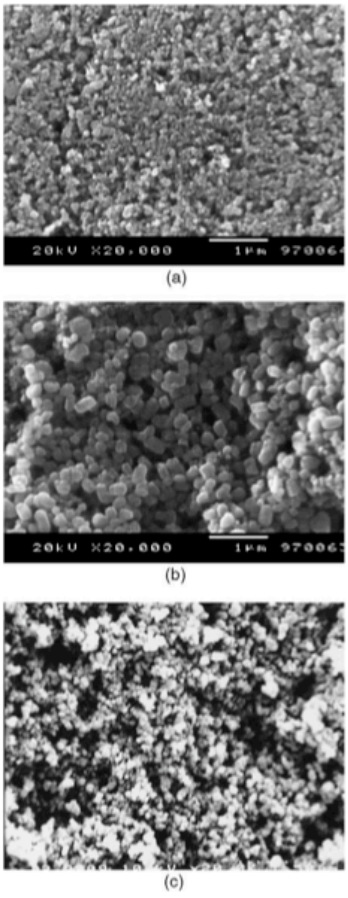

Fig. 1. SEM surface images of the gas diffusion layer (a) rolling; (b) spraying; (c) screen printing.

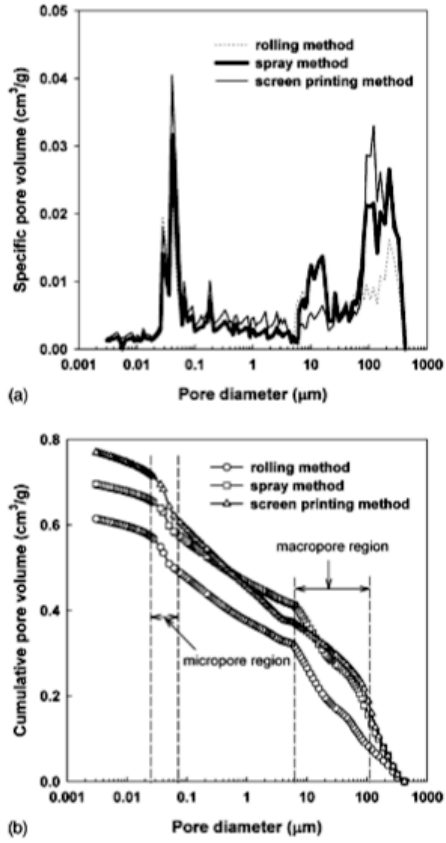

Fig. 2. (a) Specific and (b) cumulative pore volume distribution of the gas diffusion layer according to the fabrication method.

Figure 2-2. Exploration of various application methods [4]

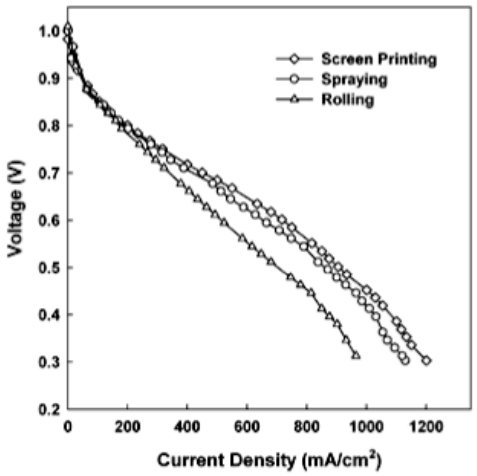

Fig. 3. Influence of different gas diffusion layer fabrication methods on cell performance of H_2/O_2 single cells.

Figure 2-3. i-v curve performance comparison for various application methods [4]

As seen in the three figures above screen-printing seems to provide the best overall performance, but the spraying method is very close to it. Further research into the method of screen-printing suggested many concerns about accuracy and repeatability, and the amount of materials and time needed to construct the apparatus.

Lim [8] apply their MSL to the GDL by using the tape-casting method. The first step of this method involves dispensing MSL solution onto the GDL. A blade is then passed over the GDL surface with a gap set to the desired MSL application thickness. Once the blade is run over the MSL, the result is the exact desired thickness. In the application of the MSL this method has much opportunity to improve. The MSL, when in its "wet" form, consists of mostly surfactants and solutes. So when it is dried, most of the material evaporates. The gap (or thickness) of the MSL established during its "wet" stage, is a very inaccurate estimate of the actual dry thickness of the MSL. This article does not say how they heat treat, or whether they sinter their MSL to the GDL.

Jordan [10] applied their MSL by brushing it onto the GDL. They did not justify why they choose this particular method, but they further elaborated on their application technique by providing the details of how they dried their MSL. Once they got the correct loading of MSL on the GDL, they sintered the two layers at 350 ^{o}C for 30 minutes. They

also did an independent study on the effect of sintering the MSL to the GDL. As previously noted Jordan [10] investigates acetylene black as well as Vulcan XC-72R carbon black. As displayed in *Figure 2-4*, they conclude their study on sintering by claiming the sintered MSL's will perform better than the non-sintered MSL's, based on polarization curve performance.

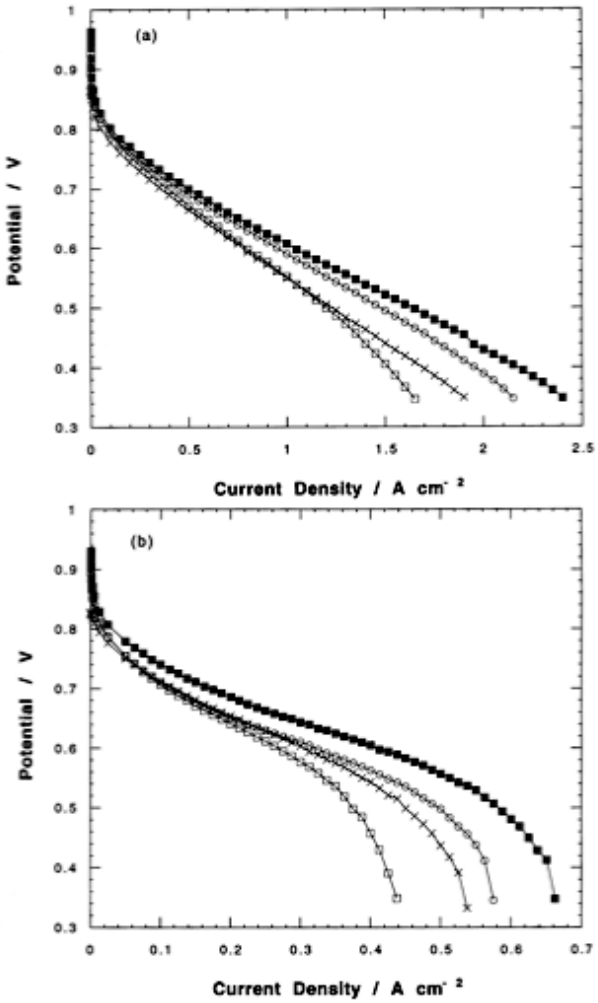

Fig. 2. Influence of diffusion layer carbon type and effect of sintering. □ Vulcan XC-72R, ○ Vulcan XC-72R sintered, × Acetylene Black, ■ Acetylene Black sintered. Diffusion layers contain 10 wt.% PTFE. (a) Oxygen, (b) air cathode supply.

Figure 2-4. Effect of sintering investigation [10]

Song [2], Qi [1], Passalacqua [14], E. Passalacqua [12], Giorgi [13], and Paganin [11] provide limited details concerning their application process. They have been

included in this review to help display the variety of accepted application techniques and drying methods that exist within the research community.

Song [2] explain that "a thin PTFE/carbon film is cast onto the treated surface…", and that they dry this film (MSL) at 180ºC for 30 minutes, and then sinter it at 330ºC for 30 minutes. Qi [1] does not provide any application details other than once the MSL is applied to the GDL it is allowed to dry at room temperature, then dried at 110 and 280ºC for 30 minutes and sintered at 350ºC for 30 minutes. Passalacqua [14] use a screen-printing method to apply their MSL. They apply the MSL onto a GDL that has had a hydrophobic treatment, and then apply the catalyst layer onto the MSL. After application of both MSL and catalyst layer they heat-treat the series of layers at 350ºC. Passalacqua [12] (a later article compared to Passalacqua [14]) utilizes a spray technique to apply their MSL to carbon paper. They then heat-treat the MSL at 350ºC. The difference between Passalacqua [14] (1998) and E. Passalacqua [12] (2001) is the change from a screen-printing application to a spray application.

Giorgi [13] apply their MSL with a spray technique. They apply it directly to the GDL. They dry the MSL at 120ºC for 1 hour, 280ºC for 30 minutes ("to remove the dispersion agent contained in PTFE"), and finally sinter it at 350ºC for 30 minutes. Paganin [11] vacuum filter their MSL onto both sides of the GDL (carbon cloth). They allow it to dry under ambient conditions, then bake it at 280ºC for 30 minutes "to help remove the dispersion agent contained in the Teflon ®". They finished the application of the MSL by sintering it at 330ºC for 30 minutes.

2.5 Literature Review Summary

Since its first use, within the structure of the PEMFC, the MSL has gotten more and more attention. Within the past 10 years researchers have identified the MSL as playing a critical role in the PEMFC. As reflected in the previous literature review, there have been several attempts to identify optimal compositions, loadings, and methods of application for the MSL in conventional fuel cell architectures.

Virginia Tech is working to develop a novel fuel cell design that utilizes a "ribbon style" stack architecture[1]. This particular design is projected to increase manufacturability and flexibility of design for the PEMFC. As displayed in *Figure 2-5*, the ribbon style architecture does not use bipolar plates to collect current or to compress the stack. In the absence of stack compression, the MSL must accomplish not only its traditional functions, but also must help to adhere the GDL to the catalyzed membrane. This is accomplished by hot pressing the MSL/GDL assembly to the catalyzed membrane.

Because conventional fuel cell stack architecture uses stack compression to maintain the integrity of the stack assembly, the adhesion of the fuel cell layers to one another is less of a concern. Therefore, a search for literature pertaining to the adhesive properties of the MSL came back with very few results. The goal of the research presented in this thesis is to evaluate the effect of MSL design and fabrication parameters on performance and adhesion in fuel cell assemblies.

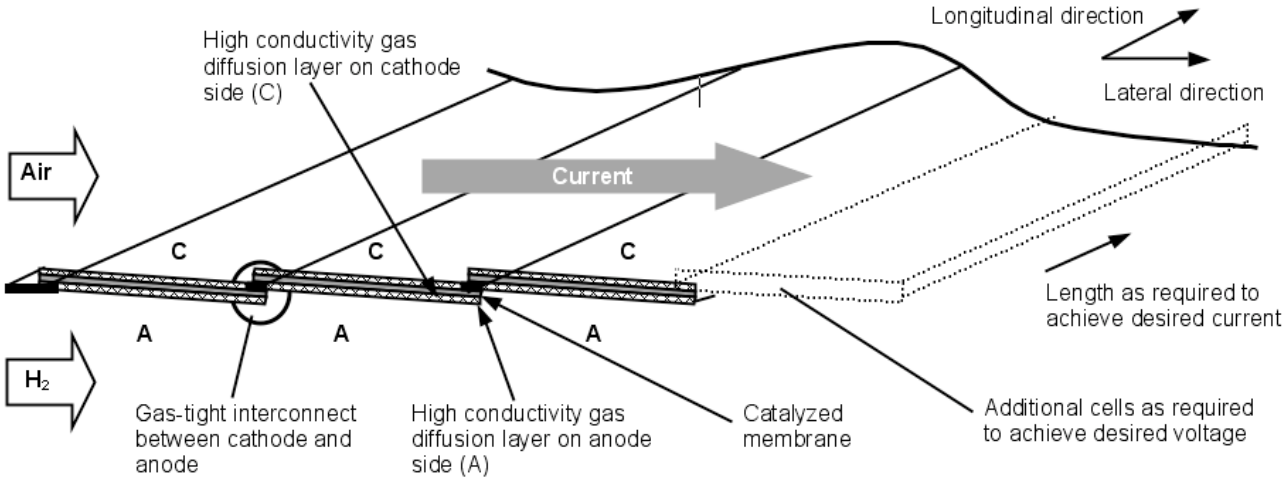

Figure 2-5. "Ribbon Style" stack architecture

As discussed in this chapter, prior research has evaluated the effects of the composition and loading of the MSL on performance in conventional cells. In the current research, the performance analysis is revisited for cells in which the GDL/MSL is

[1] VTIP Disclosure No. 03.129 "Novel PEM Fuel Cell Architectures" US Patent application no. 60/535,811.

adhered to the catalyzed membrane. Moreover, the research presented here extends the composition and loading analysis to address the role these two factors play in determining the adhesion characteristics of the assembly. In addition, since the ribbon architecture calls for the GDL/MSL to be hot pressed to the catalyzed membrane, the effects of fabrication pressure and fabrication time on performance and adhesion will also be investigated. Correlations will be developed to reflect both performance and adhesion as functions of the design/fabrication parameters. These correlations will be used to identify the loading, composition, fabrication pressure, and fabrication time that lead to overall improvements in performance and adhesion.

3 Experimental Procedures

3.1 Goals of Experiments

As stated in the conclusion of the literature review, the goal of this research is to evaluate the effect of the MSL composition and fabrication on the performance of the MEA and on the adhesion of the GDL to the catalyzed membrane. An experiment was conducted to evaluate performance and adhesion as functions of four major MSL design/fabrication factors: the MSL loading, MSL composition, pressure used while pressing the GDL to the MEA (fabrication pressure), and time the GDL-MEA combination is left in the press (fabrication time). Specifically, the performance of the fuel cell was quantified by the cell's i-v curve. The i-v curves were measured using a fuel cell test station. The fuel cell test station and its capabilities are outlined in more detail in *Section 3.8.* The adhesion of the total GDL-MEA structure, after being pressed together, was explored using a T-peel test methodology. The adhesion testing, and apparatus' used in the adhesion testing, are discussed in more detail in *Section 3.9.*

Another major goal of this research was to explain the effect of the four factors (loading, composition, fabrication pressure, and fabrication time) on performance by analyzing the major polarization losses in the cell. As reported by Springer [20], impedance spectroscopy can be used to create Nyquist plots of imaginary and real impedances within the fuel cell. These plots can be analyzed to identify the individual polarization losses, such as activation losses, ohmic losses, and mass transport losses.

With the objectives of analyzing performance and adhesion established and the factors chosen, the next step in the process was to design the experiment to optimize the number of actual test points needed, while still being able to statistically create estimates for the responses (levels of adhesion and performance) as a function of the four main factors outlined above. After the design for the experiment was in place, the next step was to establish the methodology used for creating and testing the experiment specimens. This chapter explains the design of the experiments and the experimental procedures.

3.2 Design of Experiment

As previously discussed, the experiment will have four factors; MSL loading, MSL composition, fabrication pressure, and fabrication time. Execution of a complete experimental matrix would require 256 experiments and would not be practical. To reduce the number of points tested, and still be able to draw solid statistical inferences, a program called Design-Expert®, produced by Stat-Ease, Inc., was used. Design-Expert® allows the user to choose from a variety of experimental designs. The two designs that are best suited for this particular experiment are the Central Composite Design (CCD) and the Full Factorial Design.

The advantage of the CCD is that the analysis allows for curvature between experimental points. The disadvantage of the CCD is that it still requires 28 experiments, which includes 4 center point replications. The full factorial design does not allow for curvature between points, but requires only 20 experiments, which also includes 4 center point replications. Furthermore, while the full factorial design does not allow for curvature, it does test for curvature, letting the user know the proper way to proceed with the results. Moreover, if curvature is found to be significant, the full factorial design can be augmented to a CCD. This is the approach that was taken with this research. The experiment was initially conducted using a full factorial design with four factors. The results were then evaluated to determine if augmentation to the CCD design was necessary.

For a full factorial design, Design-Expert® simply requires the input of the upper and lower limits of the factors. The limits used for these factors were established from the literature review. For composition, the upper limit was chosen to be 50 wt.% PTFE and the lower limit was chosen to be 10 wt.% PTFE, based on the data reported in *Table 2-2*. For the loading, the upper limit was 4 mg/cm^2 and the lower limit was 1.5 mg/cm^2, based on the data reported in *Table 2-3*. For the fabrication pressure, an upper limit of 10.34 MPa was used, and a lower limit of 3.45 MPa was used. Finally, the fabrication time had

an upper limit of 8 minutes, and a lower limit of 2 minutes. The range of fabrication pressures and times were dictated by experimental procedures developed in-house. With these four factors, and two levels, the full factorial design requires testing 16 individual points.

Another option that Design-Expert® provides is the ability to create "center points" for the full factorial design. These center points help to quantify the experimental error in the design. This experimental error is a mix of human/measurement error and unexplained variability stemming from a variety sources. Along with the 16 basic points needed for the full factorial design, 4 replications of the center point were conducted. In conclusion, the full factorial design results that are reported in this paper are derived from a test of 4 factors at 2 levels with 4 replicated center points.

3.3 Microporous Sublayer Preparation

The microporous sublayer (MSL) was fabricated by preparing a PTFE-carbon black mixture that is suspended in IPA. The mixture was carefully designed to avoid agglomeration of particles within the MSL. The following section will outline the procedures followed to construct a homogeneously mixed MSL.

3.3.1 Suspension Preparation. The MSL is typically composed of carbon black and polytetrafluoroethylene (PTFE). Although in some cases alternative materials have been suggested for both the carbon black and the PTFE, the results reported in this work reflect an MSL constructed of carbon black (Cabot's Vulcan XC-72R) and PTFE (ElectroChem, Inc's Teflon™ Emulsion Solution, TFE 30). Cabot's Vulcan XC-72R consists of very small (~30 nm diameter) carbon particles. TFE 30 is approximately 60% PTFE, about 40% water, with minor additives that help to keep the Teflon in suspension.

The composition of the MSL is most commonly reported as a percentage by weight (wt.%) of PTFE in the PTFE and carbon black mixture. Even though the PTFE is in a liquid/emulsion form, it is hydrophobic by nature, which makes it very hard to

further suspend in any liquid. We tried several of the chemicals reported in the literature review and chose IPA because of its ability to uniformly suspend both the PTFE and carbon black.

The MSL was applied to achieve a desired loading expressed as a mass of MSL per unit area (mg/cm^2). Knowing the area of the MSL and the required loading, the required MSL mass can be determined by:

$$m_{msl} = A_{msl} L_{msl} \tag{3-1}$$

The PTFE content of the MSL, f_{PTFE}^{msl}, is expressed as a wt.% so that the mass of the PTFE is:

$$m_{PTFE}^{msl} = m_{msl} f_{PTFE}^{msl} \tag{3-2}$$

The PTFE content of the emulsion, f_{PTFE}^{eml}, is also expressed as a wt.% so that the mass of the emulsion is:

$$m_{eml} = \frac{m_{PTFE}^{msl}}{f_{PTFE}^{eml}} \tag{3-3}$$

Trial and error revealed that a 1-1.5 wt.% mixture of PTFE in IPA provided the most homogeneous mixtures when the carbon black was added. Thus the required mass of IPA is:

$$m_{IPA} = m_{PTFE}^{msl} \left(\frac{1}{f_{PTFE}^{susp}} - 1 \right) \tag{3-4}$$

where f_{PTFE}^{susp} is the wt.% of the PTFE in the suspension. As an example, if 5 cm ^{2} of MSL is to be prepared with a loading of 4 mg/cm^2 and a composition of 50 wt.%, the required

amount of PTFE is 10 mg. This is provided by 16.7 mg of PTFE emulsion that is mixed with 656.7 mg of IPA to yield the suspension required to prepare the MSL. In practice, more MSL is made due to the amount that is wasted in the application process. The exact MSL loading is then determined by measuring the additional weight added to the GDL and the area upon which the MSL is applied.

The next step in the mixing process was to ultrasonically mix the IPA and PTFE with a BioLogics, Inc Ultrasonic Homogenizer (model 300 V/T). A "micro-tip" was used on the ultrasonic homogenizer, and the power level was set to approximately 40% with a 50% pulse. The PTFE and IPA were mixed for two three-minute intervals; with a 30 second break in between them.

The next step was to determine the appropriate amount of carbon black. Since the MSL is comprised only of carbon black and PTFE, the mass fraction of carbon black is simply 1- f_{PTFE}^{msl} . Thus the required mass of the carbon black is:

$$m_{CB}^{msl} = m_{msl}\left(1 - f_{PTFE}^{msl}\right) \tag{3-5}$$

Keeping with the above example, the required mass of carbon black would be 10 mg. It is worth emphasizing that when calculating the amount of carbon black, the amounts of IPA, water, and minor constituents[2] in the PTFE emulsion are not included because these constituents evaporate from the MSL.

After the desired amount of carbon black was obtained, the next step was to add it to the IPA and PTFE mixture. Once the carbon black has been added to the IPA and PTFE, the mixture is sealed and shaken by hand. The hand shaking provides a decent initial mix, but the final, and more thorough, mix is accomplished with the ultrasonic homogenizer. The same procedure, as used when mixing the IPA and PTFE, was used

[2] Minor constituents found in PTFE Emulsion (not including water)

Surfactant:	<6%
Octyl Phenoxypolyethoxyethanol	0-5%
Nonyl Phenoxypolyethoxyethanol	0-5%
Ammonium Perfluorooctanoate	<0.5%

when mixing the carbon black into MSL suspension. The ultrasonic homogenizer was set to approximately 40% power with a 50% pulse, and the MSL was mixed, using the micro-tip, for two three-minute intervals with a 30 second break in between them. The final mixture is referred to as the MSL ink.

Following the above procedures yields a mixture that has the consistency and transparency of ink, provided the proper amount of IPA is used. It was mentioned above that, in order to thin the PTFE, various amounts of IPA were tested. Due to the price (compared to water) and flammability of it, the desire was to use less IPA. A review of the MSL literature suggested that using combinations of water and small amounts of IPA, instead of pure IPA, should provide a homogenous mixture when the carbon black is added. To create a well-homogenized 25 wt.% PTFE MSL we added PTFE emulsion and carbon black to three different solutions – 50% deionized (DI) water and 50% IPA; a few drops of IPA and the remainder DI water; and 100% IPA. After adding PTFE emulsion and carbon black, the first two solutions contained agglomerations of carbon black particles. Only the final solution, containing 100% IPA, allowed homogenization of the PTFE/carbon black mixture.

The design of this experiment required the construction of a 10, 30, and 50 wt.% PTFE MSL. When first preparing these MSL's the thought was to use the same method that was used when constructing the 25 wt.% PTFE MSL. Unfortunately, this approach did not work for the 10 and 50 wt.% PTFE MSL. When constructing a 10 wt.% MSL ink, the key to creating a homogenous mixture is to hold the ratio of carbon black to IPA the same as from the 25 wt.% PTFE MSL (i.e. 0.029). Otherwise, if the IPA is reduced as the PTFE is reduced, the carbon black will not homogeneously suspend in that smaller of an amount of IPA. However, when constructing the 50 wt.% PTFE MSL, the MSL became too watery. By a trial-and-error series of experiments, it was identified that the original mixture (for preparing 25 and 30 wt.% PTFE MSL) of 1 wt.% PTFE and 99 wt.% IPA, had to be adjusted to 1.5 wt.% PTFE and 98.5 wt.% IPA for the 50 wt.% PTFE MSL ink. This small adjustment gave the MSL a much more ink-like consistency, that made it more feasible to apply.

After some time of sitting without agitation, even the most homogeneous MSL mixtures will begin to separate. It was observed that a clear fluid rises to the top of the container over time. After drawing a small amount of this fluid from the top of the container, and depositing it in a Petri dish to allow evaporation, it was concluded that this fluid is mostly IPA, suggesting that the mixture separates over relatively short periods of time. To investigate the homogeneity of the suspension, samples of the MSL suspension were taken from the top and bottom of the storage container. These samples were taken approximately 15 minutes after mixing in the ultrasonic homogenizer. This time frame, of 15 minutes, was thought to be the longest the MSL ink would have to sit before being applied onto the GDL. These samples were then taken to a TA Instruments Q500 Thermogravimetric Analyzer (TGA). The TGA instrument heats a sample through a range of temperatures while measuring the mass of the sample. The mass of the sample changes as constituents within the mixture are evaporated. Knowing the temperatures at which species vaporize, and the change in sample mass, allows the mass of each species to be determined. The first step in this process is to run the constituents of the suspension (PTFE and carbon black) through the TGA instrument individually. This identifies the temperatures at which the individual constituents vaporize. In the case of the MSL, both PTFE and carbon black were first run in the TGA instrument separately, and then the mixture was evaluated. The mixture was evaluated by extracting samples from the top and bottom of the ink container and depositing them in separate Petri dishes. After complete evaporation of the IPA, the resulting MSL was scrapped from the Petri dish and taken to the TGA. *Figure 3-1* illustrates the wt.% of PTFE in the top and bottom samples. Since the mass loss corresponding to PTFE variation was the same, it can be concluded that both ink samples contained the same amount of PTFE, approximately 25wt.% which is consistent with the mixture design.

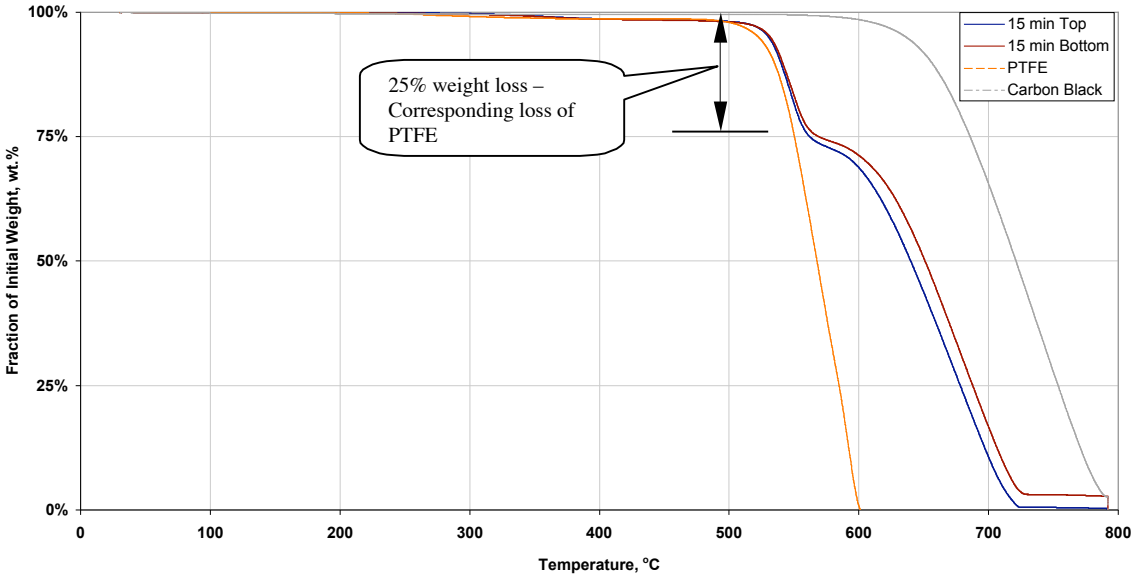

Figure 3-1. TGA analysis of sample from top and bottom of MSL container.

These results confirm that the MSL remains homogenously mixed for at least the first 15 minutes after preparation. If the application process is executed efficiently, 15 minutes should be adequate to complete at least one application of MSL.

3.3.2 Application Method. As discussed in the literature review, there are many different methods to apply the MSL. The literature review revealed that screen-printing, tape casting, and spraying could be used to prepare the MSL. Screen-printing is a process in which a substance is forced through a screen onto a substrate. The screens are carefully chosen according to thread count and durability. Once the appropriate material is acquired, the screen is masked to create the desired shape or pattern. The next step is to apply the ink, or in this case the MSL, to one edge of the screen and pull it across the screen with a squeegee. This process has many disadvantages. For example, the screen must be thoroughly cleaned after every use, and the screen has a limited lifetime. The ink consistency and screen porosity must be carefully considered. For these reasons screen-printing was not the chosen method of application for the MSL's studied in this research.

Tape casting was another method mentioned in the literature review. The first step of this method involves dispensing MSL solution onto the GDL. A blade is then passed

over the GDL surface with a gap set to the desired MSL application thickness. Once the blade is run over the MSL, the result is a MSL with the exact desired thickness. Tape casting was not used in this research because, tape casting works best when the goal is to apply one thick layer. When applying the MSL, the application process must be done in thin layers to avoid surface cracks that will form due to rapid evaporation of the IPA.

Spraying was determined to be the best approach for applying the MSL because it offers more control over the amount of MSL applied to the GDL, therefore reducing the risk of surface cracking. The use of a hobby-style airbrush was thought to be the best method. Specifically, this type of airbrush works best with a substance that has the consistency of milk. Most MSL compositions will satisfactorily meet this requirement. Most hobby-style airbrushes also have relatively small paint reservoirs when compared to the spray guns typically employed in the automotive industry. This is an advantage because the amount used for one MSL application will most likely not exceed 3 ounces.

When considering the purchase of an airbrush, there are a few key decisions to make. There are two different ways to feed the MSL ink into the airbrush. The first way to feed the ink into the airbrush is a called gravity feed. Gravity fed airbrushes have a small cup that rests on the top of the airbrush. The paint falls from the cup into the spraying orifice of the airbrush. This cup is usually open on the top, which would expose the MSL ink to the air. The second type of airbrush is a siphon fed airbrush. A siphon fed airbrush draws the MSL ink out of a sealed reservoir located below the airbrush. Since the IPA used in the MSL suspension has the tendency to evaporate quite rapidly, the siphon fed option seemed most appropriate for the MSL application.

Most of the airbrushes have an adjustment clutch that positions a needle that passes through the center of the airbrush, controlling the rate at which ink is drawn from the reservoir. The position of this needle is adjusted by the threaded clutch assembly at the back of the airbrush. As the clutch assembly is threaded out of the airbrush, MSL ink will be drawn more rapidly from the reservoir and in turn sprayed from the nozzle.

There are two main types of airbrushes - single action airbrushes that only allow on-off control of the spray. Double action airbrushes also allow for on-the-go adjustment of the clutch assembly, and thus the feed rate. In the application of the MSL, the single action airbrush is more advantageous than the double action because once the airbrush has been optimized; only one feed rate setting will be used. Changing the feed rate during spraying can cause an undesirable finish on the MSL. Therefore, use of a double action airbrush would only increase the likelihood for operator error. Based on the previous considerations, we selected a siphon-fed, single action hobby style airbrush (Paasche SA2000).

The final consideration, when using an airbrush to apply the MSL, is the choice of propellant. Since shop air can have traces of oils, and other impurities that would pollute the MSL, bottled nitrogen was used as the propellant.

3.3.2 Application Optimization. The airbrush settings that produced the best MSL layers were determined by an initial exploration. As mentioned above, the user has the ability to adjust the clutch assembly, which in turn will adjust feed rate at which MSL ink is drawn from the reservoir. The user also has the option of adjusting the pressure of the propellant (nitrogen) that is supplied to the airbrush. This affects both the rate of application and atomization of the ink. The pressure of the propellant can be adjusted by a regulator located on the outlet of the compressed nitrogen tank. These two variables provide an opportunity for an optimization of the combination of pressure and feed rate setting.

During this study the clutch was tested at two significantly different feed rate settings, and the pressure was adjusted to two different pressures. The location of the clutch assembly was measured by the number of turns it was unscrewed and by the distance (millimeters) the body of the clutch assembly was from the body of the airbrush. The clutch assembly was tested at 1.43 mm (1.75 rotations out) from the body and 3.7 mm (4.75 rotations out) from the body, and the pressure of the propellant was tested at 103.4 kPa PSI and 275.8 kPa.

During the study the airbrush was positioned 203-305 mm from the specimen. With the feed rate, propellant pressure, and spray distance established, the only other variable involved in the application of the MSL is the amount applied before a drying is needed. Only a limited amount of MSL can be applied before drying it, and evaporating the IPA. If too much MSL is applied before drying, the surface of the MSL will contain large cracks. This texture is similar to a desert when all of the water has been evaporated. Since one of the goals of applying the MSL is to create a uniform surface to which the catalyst surface can bond, these surface cracks are very undesirable. Therefore, the procedure for applying the MSL consists of a series of spraying and drying steps.

This study was done in two stages. The first stage explored the effect of varying the pressure and feed rate setting. During this stage the number of times the airbrush passes over the GDL, while applying the MSL, was recorded but not controlled. The MSL was applied until the surface onto which it was being applied became glossy. At this point the GDL, onto which the MSL was applied, was allowed to dry in room temperature until the glossy finish (meaning the MSL was still wet) turned to a flat finish. At this point the GDL was then taken to an oven where it was dried at 140ºC for 30 minutes. It was then weighed, and the loading in mg/cm^2 was recorded. This procedure was continued until the desired amount of MSL was applied.

The second stage of the study was to explore whether the number of passes between each dry had an effect on the overall characteristics and appearance of the MSL. This was done by picking a pair of settings attempted above (pressure and feed rate), and controlling the number of passes the airbrush made over the top of the GDL during application to a relatively low value and then to a relatively high value. The same drying and recording procedure as described in the previous paragraph was used.

After the desired amount of MSL was applied, during both of the stages of the study, the GDL was then subjected to its final drying and sintering stages. It was baked, once again, at 140ºC for 30 minutes. Then it was ramped, at 40ºC per minute, to 280ºC,

where it was baked for 30 minutes. This stage is designed to finish evaporating the water and IPA out of the MSL. The final stage of sintering the MSL to the GDL was to raise the temperature of the GDL to 350ºC for 30 minutes. The melting point for PTFE is between 327 - 342ºC, so at this temperature the PTFE in the MSL will bond with the PTFE from the hydrophobic treatment of the GDL, providing a strong bond between the GDL and MSL. During this study, 8 specimens were created, each one with a different combination of pressure, feed rate setting, and number of passes.

The final step in the study was to inspect the specimens created. During this inspection, under the naked eye and under Scanning Electron Microscopy (SEM), the specimens were judged based upon surface uniformity, apparent density, uniformity of thickness, and quality of the MSL/GDL interface. Surface uniformity includes both how flat the surface is and whether there are surface cracks (and if there are how prevalent they are). As previously discussed, the MSL serves as a catalyst support and a way to reduce contact resistance between the GDL and catalyst layer. Thus, a flat surface is desired to better support the catalyst layer and reduce contact resistance between the MSL and catalyst layer. Also previously discussed, another major function of the MSL is water management. The formation of cracks within this layer can disrupt the capillary effect of the MSL pores, effectively reducing the ability of the MSL to manage the water.

Initially, specimens 1, 3, 5, and 6 were discarded from further consideration based on the fact that even to the naked eye they exhibited a very rough surface, with what looked like tiny agglomerations randomly appearing on the surface. Specimen numbers 1, 3, 5, and 6 were all specimens that were prepared using the low feed rate setting. The low feed rate setting reduces the feed rate of MSL ink that is applied, while holding the flow of nitrogen constant. With this in mind, it was concluded that a higher feed rate of the MSL ink (or ratio of MSL applied to nitrogen flow) is desirable. It was concluded that, while the lower feed rate can assist in keeping MSL layers thin, it allows too much nitrogen to blow across the MSL substrate and leads to the formation of agglomerations of MSL. These surface non-uniformities can be observed in the SEM image of specimen 6 displayed in *Figure 3-2*.

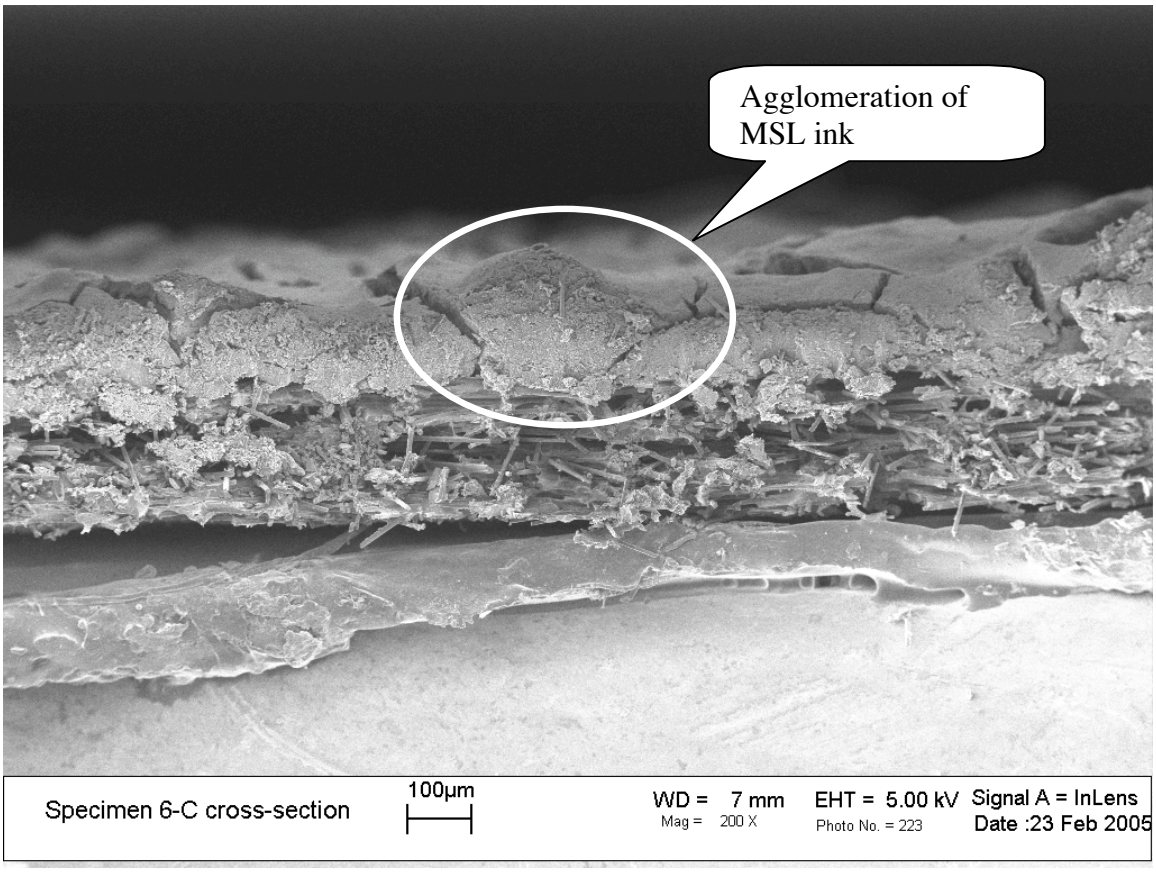

Figure 3-2. SEM cross-section from the center of specimen 6

Specimens 2, 4, 7, and 8 were investigated further using SEM. Two samples of each of these specimens were prepared for SEM viewing. A sample from the center was taken, and a sample from the very side of the specimen was taken. To assist in capturing higher quality results, a 15-nanometer conductive layer of gold was applied (via sputter coating) to all specimens viewed under SEM. Using the inspection guidelines outlined above, 5 images from looking down on the surface and 2 cross-sections were captured. The five images of the surface, 200x, 1000x, 5000x, 20000x, and 100000x were taken in an attempt to examine both the broad and very fine differences that might exist. Two additional cross-section images, 200x and 400x, were taken from each of the specimens to examine these differences from another angle.

Specimen 2 was applied with a lower (103.4 kPa) propellant pressure, and a high feed rate setting. Specimen 4 was applied with a higher (275.8 kPa) propellant pressure, and a high feed rate setting (MSL to nitrogen ratio). The MSL on specimen 7 and 8 was applied in almost the same way, with a high propellant pressure and a high feed rate. The only difference between 7 and 8 was in the amount of MSL that was applied before it was dried. As discussed earlier, the MSL is applied in layers, drying it in an oven between each of the layer applications. The MSL was applied to specimen 7 in very thin layers (6 layers were required to meet the desired loading for specimen 7) between drying. For specimen 8, the MSL was applied in thicker layers (3 layers were required to meet the desired loading for specimen 8), meaning it took fewer application and dry cycles than specimen 7. A SEM image of the cross-section of the center of specimen 7 is displayed in *Figure 3-3*.

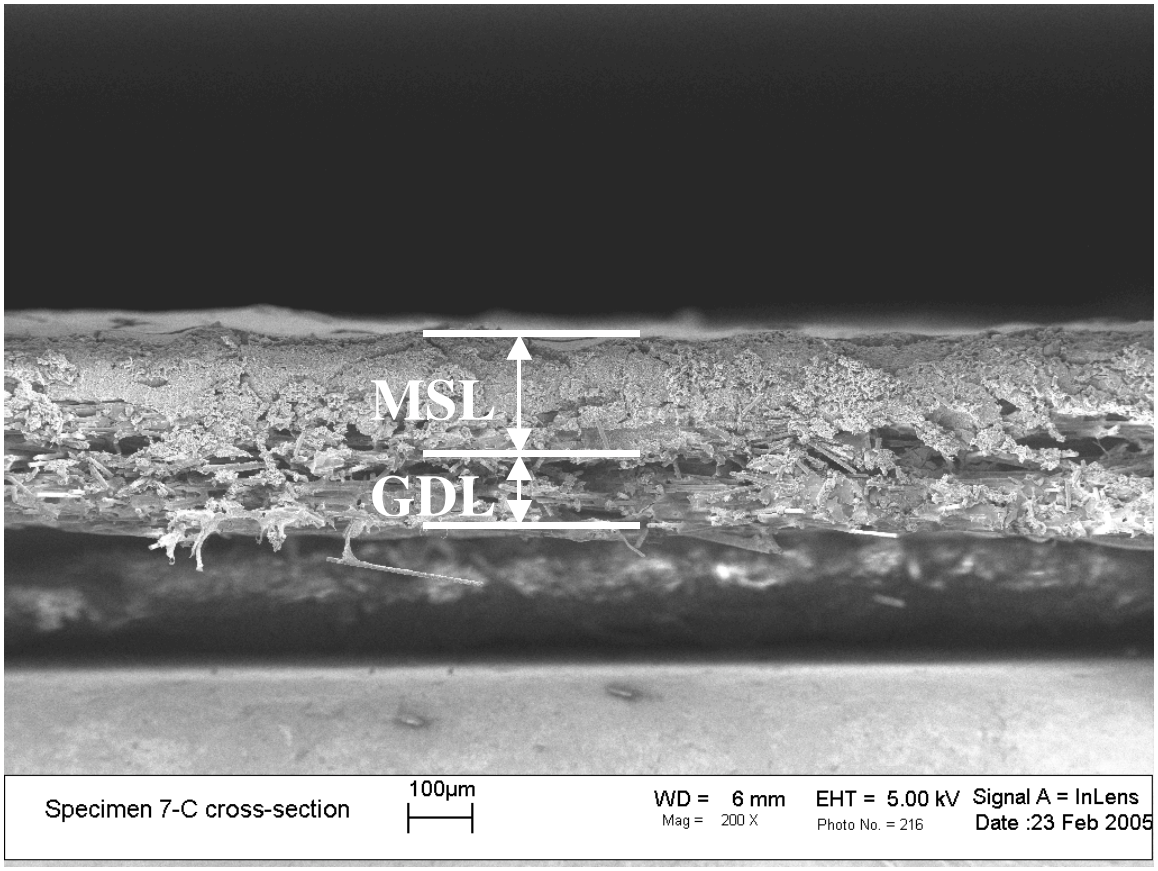

Figure 3-3. SEM cross-section from the center of specimen 7

When viewed under 100,000x magnification specimens 2, 4, and 8 seem to exhibit small agglomerations of particles. The commonality between specimens 2, 4, and 8 is that during the application process they received relatively thicker MSL layers between drying. As discussed in the previous paragraph, the MSL on specimen 7 was applied in very thin layers between drying. From the 200x magnification images taken from the surfaces of these four specimens, it appears that specimens 2, 4, and 8 also have larger surface cracks. This observation is as expected since the majority of the MSL (when in "sprayable" form) is IPA, and during the drying process the IPA evaporates from the MSL, leaving stress cracks as evidence of the shrinkage that occurs when the IPA evaporates. In conclusion, the thicker layers of MSL require more evaporation, leading to larger surface cracks. Based on the agglomerations observed at large magnifications, and the cracking observed at low magnifications, we concluded that application of thin layers (as in specimen 7) was desirable.

Results from the application study suggest that it is better to apply the MSL in thin layers, to prevent surface cracking. The study also suggests applying the MSL with a high MSL ink feed rate will provide a better surface finish. Propellant pressure did not seem to be a significant factor in the quality of the surface finish. Although there are a few extraneous variables, such as the speed at which the airbrush passes over the substrate during application, and the true distance of which the operator is holding the airbrush from the substrate, the characteristics outlined above are have been determined to assist in providing a more uniform MSL application.

The spray tests described above were done using a carbon paper as the GDL. The results are believed to be applicable to papers and tightly woven cloths. However, the spraying parameters need to be re-evaluated for very porous or loosely woven GDL's. It was observed that when applying the MSL with high propellant pressure to loosely woven GDL, there was a greater tendency for the formation of surface agglomerations. It appeared that the spray passes through the loosely woven GDL's with so much velocity that it splashes off the GDL's support and back through the GDL, causing uneven distribution. The solution to avoid the agglomerations, and stop the recirculation of spray,

was to place a piece of tape on the backside of the GDL as the MSL was being sprayed onto it. The tape effectively decreased the porosity of the GDL, and minimized the movement of propellant on the backside of the GDL.

3.4 Membrane Electrode Assembly Preparation

Since the MSL joins the catalyst layer to the GDL, the fabrication of these two elements had to be carefully considered. Catalyst layers for adhesion testing were prepared in-house using the decal transfer procedure [23]. Catalyst layers for performance testing were purchased from ION Power to reduce the time required to conduct experiments and because ION Power's MEA's were found to have relatively repeatable performance. The in-house procedure used to prepare the membrane electrode assemblies (MEA) for adhesion testing is broken into two parts; preparing the catalyst layer and preparing the membrane. Preparing the catalyst layer consists of mixing the necessary ingredients to prepare the catalyst ink, then applying the correct amount of catalyst ink to a decal. These decals are then pressed to the membrane, to transfer the catalyst layer. Before catalyst transfer, the membrane is placed in its sodium form, by an ion transfer process, to improve its temperature tolerance. Once the catalyst layers have been transferred, the final step in the preparation of the MEA is to return the membrane to its acid form.

3.4.1 Catalyst Layer Preparation. The first step in preparing the catalyst layer is to create the catalyst ink. This ink is prepared by mixing 33% Nafion solution (ElectroChem, Inc. EC-NS-05-250) and 67% carbon supported platinum catalyst (E-TEK Inc C-2 HP). The Nafion solution contains only 5% Nafion, 15-20% water, and the remaining amount as lower aliphatic alcohols. The carbon supported platinum catalyst (C-2 HP) contains about 20% platinum that is supported on Vulcan XC-72R carbon. To assist in making this mixture more "paintable", a small amount of glycerol reagent (ACROS 41098-5000) is added. The exact amount that is added is insignificant due to the fact that it evaporates when the catalyst layer is baked. A small stirring ball is dropped into the bottle containing the mixture, and the bottle is placed on a stirring plate for about

20-30 minutes. After mixing on the stirring plate, the mixture is taken to a sonic bath in which it is submerged for another 20-30 minutes, and finally it is ultrasonically homogenized using a BioLogics, Inc Ultrasonic Homogenizer (model 300 V/T).

Once the catalyst layer mixture is thoroughly mixed, it is painted onto the decals. The decals are small pieces of woven fiberglass that have been coated with PTFE (Alpha Associates, Inc Alphaglass 810). The decals are 5 cm^2 in size, corresponding to the size of the active area in the test fixture. The decals are initially cleaned with isopropyl alcohol (IPA), and sprayed with a flouropolymer dry lubricant (Saint-Gobain's Flouroglide CP*)*. This coating allows the decal to be peeled off after compression onto the membrane. After the coating of *Flouroglide,* the decal is weighed and recorded. The first coat of catalyst layer ink is then added to the decal, by painting it on with a paintbrush. The decal is then baked in an oven at 140ºC, for 15-20 minutes or until dry. Baking the decal causes the suspension agents and additives to evaporate, leaving only the desired Nafion, carbon black, and platinum. After baking, the decal is weighed and recorded. This series of painting, drying and recording is repeated until a loading of 0.325 mg-Pt/cm^2 of platinum is reached. *Table 3-1* summarizes the MEA characteristics.

Table 3-1. MEA Characteristics

Membrane	Nafion 112
Catalyst Description	33% Nafion
	67% Carbon Support Platinum (20% pt)
Catalyst Loading	0.325 mg-Pt/cm^2 (Per side)

3.4.2 Membrane Preparation. Nafion (Dupont's N112) was used for the membrane of the MEA's constructed in-house. The first step in preparing a piece of Nafion, for the pressing of decals, is to boil it in deionized water with a slow stirring, for about 1 hour. The next step is to boil it in a sodium hydroxide solution, with a slow stirring, for 1 hour. This solution contains 1% sodium hydroxide (Mallinckrodt 7708 NaOH), and 99% deionized water. After boiling the membrane in NaOH, it is boiled in deionized water for 1 hour.

Boiling the membrane in a sodium hydroxide solution causes the hydrogen ions in the membrane to be replaced with sodium. After boiling the membrane in NaOH, the membrane is considered to be in sodium form. Due to its advantages in thermal stability [17], when compared to the acidic form of Nafion, the sodium form of the membrane is desired for the high temperature compression it experiences when the catalyst decals are applied.

After the Nafion has been transformed to sodium form, the next step in constructing the MEA is to press the catalyst decals to both sides of it. The pressing process consists of applying 6.89 MPa of pressure at 210ºC to the combination of the membrane and catalyst decals. This pressure is applied continuously for 5 minutes. After the compression process is completed, the MEA is allowed to cool at room temperature for 20 minutes. Once cool, the decals, to which the catalyst layer was applied, are peeled off of the membrane, leaving the catalyst layer bonded to the Nafion membrane.

The MEA, still in sodium form, must be returned to its acidic form for operation in the PEMFC. In order to do this, the MEA is boiled in sulfuric acid solution for 1 hour. This solution consists of 99.5% (by volume) deionized water and 0.5% (by volume) sulfuric acid. After boiling in this solution, the completed MEA is removed and boiled in deionized water for 1 hour to remove excess acid.

The MEA's used for the adhesion study reported in this paper were prepared in a similar manner as described above, except a catalyst decal was only pressed to one side of the Nafion. Due to its higher mechanical strength, a thicker (127 μm more thick than Nafion 112) membrane material, Nafion N117, was used for the adhesion study. It was discovered that pressing a decal to Nafion N117 at 6.89 MPa would cause deformation of the catalyst/membrane interface. So for the adhesion study, the pressure at which the catalyst decals were applied to the Nafion was reduced to 3.45 MPa. During the actual testing, no failures were observed at the catalyst/membrane interface.

The MEA's used for the performance study were provided by ION Power Inc. The Ion Power MEA's used were 3.5 x 6.5 cm fully-catalyzed Nafion N112 membrane with a catalyst loading of 0.3 mg-Pt/cm^2. The performance of an ION Power MEA is very similar that of the MEA's produced in-house at Virginia Tech. We have investigated the consistency of Ion Power MEA's, and found the current density to be repeatable within plus or minus 8% at 0.5 volts.

3.5 Gas Diffusion Layer Preparation

The gas diffusion layer (GDL), as described in the introduction of this paper, is typically either a continuous carbon fiber weave or chopped and compressed carbon fibers that form a paper. During the experiments conducted in this research, a carbon weave (fabric) was used. The carbon weave used throughout this research, unless otherwise stated, was ETEK B-1/A.

This particular carbon weave does not have any hydrophobic pretreatment. As briefly described in the introduction of this paper, the addition of a hydrophobic substance will enhance the ability of the GDL to transport water. The hydrophobic treatment applied to the GDL's is a mixture consisting of 10 wt.% PTFE solution (ElectroChem, Inc's, TFE 30) and 90 wt.% deionized water.

Before applying the hydrophobic treatment, the GDL's were baked at 280ºC for 30 minutes to help remove impurities. The treatment procedure began by completely submerging the GDL's in the hydrophobic treatment. The GDL is submerged for 45 seconds. After 45 seconds, the GDL is removed and placed on a specially designed drying rack for 5 minutes. After 5 minutes, the GDL is rotated, placed back on the rack, and dried until the glossy look of the hydrophobic treatment disappears. After the glossy look disappears, the rack with the GDL's is placed in an oven and baked at 140ºC for 30 minutes. This baking process allows the liquid components of the hydrophobic treatment to evaporate, thus leaving behind only the PTFE. This process (soaking and drying) is

repeated until the desired amount (wt.%) of PTFE is added to the GDL. The wt.% PTFE added to the GDL is calculated by;

$$f_{wt.\%PTFE}^{GDL} = \frac{m_{GDL+PTFE} - m_{GDL}}{m_{GDL+PTFE}} \tag{3-6}$$

where $m_{GDL+PTFE}$ is the resulting mass of the GDL after hydrophobic treatment, and m_{GDL} is the original mass of the GDL. Based on data from the literature (see literature review) 10-30 wt.% PTFE was the target for the GDL's used in this research.

The drying rack, as mentioned in the previous paragraph, consists of stainless-steel pins, 1.6 mm in diameter, inserted in holes drilled into an aluminum block. The spacing between each of the pins is approximately 8 mm, and the length, from the top of the pin to the aluminum block is about 41 mm. The goal is to provide convective drying from both sides of the GDL simultaneously, thus encouraging a uniform dispersion of PTFE throughout the GDL. A similar design is used, and suggested, for "uniform distribution" of the hydrophobic substance within the GDL by Lim [8]. Bevers [18] report using a similar 13 pin apparatus, and discover that migration to the corners of the GDL is a natural occurrence. Although wasteful, Bevers [18] suggest that the desired piece of GDL be cut from the center of a piece to which hydrophobic treatment has been applied, to avoid the possibility of PTFE accumulation in the corners of the GDL. All GDL used in this research was cut from a larger piece of GDL after the hydrophobic treatment was added and the MSL was applied.

Once the desired wt.% of PTFE was reached, the GDL's were placed back in the oven and baked at 140ºC for 30 minutes, 280ºC for 30 minutes, and 350ºC for 30 minutes. The 140ºC and 280ºC temperatures are designed to assure the removal of any remaining liquid from the PTFE solution. The final temperature of 350ºC, being right above PTFE's first melting point of 342ºC, sinters the PTFE particles in hydrophobic treatment to the GDL. The sintering process creates a strong bond between the PTFE and GDL fibers. Similar procedures are reported by Qi [1], Song [2], and Park [9].

3.6 Sample Assembly for Performance Testing

The MSL coated GDL was then cut into two square 5 cm^2 pieces (2.24 x 2.24 cm). One of these pieces was placed MSL side up on a stainless steel plate. An Ion Power catalyzed membrane was then placed on top of the GDL, and the second piece of MSL coated GDL was placed on top of the catalyzed membrane, with the MSL side towards the catalyst layer. A second stainless steel plate was then placed on top of the whole assembly, and the assembly was placed in a hot press at 135ºC [17] at the specified fabrication pressure (P_f) and for the specified fabrication time (t_f) (see *Figure 3-4*). The fabrication pressure was the pressure applied to the 5 cm^2 GDL, and was recorded as megapascals (MPa). The fabrication time is simply the period of time of which this pressure was applied to the assembly. *Figure 3-4* illustrates this fabrication process.

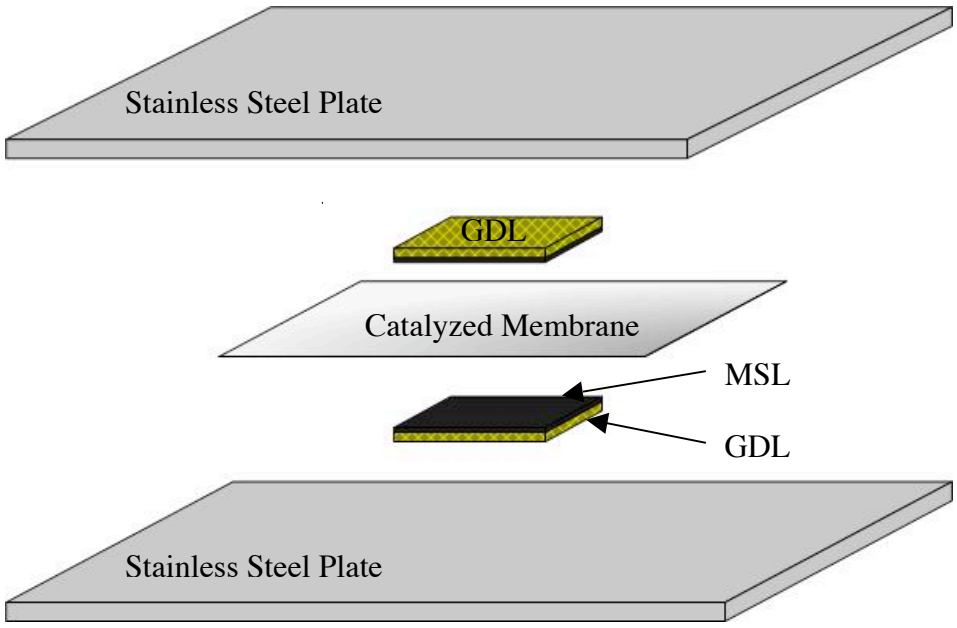

Figure 3-4. Diagram of fuel cell fabrication

After the MSL coated GDL was pressed to the catalyzed membrane, it was ready to be tested. Each fuel cell was tested at three different compressions. This operation compression is not to be confused with the initial fabrication pressure that the fuel cell

experienced when the MSL coated GDLs were pressed to the catalyzed membranes for a specific time and pressure. The operating compression is the change in thickness of the fuel cell components on each side of the membrane (GDL + MSL + catalyst layer) during assembly. This change in thickness is assumed to correspond to the difference in thickness between the fuel cell components (after fabrication) and the gasket material. Although the pressure experienced by the fuel cell components (at the various levels of compression) is probably a better metric to report, it is however much more difficult to accurately quantify.

3.7 Sample Assembly for Adhesion Testing

The MSL was applied to the GDL in the same manner as described in previous sections. The only difference in the MSL application for adhesion, compared to its application for performance, is that for the adhesion study the GDL is not entirely coated with MSL. The GDL's used for the adhesion study were approximately 76 mm in length by 20 mm in width. During the MSL application process, the surface of the GDL was masked off except for a 5 cm^2 area on one of the ends.

Once the GDL is loaded with MSL to the desired amount, it is placed MSL side up on a stainless steel plate. The catalyzed membrane (catalyzed N112 supplied by Ion Power Inc.) was then placed on top of the GDL, with the catalyst layer towards the MSL. A second stainless steel plate is then placed on top of the whole assembly, and the assembly hot pressed at 135ºC [17] at the specified fabrication pressure and for the specified fabrication time (see *Figure 3-5*). The fabrication pressure was the pressure applied to the 5 cm^2 MSL coated portion of the GDL, and was recorded as megapascals (MPa). The fabrication time is simply the period of time for which this pressure was applied to the assembly. *Figure 3-5* illustrates this fabrication process.

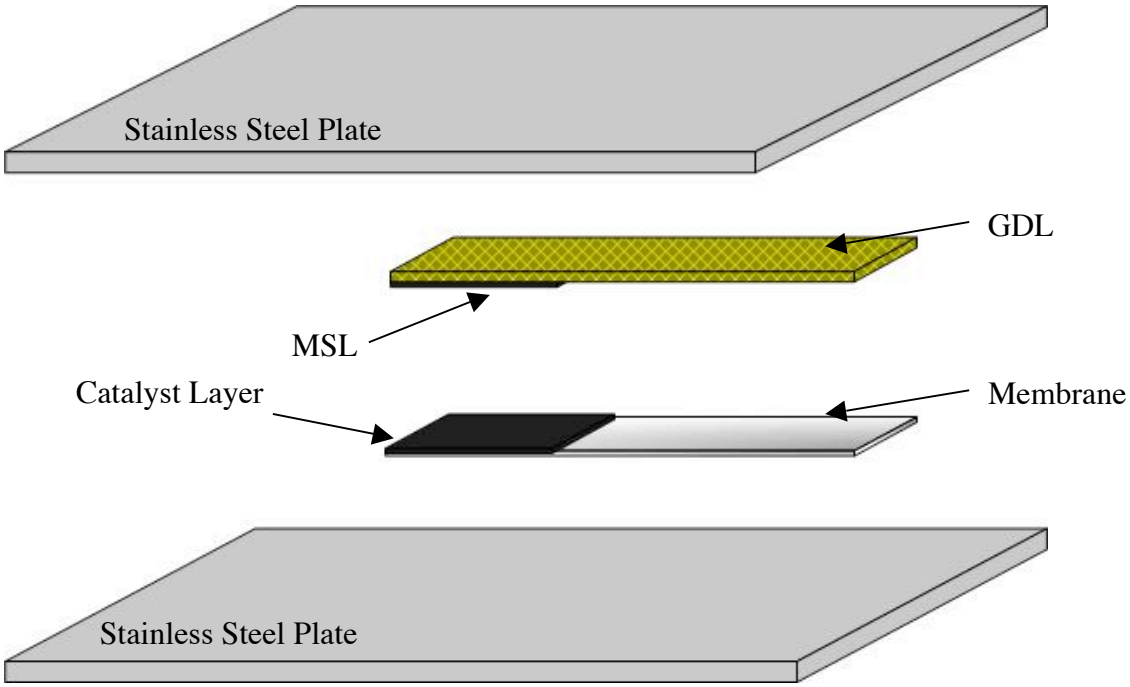

Figure 3-5. Diagram of pseudo fuel cell assembly used for adhesion test

3.8 Fuel Cell Test-Stand Description

The results for fuel cell performance, expressed as *i-v* curves or impedance measurements, were produced using a fuel cell test station (Fuel Cell Technologies, Inc 100-Amp, 150-Watt Fuel Cell Test Station), as displayed in *Figure 3-4*. This test station automates the monitoring and control of a single fuel cell or a stack. The test station links to a PC via GPIB protocol, and utilizes a LabVIEW program, supplied by Fuel Cell Technologies, Inc, as a user interface. Using the LabVIEW software, the user can adjust the reactant gas flow rates, cathode and anode backpressures, cell temperature, and relative humidity of either gas stream. The test station also has the capabilities to hold the stoichiometry constant under varying load conditions. The LabVIEW interface can also operate the fuel cell in constant current or constant voltage modes by automatically adjusting the voltage or current respectively. The reactant gases used in the test station are compressed ultra high purity (99.999%) hydrogen and compressed grade D breathing air.

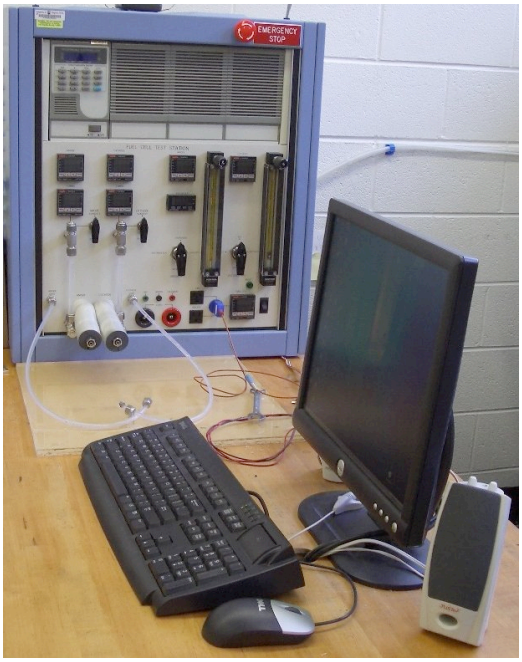

Figure 3-6. Fuel cell test stand

The LabVIEW software also provides the ability to automate the creation of polarization curves and impedance spectroscopy plots. In addition, the data can also be exported into a format that is compatible with various databases such as Excel. This feature is very useful since the polarization curves and impedance results are two of the critical responses upon which the statistical relationships of the four main factors will be formed.

All performance-based tests conducted on the test stand are conducted with a cell temperature of 80°C, reactant gases at 100% relative humidity, hydrogen flow rate of 250 SCCM, air flow rate of 500 SCCM, and no backpressure on either anode or cathode (neglecting the small amount of pressure change experienced while passing through the serpentine path of the flow fields). The flow rates used here correspond to a stoichiometry at 1 A/cm^2 of 6.7 on the anode side, and 5.5 on the cathode side.

3.9 Adhesion Testing and Apparatus Description

The adhesion tests conducted in this study were done using a "T-peel" test. The T-peel test was conducted on an Instron 4500 load frame (see *Figure 3-7*) equipped with a 1 kN load cell. There was a computer interface, associated with the Instron 4500, which allowed for the use of a LabVIEW program to control and compile the results. The tests were conducted with a crosshead speed of 50 mm/min, while recording 10 data points/second. The LabVIEW program monitors the load, time, and displacement and records them to an electronic format.

Figure 3-7. Instron load frame

The T-peel tests are conducted in accordance with ASTM standard D 1876-01. Fabrication of test specimens include adhering two substrates for a specified length. The actual substrates extend beyond the area of adhesion to allow for connection to the load frame. *Figure 3-8* illustrates this process.

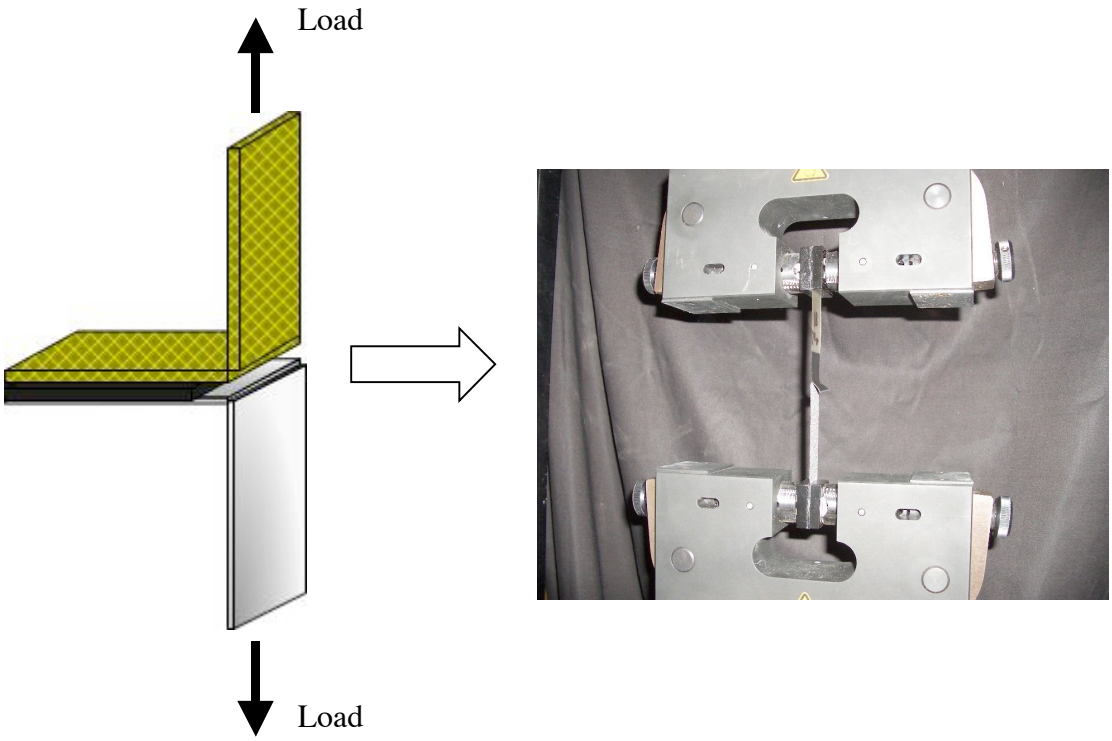

Figure 3-8. T-peel test (Drawing does not show proper curvature)

4 Experimental Results

4.1 Fuel Cell Performance

To investigate how the design and fabrication of a MSL can affect the performance of a fuel cell, 20 fuel cells were tested, each with a unique MSL design/fabrication. *Table 4-1* illustrates the design/fabrication characteristics of these 20 MSL's. The MSL was applied to the GDL and the cell was assembled using the procedure described in Chapter 3.

Table 4-1. Performance Matrix

Design Point	Factor 1 A: Loading (mg/cm^2)	Factor 2 B: Composition (wt.% PTFE)	Factor 3 C: Pressure (MPa)	Factor 4 D: Time (Minutes)
1	1.5	10	3.45	2
2	1.5	10	3.45	8
3	1.5	10	10.34	2
4	1.5	10	10.34	8
5	4	10	3.45	2
6	4	10	3.45	8
7	4	10	10.34	8
8	4	10	10.34	2
9	2.75	30	6.89	5
10	2.75	30	6.89	5
11	2.75	30	6.89	5
12	2.75	30	6.89	5
13	1.5	50	3.45	2
14	1.5	50	3.45	8
15	1.5	50	10.34	8
16	1.5	50	10.34	2
17	4	50	3.45	2
18	4	50	3.45	8
19	4	50	10.34	2
20	4	50	10.34	8

As noted in *Chapter 3*, each MSL design/fabrication sample was tested at three different operating compressions. At each of these levels of compression, five tests were run on the fuel cell – 3 polarization curves, and 2 spectral impedance plots. Each

polarization curve was run from 0.92 to 0.1 volts, and then back to 0.92 volts in steps of 0.05 volts. Performing a polarization curve in both increasing and decreasing voltage allows for the identification of hysteresis. The final polarization curve reported is an average of the increasing and decreasing (in voltage) polarization curves, and an average of the 3 trials that are done at a single compression.

After completing all 20 tests, the results were compiled and the compression corresponding to the best performance of each of the 20 fuel cells was reported. At this compression the current density (A/cm^2) at 0.5 volts was recorded for each of the fuel cells. *Table 4-2* tabulates these results, and the respective optimum compression for each of the cells is displayed. It should be noted that design point 12 was deemed a statistical outlier, and not included as part of the data used to create the performance correlation.

Table 4-2. Performance Results and Optimum Compression

Design Point	Factor 1 A: Loading (mg/cm^2)	Factor 2 B: Composition (wt.% PTFE)	Factor 3 C: Pressure (MPa)	Factor 4 D: Time (Minutes)	Response 1 I@0.5 V A/cm^2	Amount of Compression (μm)
1	1.5	10	3.45	2	1.20	105
2	1.5	10	3.45	8	1.23	105
3	1.5	10	10.34	2	1.07	55
4	1.5	10	10.34	8	1.29	55
5	4	10	3.45	2	1.17	160
6	4	10	3.45	8	1.00	120
7	4	10	10.34	8	0.96	30
8	4	10	10.34	2	0.94	70
9	2.75	30	6.89	5	1.27	90
10	2.75	30	6.89	5	1.26	90
11	2.75	30	6.89	5	1.11	85
12	2.75	30	6.89	5	0.82	40
13	1.5	50	3.45	2	1.08	75
14	1.5	50	3.45	8	1.14	90
15	1.5	50	10.34	8	0.82	60
16	1.5	50	10.34	2	1.03	65
17	4	50	3.45	2	1.12	80
18	4	50	3.45	8	1.15	65
19	4	50	10.34	2	0.89	35
20	4	50	10.34	8	0.92	50

4.1.1 Performance Correlation. After recording and compiling all of the current densities at 0.5 volts, the results were analyzed using the statistical package, Design Expert®. The actual polarization curves, at each fuel cells optimum compression, are displayed in *Appendix C*. This statistical package will analyze the results, provide the user with the information needed to choose the significant factors, provide an analysis of variance (ANOVA) table, provide transform suggestions/diagnostics, and provide solutions that will optimize the performance based on the results.

Factors and combinations of factors were investigated to determine those which had the most significance. *Figure 4-1* presents the results from Design Expert®. The factors for the correlation are chosen by observing their "percent contribution" (see *Figure 4-2*) and by examining a half-normal plot (an additional tool used to determine significant factors). The overall decision as to which factors to keep in the correlation comes from many sources, one of which is the "Prob > F" value. Ideally, it is desired that this value is less then 0.05, but for experimental data a value a slight bit higher is acceptable. After choosing which factors to include in the correlation, an ANOVA table was created. For fuel cell performance, the most significant factors related to the MSL design/fabrication were loading, composition, and fabrication pressure. *Table 4-3* is the ANOVA table produced by Design Expert® from the performance-based tests.

	Term	Stdized Effects	Sum of Squares	% Contribution
	Intercept			
M	A	-0.087	0.030	9.04
M	B	-0.088	0.031	9.13
M	C	-0.15	0.084	25.06
e	D	1.250E-003	6.250E-006	1.862E-003
M	AB	0.091	0.033	9.93
e	AC	-0.035	4.784E-003	1.43
e	AD	-0.024	2.336E-003	0.70
e	BC	-0.063	0.016	4.78
e	BD	-0.024	2.256E-003	0.67
e	CD	0.014	7.563E-004	0.23
e	ABC	0.014	7.562E-004	0.23
e	ABD	0.077	0.024	7.16
e	ACD	0.033	4.444E-003	1.32
e	BCD	-0.081	0.026	7.87
e	ABCD	0.035	4.900E-003	1.46
M	Curvature	0.12	0.056	16.72
e	Lack Of Fit		0.000	0.000
e	Pure Error		0.014	4.29
	Lenth's ME	0.12		
	Lenth's SME	0.22		

A-Loading
B-Composition
C-Fabrication Pressure
D-Fabrication Time

Figure 4-1. Percent contribution for correlation factors

Table 4-3. ANOVA Table of Performance Results

Source	Sum of Squares	DF	Mean Squares	F Value	Prob > F
Model	0.180	4	0.045	5.73	0.0069
A	0.030	1	0.03	3.9	0.0699
B	0.031	1	0.031	3.94	0.0687
C	0.084	1	0.084	10.81	0.0059
AB	0.033	1	0.033	4.28	0.0590
Curvature	0.056	1	0.056	7.21	0.0187
Residual	0.100	13	7.78E-03		
Corrected Total	0.340	18			

Using the factors outlined above, Design Expert® suggests the following relationship between the design of an MSL and the performance of a fuel cell.

$$i(Amp/cm^2) = 1.51906 - 0.089584\, L_{msl} - 0.00720637\, C_{msl} - 0.02103\, P_f + 0.00182503\, L_{msl}\, C_{msl} \quad (4\text{-}1)$$

where L_{msl} is the MSL loading (mg/cm^2), C_{msl} is the MSL composition (wt.% PTFE), and P_f is the fabrication pressure (MPa).

The *sum of squares,* as observed in *Table 4-3,* for each of the terms is defined as the sum of the squared deviations from the mean due to the effect of the term. The sum of squares represents the variation due to the effect of each term. The *mean square* for each term is the variance associated with the term and is calculated by dividing the sum of squares for the term by the degrees of freedom associated with the term. The residual is the difference between the data and the model prediction. The residual reflects the variation that is not described by the model and must be attributed to noise, or unexplained sources. The *residual sum of squares* is defined as the sum of squared values for the residual. The *residual mean square* is an estimate of the variance that is not explained by the model, and is calculated by dividing the residual sum of squares by the degrees of freedom not reflected in the model (i.e. the total degrees of freedom less the degrees of freedom associated with the model). The *F-value* for each term is calculated by dividing the mean square of the term by the residual mean square. The F-

value compares the variance of each term to the residual variance and is an indicator of the significance of a term. The *pure error mean square* (not reported in the ANOVA table but provided in the following discussion of the correlation) is defined as the variance associated with error of replication and quantifies the repeatability of the experimental results. [25]

Design Expert® provides several ways to quantify how well this correlation fits the actual data. An estimate of the "lack of fit" that this correlation contains is given by a ratio of the residual error over the pure error. The "lack of fit" for this correlation is 1.10, which suggests that the there is no significant "lack of fit" for this correlation. According to the statistical consultants at Stat-Ease Inc., the designers of Design Expert®[25], if the "lack of fit" value is approximately 1, it can be said that the replications are correctly quantifying the error in the system.

To further quantify the fit of this correlation and variation in data, the R-Squared, Adjusted R-Squared, and Predicted R-Squared are investigated. As displayed in *Table 4-4*, the R-Square value for this correlation is 0.6382. Since the R-squared value will simply increase as the total number of factors increases, is not a very reliable judge of variation in the data. Therefore, the adjusted R-squared value is a much better judge of the variation within the correlation. The predicted R-squared value quantifies the variation in predictions by the correlation. According to the statistical consultants at Stat-Ease Inc., the maximum acceptable difference between the adjusted and predicted R-squared values should be no more than 0.2.

Table 4-4. Performance Correlation R-Squared Table

R-Squared	0.6382
Adj R-Squared	0.5269
Pred R-Squared	0.3568

The ANOVA table, *Table 4-3*, displays a curvature F-Value of 7.21. This F-Value "implies that there is significant curvature (as measured by difference between the average of the center points and the average of the factorial points) in the design space.

There is only 1.87% chance that a "Curvature F-Value" this large could occur due to noise." [see Performance Design Expert Output, *Appendix E*] *Figure 4-2* illustrates how the center points do not lie within the linear relationship drawn for current density as a function of pressure. Although the full factorial design, with replications, can be used to identify curvature, it does not allow for the creation of a correlation that is nonlinear between its high and low design points. This explains the low R-squared values in *Table 4-4*. If curvature is identified as being very significant, then the full factorial design should be augmented to a central composite design (CCD). Augmenting to a CCD would require the addition of 8 design points, and would suggest additional center points. However, *in the experiment the maximum center point does not exceed the maximum design space point; suggesting that the best performance lies at the boundary of the factor domain*. Therefore, while augmenting the experiment to a CCD would be required to establish the functional relationship, it is not necessary for identifying the best values for the factors. In *Figure 4-2* the "Design Points" are the center points of the experiment.

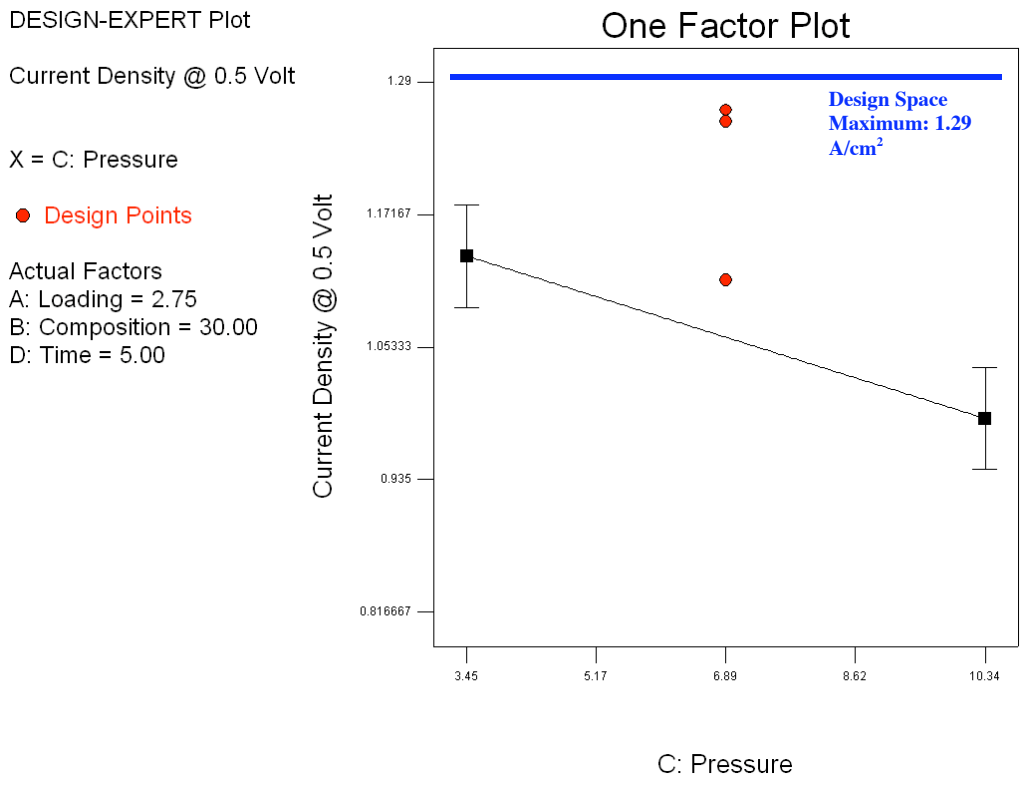

Figure 4-2. Current density as a function of pressure

4.1.2 Effect of MSL Design/Fabrication Factors on Performance

While additional experimentation is necessary to yield a correlation that characterizes the effect of MSL design/fabrication factors across the entire design space, conclusions can be drawn about the factor values that lead to best performance. This is possible because the curvature identified by the center points of the experiment does not lead to performance in excess of the values found on the design space boundaries. The correlation is still complicated by the presence of higher order and interaction terms. However, one approach to understanding the factor values that lead to best performance is to optimize the correlation, *Equation 4-1*, to identify a set of near optimal points and then evaluate the characteristics that are common to these points. Design Expert has the ability to optimize the correlation to identify near-optimal solutions for the set of MSL design/fabrication parameters. *Table 4-4* displays the top 10 solutions. Common characteristics of these solutions are low loading, low PTFE content, and low fabrication pressure. As shown by the results in *Figure 4-1*, fabrication time as an independent factor has no effect on performance. Fabrication time is present in higher order terms that, as indicated by *Figure 4-1*, can have a small contribution to the correlation. But if the higher order terms were included the correlation would be weakened, as the difference between the adjusted and predicted R-squared would increase greatly. Thus, the value of fabrication time in the near-optimal solutions varies at random through the allowable design space of 2 - 8 minutes.

Table 4-5. Top 10 Performance Solutions suggested by Design Expert

Solutions Number	Loading (mg/cm^2)	Composition (wt.% PTFE)	Fabrication Pressure (MPa)	Fabrication Time* (Minute)	Current Density @ 0.5 Volt
1	1.5	10	3.45	6.35	1.2675
2	1.5	10	3.45	7.18	1.2675
3	1.5	10	3.45	7.05	1.2675
4	1.5	10	3.45	2.38	1.2675
5	1.5	10	3.45	4.64	1.26747
6	1.5	10	3.45	2.34	1.26729
7	1.5	10	3.49	4.25	1.26654
8	1.5	10	4.34	2	1.24856
9	1.5	10	5.76	2	1.21884
10	1.5	10	6.21	2	1.20949

*Has no effect on optimization results.

Figure 4-3 is a 3-D representation of the correlation, *Equation 4-1*, which shows the effects of composition and loading on performance while holding time at 5 minutes, and pressure at 3.45 MPa.

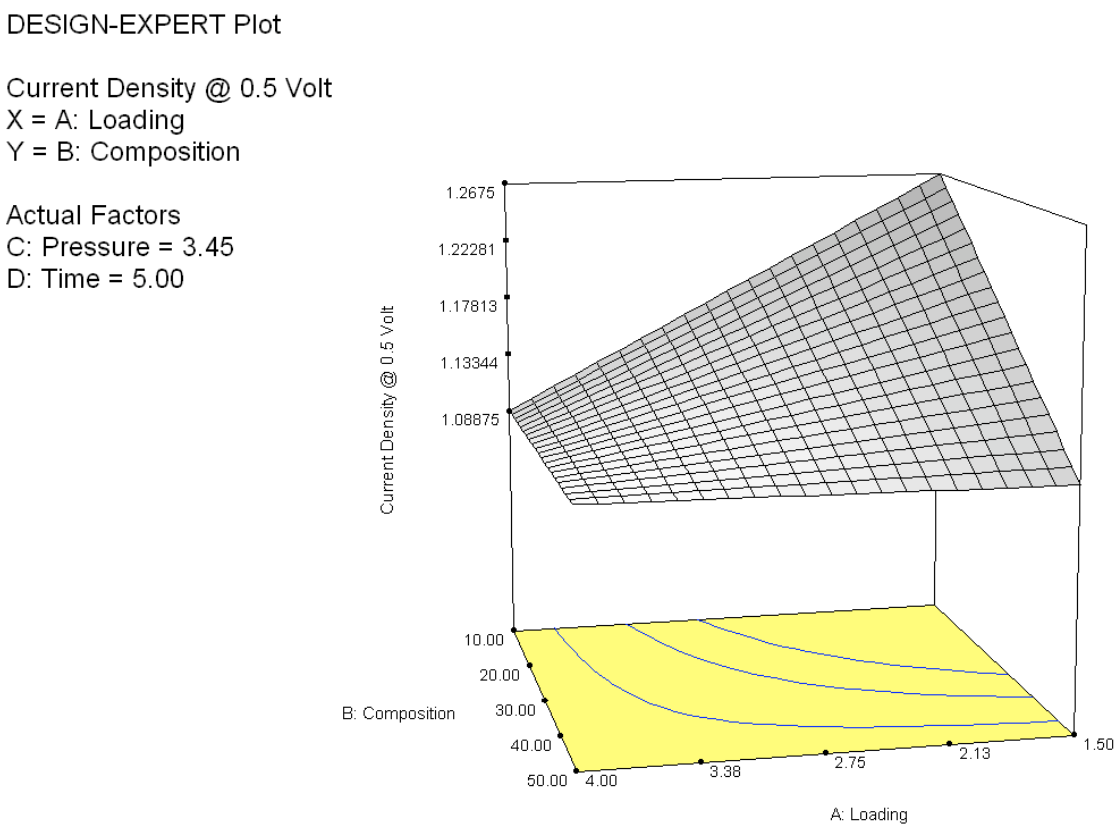

Figure 4-3. Current density as a function of composition and loading - Low pressure.

As identified by the Table 4-3, MSL composition can have a significant effect on the performance of the PEMFC. *Table 4-4* displays the top 10 optimum combination of MSL design factors, in which composition is always 10 wt.% PTFE. Similarly, *Table 4-3* also identifies the loading of the MSL as a significant factor. The top 10 solutions, as displayed in *Table 4-4*, all have a low MSL loading. Further, inspection of the composition-loading interaction depicted in *Figure 4-3*, illustrates that for any composition, reduced loading leads to higher performance. The typical cost of PTFE is $0.11 per gram, and the typical cost of carbon black is $0.0057 per gram. Thus, economically, a lower PTFE content and a lower loading MSL are both advantageous because materials cost are reduced. Furthermore, because the MSL is applied in small layers, lower loadings mean less time is required to apply the desired amount. Therefore, when considering this process in a high speed manufacturing line, low loadings could save time and material cost.

Fabrication pressure is also identified as a significant factor in the correlation. Inspection of the top 10 optimal solutions, *Table 4-4*, reveal 7 out of 10 of those optimal solutions recommend approximately 3.45 MPa of pressure, which is at the low end of the design range (3.45 – 10.34 MPa). Since the GDL, used in this research has a somewhat loose weave, it has a greater tendency to become compacted at higher fabrication pressures. When the GDL is compacted too much, movement of reactant gas and product water will be hindered, and mass transport limitations will decrease the performance. *Figure 4-4* illustrates the same 3-D interaction between composition and loading as in *Figure 4-3*, but with the fabrication pressure changed to 10.34 MPa. As expected, the maximum performance that the correlation predicts decreases by 11% from the results at 3.45 MPa.

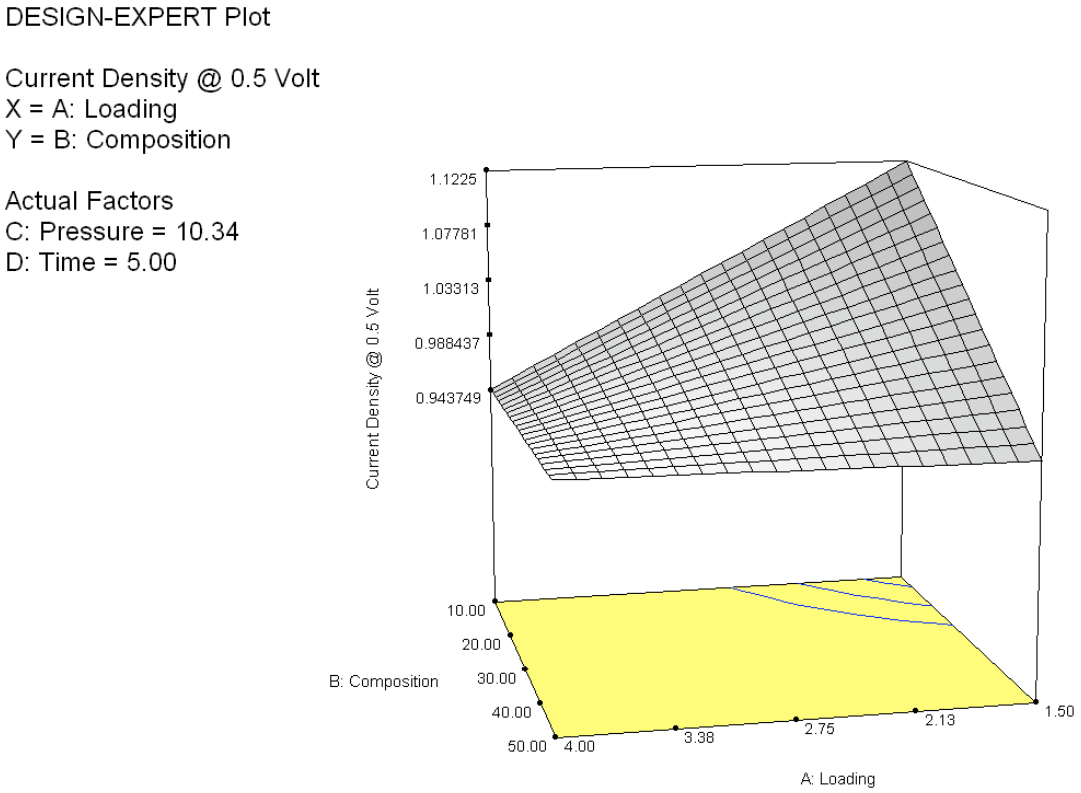

Figure 4-4. Current density as a function of composition and loading - High pressure

The one MSL design factor that did not emerge as a significant correlation factor is fabrication time. Fabrication time is the period of time that the MSL coated GDL's are initially pressed to the catalyzed membrane. The results presented in *Figure 4-1* demonstrate that time and associated interaction terms do not contribute significantly. The fact that fabrication time has no significant effect on the performance becomes advantageous when considering this part of the process in a high speed manufacturing line. Less time required means more units can be produced over a given time period, and that can lead to reduced manufacturing costs.

Although the correlation does not find fabrication time significant, and therefore does not recommend any certain value for this time, it is desired to keep this factor as low as possible, without effecting performance. The fabrication process takes place at 135ºC, which is very close to the region (around 145ºC) above which transition of ionic clusters within the Nafion membrane will take place [17]. It becomes a trade-off, because with increased fabrication time and a higher fabrication temperature, better adhesion is

expected. But too high of temperatures for long periods of time will damage the Nafion membrane. So if the fabrication time does not have a significant effect on performance, the fabrication process can be completed using high temperatures (such 135ºC) with a short fabrication time without compromising the structural integrity of Nafion.

As noted in previous paragraphs this correlation is limited to drawing linear relationships. Although, the experimental data contains a significant amount of curvature, meaning that it is possible for a composition that is between 10 and 50 wt.% PTFE, a loading that is between 1.5 and 4 mg/cm^2, or a pressure that is between 3.45 and 10.34 MPa to produce better performance. A comparison of the best center point (30 wt.% PTFE, 2.75 mg/cm^2, and 6.89 MPa) performance (1.27 A/cm^2) and the (10 wt.% PTFE, 1.5 mg/cm^2, and 10.34 MPa) performance (1.29 A/cm^2), illustrate this concept. With this in mind, it is recommended that further experimental research be conducted to explore the interior of the design space, possibly augmenting this full-factorial design to a central composite design, which would allow for a nonlinear correlation.

An additional study was done to investigate the consistency of the Ion Power catalyzed membranes. During this study, ETEK B-1/A GDL, the same GDL used for the performance based experiments, with no MSL was used. The results from this consistency study serve as a baseline for comparison of the various MSL designs. The GDL with no MSL has a current density of about 0.95 A/cm^2 at 0.5 Volts. Investigation of the actual performance data from the 20 design points, *Table 4-2*, reveals that the addition of an MSL can actually decrease the performance of the PEMFC. The fact that the MSL can decrease the performance, if not properly designed, further supports the need for the correlation created with this research. *Figure 4-5* displays the best MSL design, worst MSL design, and an average of 2 fuel cells with no MSL applied to the GDL (from the consistency investigation).

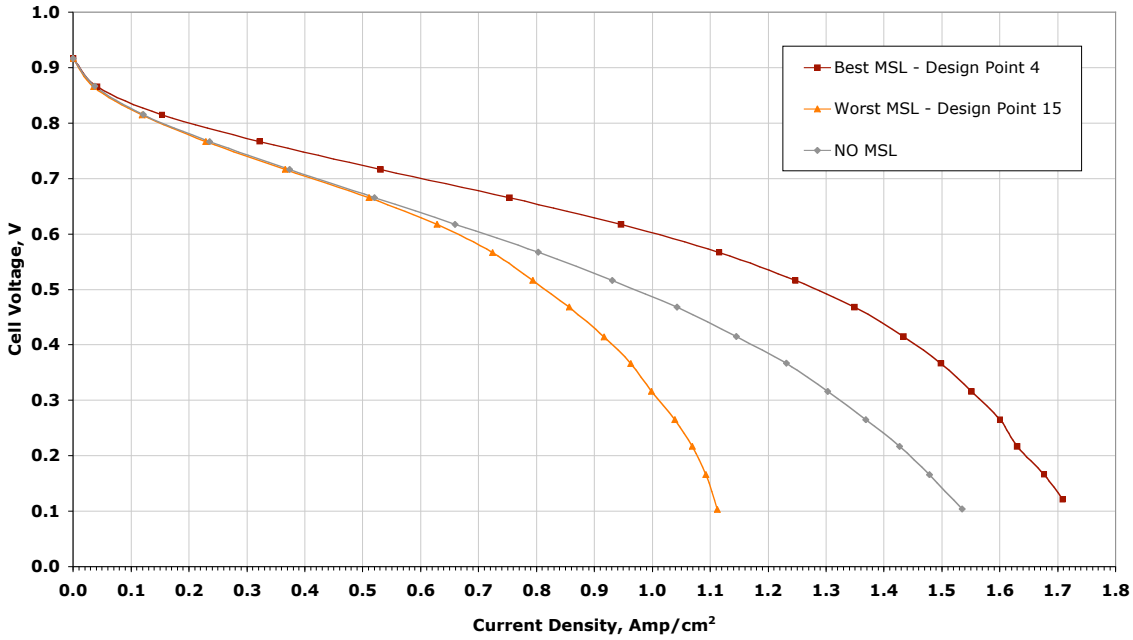

Figure 4-5. Best, worst, and no MSL comparison

4.1.3 Effect of MSL Design/Fabrication on Polarization Losses **.** Polarization losses within a fuel cell are categorized as activation, ohmic, and diffusive losses. During this study, electrochemical impedance spectroscopy (EIS) was used to distinguish between ohmic losses and other types of losses. Electrochemical impedance spectroscopy relies on the development of a charge double-layer at the electrode/electrolyte interface. This double-layer behaves like a capacitor and the resulting equivalent circuit for a fuel cell is depicted in *Figure 4-6*. In this figure, the capacitor C represents the charge double-layer; resistor R_o represents the ohmic losses (both electrical and ionic) within the fuel cell; and resistor R_a represents the *activation and diffusive losses* associated with the electrochemical kinetics of the fuel cell reaction. [15]

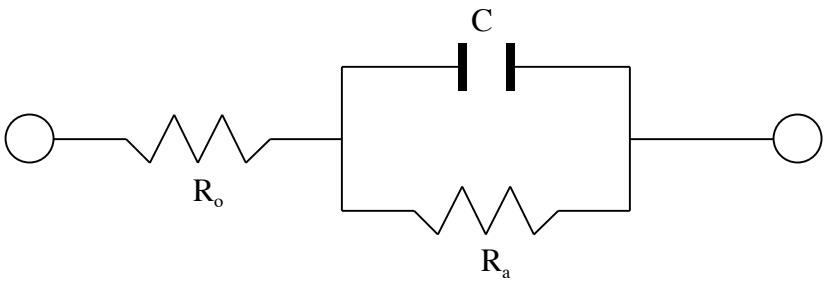

Figure 4-6. Fuel cell equivalent circuit

The first step in an EIS analysis is to apply an alternating current to the fuel cell while measuring the voltage. For a high frequency current, the impedance associated with the capacitor is small, and the activation/diffusive losses (R_a) are essentially bypassed leaving only the ohmic losses (R_o). At low frequency, both the ohmic and the activation/diffusive losses are important. The phase shift between the voltage and current waveforms can be used to determine the real and imaginary parts of the cell impedance. This information is used to construct a Nyquist plot which is simply the imaginary part of the impedance plotted against the real part of the impedance for various frequencies (e.g., 1-10,000 Hz, recording 6 points/decade). The high frequency termination point of a Nyquist plot indicates the real resistance (R_o) or ohmic losses associated with the fuel cell. This resistance will be the sum of the ohmic resistances from all the layers (membrane, catalyst, MSL, and GDL) found within the fuel cell. The magnitude of the impedance at lower frequencies is indicative of the total loss (ohmic, activation, and diffusive).

In the original design of the experiment used in this study, the idea was to construct an impedance plot for each fuel cell tested. In doing this, the desire was to identify a relationship between the MSL and overall fuel cell ohmic loss. For example, it was thought that, since PTFE is an electrical insulator, as the PTFE wt.% in the MSL was increased, a higher value for the ohmic loss could be expected.

As testing proceeded, it was identified that changing the fuel cell's operating compression had a large effect on the overall performance and on the relative importance of ohmic and diffusive losses. As outlined in previous sections, the performance testing scheme includes testing the fuel cells at various compressions. *Figure 4-7* illustrates how the performance, as characterized by an *i-v* curve, can change dramatically due to a change in the amount of compression.

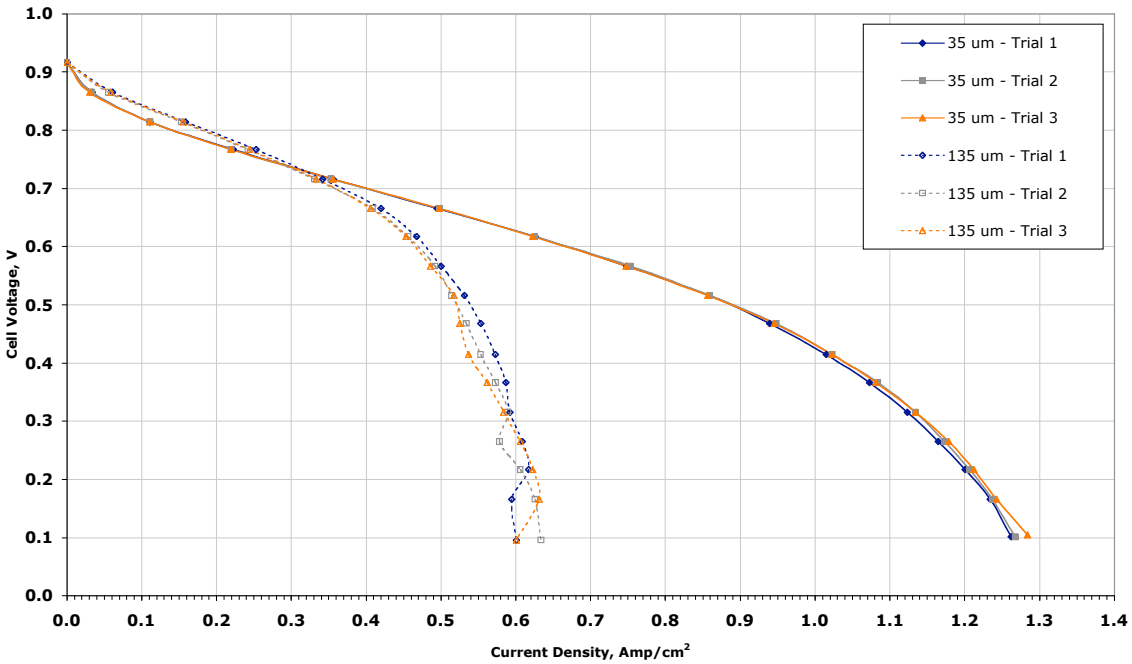

Figure 4-7. Polarization curve for various fuel cell compression levels

In *Figure 4-7*, it is noted that the fuel cell's optimum performance occurs at a lower compression (i.e. 35 μm versus 135 μm). This polarization curve was taken from fuel cell number 19, as found in the performance design point plots (see *Appendix C*). Fuel cell number 19 is constructed with a fabrication pressure of 10.34 MPa for 2 minutes. When prepared with this much fabrication pressure, the fuel cell does not require much operating compression to reach its optimum performance. Hence, number 19 reaches it's optimum performance with only 35 μm of compression.

The optimum performance represents a balance of ohmic losses and diffusive losses. This is illustrated in *Figure 4-8,* which displays two Nyquist plots, one for the low (35 μm) compression, and one for the higher (135 μm) compression. As the operating compression increases, the contact resistance between the individual tows of fiber, between the GDL and collector plate, and between the MSL and catalyst layer are reduced, leading to lower ohmic losses (indicated by the lower value of the x-axis intercept).

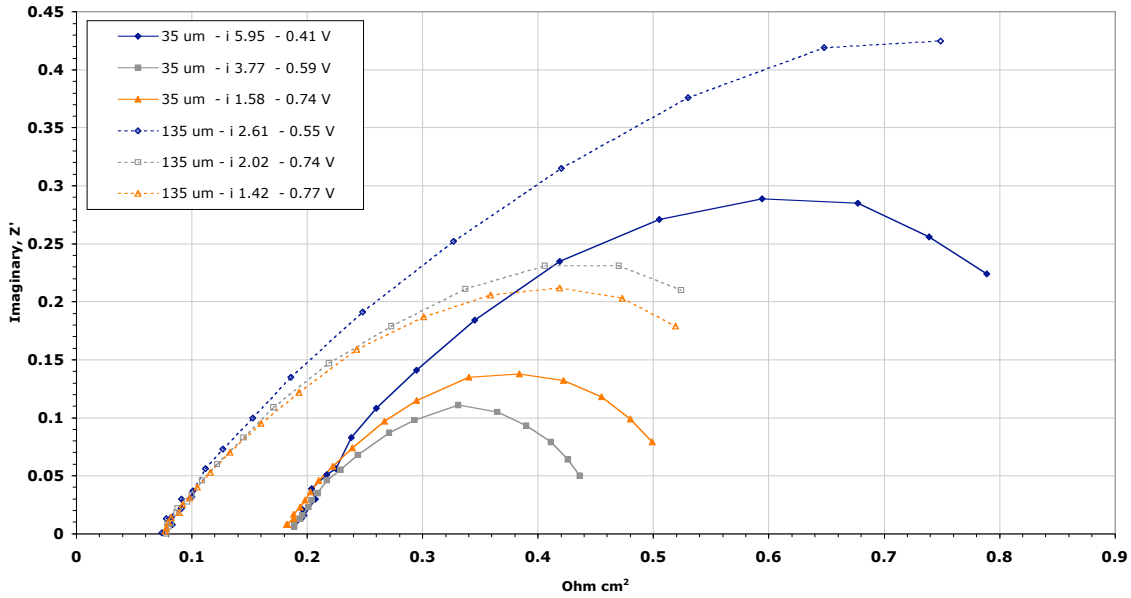

Figure 4-8. Nyquist plot for various fuel cell compressions

On the other hand, the higher compression of the GDL leads to higher diffusive losses as suggested by the larger radius of the 135 µm curves. This same trend is observed in *Figure 4-7* where at a cell voltage of approximately 0.7 the performance of the higher compression cell is actually better, but at higher current densities where diffusive losses are critical, the lower compression cell performs better.

Thus, it is not appropriate to evaluate MSL's in terms of the their effect on one aspect (e.g. ohmic losses) of the overall cell behavior. Rather, each MSL design/fabrication should be viewed as establishing a design space within which ohmic and diffusive losses can be balanced by choosing the operating compression. As stated in previous sections, this study tested three different compression levels for each of the 20 fuel cells tested, starting with the lowest compression and moving to the highest compression to avoid compression set. The reported performance corresponds to the compression that produces the highest current density at 0.5 volts. 0.5 volts was chosen because it generally corresponds to the fuel cells peak power. Also, a higher cell voltage would likely have favored cells with lower ohmic losses. Conversely, a lower cell voltage would favor cells with lower diffusive losses.

4.2 Fuel Cell Adhesion

To investigate how the design of a MSL can affect the adhesion of the GDL to the catalyst layer within a fuel cell, 28 pseudo fuel cell assemblies were tested, each with a unique MSL application. *Table 4-6* illustrates what characteristic of the application process is unique to each of these 28 pseudo fuel cell assemblies. The MSL adhesion test samples were prepared using the procedures described in *Chapter 3*.

Table 4-6. Adhesion Matrix

Design Point	Factor 1 A: Loading (mg/cm^2)	Factor 2 B: Composition (wt.% PTFE)	Factor 3 C: Pressure (MPa)	Factor 4 D: Time (Minutes)
1	1.5	10	500	2
2	1.5	10	500	8
3	1.5	10	1500	2
4	1.5	10	1500	8
27	2.75	10	1000	5
5	4	10	500	2
6	4	10	500	8
7	4	10	1500	8
8	4	10	1500	2
21	1.5	30	1000	5
22	2.75	30	500	5
23	2.75	30	1000	2
9	2.75	30	1000	5
10	2.75	30	1000	5
11	2.75	30	1000	5
12	2.75	30	1000	5
24	2.75	30	1000	8
25	2.75	30	1500	5
26	4	30	1000	5
13	1.5	50	500	2
14	1.5	50	500	8
15	1.5	50	1500	8
16	1.5	50	1500	2
28	2.75	50	1000	5
17	4	50	500	2
18	4	50	500	8
19	4	50	1500	2
20	4	50	1500	8

Indicates Point was added for CCD Augmentation

The adhesion tests conducted in this study were done using a "T-peel" test. The test specimens were prepared in two phases. A catalyzed membrane was first prepared, and then a piece of GDL was loaded with a specified amount of the desired composition MSL. The MSL coated GDL was then pressed together with the catalyzed membrane with a specific fabrication pressure and for a specific fabrication time. The catalyzed membrane was prepared in the manner described in *Chapter 3*, with one exception; a decal was only applied to one side of the membrane. For simplicity, during the adhesion study it is assumed that, since the layers within the fuel cell are symmetric, the level of adhesion observed between the layers on one side of the fuel cell (membrane to GDL#1) should equivalent to the level of adhesion observed between the layers on the other side of the fuel cell(membrane to GDL#2). Therefore, it is only necessary to investigate half of the traditional PEMFC assembly; which includes all of the layers from the membrane to the GDL (pseudo fuel cell assembly).

The T-peel tests were conducted as suggested in ASTM D 1876–01. The dimensions of the specimens used for this study are similar to those suggested in this standard. No additional hydration was added to the specimens after being pressed together at 135ºC, and the specimens were tested at ambient temperature, pressure, and relative humidity. The results are reported as the apparent fracture energy, G_c (J/m^2), which is based on the amount of work that the load frame does in debonding a unit area. Fracture energy is the work (energy) per unit area required to separate the pseudo fuel cell assembly. The apparent fracture energy is the sum of the true facture energy associated with the delamination process and the energy, per unit area, associated with the plastic deformation of the adherends. Fracture energy can be calculated using the following equation.

$$G_c = \frac{Work}{Area} = \frac{FD_T}{wa} = \frac{F2a}{wa} = \frac{2F}{w} \tag{4-2}$$

where F is the force required peel the assembly apart, a is the length of the MSL-catalyst area, w is the width of the MSL-catalyst area, and D_T is the total distance traveled by the

machine applying the force, which for a T-peel test is equal to twice the length of the debond, assuming negligible stretching of the adherends. As illustrated by this equation, the length (a) of the specimen does not matter, but the actual width of the specimen (w) becomes important. After fabrication (pressing the MSL coated GDL to the catalyzed membrane), each specimen was trimmed to a width of 20 mm. *Figures 4-9 and 4-10*, display the best performing adhesion design point (*Figure 4-9*), and the worst performing adhesion design point (*Figure 4-10*). These figures represent the raw data acquired from the load frame, load (force required to debond the adherends) as a function of extension of the load frame.

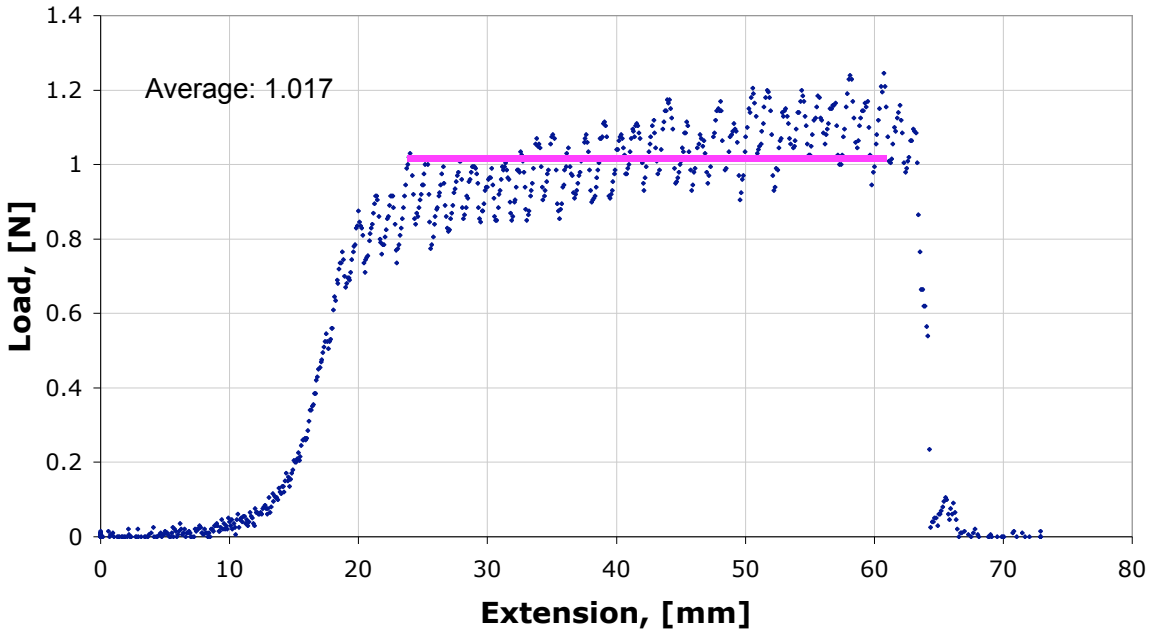

Figure 4-9. Best performing adhesion design point

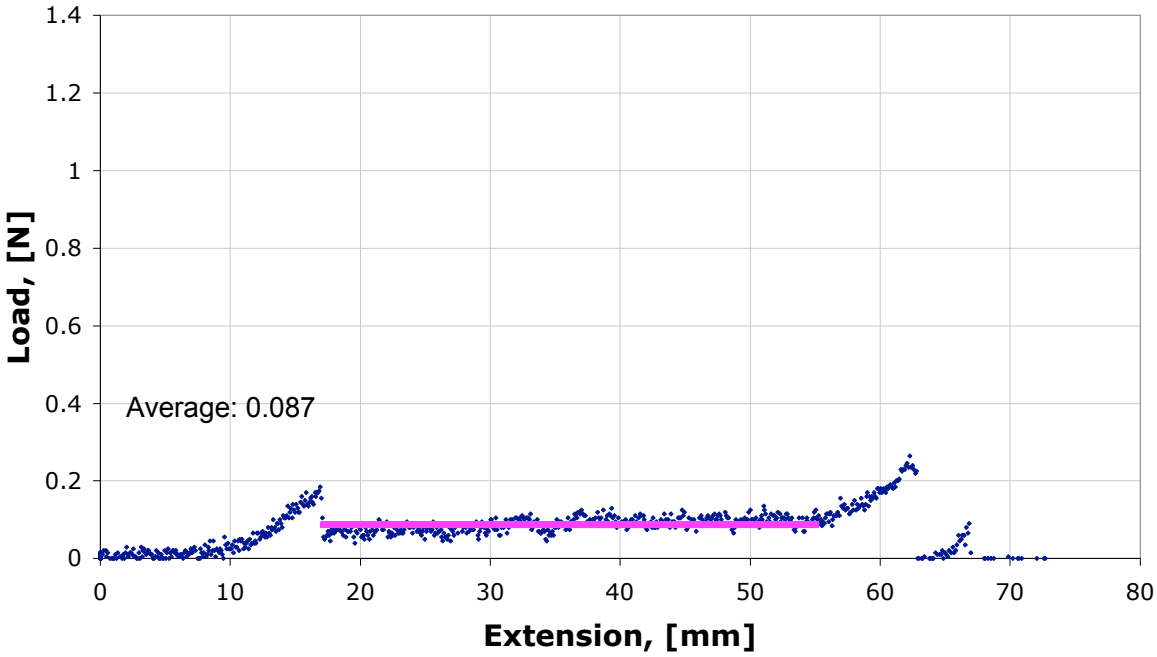

Figure 4-10. Worst performing adhesion design point

Once all 28 of the tests were completed, the results were compiled and the fracture energy of each of the 28 pseudo fuel cell assemblies was reported. *Table 4-7* tabulates these results, and *Appendix D* graphically displays the actual data taken from the Instron load frame.

Table 4-7. Adhesion Testing Results

Design Point	Factor 1 A: Loading (mg/cm^2)	Factor 2 B: Composition (wt.% PTFE)	Factor 3 C: Pressure (MPa)	Factor 4 D: Time (Minutes)	Response Fracture Energy (J/m^2)
1	1.5	10	500	2	16.1
2	1.5	10	500	8	28.0
3	1.5	10	1500	2	41.9
4	1.5	10	1500	8	34.4
27	2.75	10	1000	5	30.3
5	4	10	500	2	25.9
6	4	10	500	8	34.8
7	4	10	1500	8	48.9
8	4	10	1500	2	41.6
21	1.5	30	1000	5	61.8
22	2.75	30	500	5	42.6
23	2.75	30	1000	2	74.2
9	2.75	30	1000	5	70.3
10	2.75	30	1000	5	83.7
11	2.75	30	1000	5	74.8
12	2.75	30	1000	5	76.2
24	2.75	30	1000	8	91.7
25	2.75	30	1500	5	101.7
26	4	30	1000	5	83.7
13	1.5	50	500	2	17.2
14	1.5	50	500	8	24.7
15	1.5	50	1500	8	63.1
16	1.5	50	1500	2	57.5
28	2.75	50	1000	5	43.1
17	4	50	500	2	8.7
18	4	50	500	8	12.1
19	4	50	1500	2	42.8
20	4	50	1500	8	60.9

Indicates Point was added for CCD Augmentation

4.2.1 Adhesion Correlation. As indicated by *Tables 4-6 and 4-7*, the adhesion correlation started with the same 20 design points used for the performance test, as required for a full factorial design. The results produced from the original full factorial adhesion correlation exhibited severe curvature. The curvature was so severe that it became obvious that the optimum solution was not in the full factorial design space, and in order to accurately predict adhesion, the correlation needed to be augmented to a central composite design (CCD). As discussed in the performance study, a CCD has the

capability to produce non-linear relationship between the design factors. Augmenting to a CCD required the creation of 8 more design points, as identified in *Table 4-7*.

After recording and compiling all of the fracture energies, the results were analyzed using the statistical package, Design Expert®. This statistical package was used to analyze the results, provide the user with the information needed to choose the significant factors (or in the CCD, choose those factors in one of three methods for the user), provide an analysis of variance (ANOVA) table, provide transform suggestions/diagnostics, and produce solutions that will optimize the adhesion based on the results. *Table 4-8* is the ANOVA table produced by Design Expert® from the adhesion tests.

Table 4-8. ANOVA Table of Adhesion Results

Source	Sum of Squares	DF	Mean Square	F Value	Prob > F
Model	94.76	7	13.54	56.27	< 0.0001
A	2.42E-03	1	2.42E-03	0.01	0.9212
B	9.72E-03	1	9.72E-03	0.04	0.8427
C	30.38	1	30.38	126.29	< 0.0001
D	1.98	1	1.98	8.24	0.0094
B2	54.75	1	54.75	227.57	< 0.0001
AB	2.75	1	2.75	11.41	0.003
BC	4.88	1	4.88	20.3	0.0002
Residual	4.81	20	0.24		
Cor Total	99.57	27			

The factors chosen for the correlation were automatically chosen by Design Expert® [25]. The routine used to eliminate factors from the correlation was a backwards step routine, which Design Expert deemed the most robust routine. The overall decision as to which factors to keep in the correlation comes from many sources, one of which is the "Prob > F" value. The backwards elimination routine starts with all the factors in the correlation, then analyzes the correlation stepping one factor at a time out of the correlation. Ideally it is desired that the P-value (Prob>F) is less then 0.05, but for experimental data a value a slight bit higher is acceptable. A detailed investigation of the P-values reveal high values for factors A and B (loading and composition). Initially these

factors were eliminated from the correlation, but then added back to satisfy higher order interactions, such as B^2, AB, and BC.

Design Expert® [25] also provides the ability to identify whether a certain transform should be used to produce a more accurate correlation. For the adhesion correlation described above, Design Expert® suggested a square root transform for the data. To suggest such a transform, Design Expert® will produce a Box-Cox plot, as displayed by *Figure 4-11*.

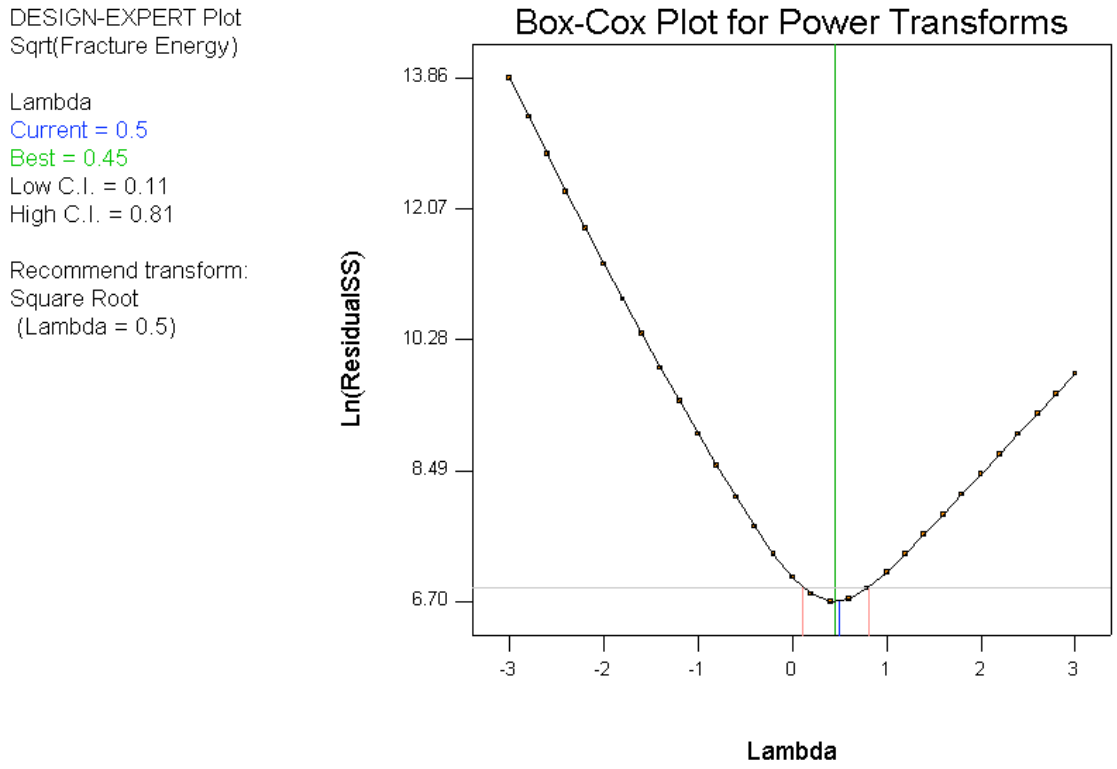

Figure 4-11. Box-Cox plot to support adhesion transform

Using the factors outlined above, Design Expert® suggests the relationship between the design/fabrication factors of an MSL and the square root of the fracture energy of the adhesive bond, $\sqrt{G_c}$, is as follows:

$$\sqrt{G_c}(J/m^2) = -0.81587 + 0.50631\,L_{msl} + 0.42924\,C_{msl} + 0.13650\,P_f + 0.11065\,t_f - 0.00729607\,C_{msl}^2 - 0.016568\,L_{msl}\,C_{msl} + 0.00801223\,C_{msl}\,P_f \quad (4\text{-}3)$$

where L_{msl} is the MSL loading (mg/cm^2), C_{msl} is the MSL composition (wt.% PTFE), P_f is the fabrication pressure (MPa), and t_f is the fabrication time (mintues). It is interesting to note that this relationship, being $\sqrt{G_c}$, is similar to the stress intensity factor (K_c). The stress intensity factor is defined as:

$$K_c = \sqrt{(G_c E)} \tag{4-4}$$

where E is the modulus of elasticity.

Design Expert® provides several ways to quantify how well this correlation fits the actual data. An estimate of the "lack of fit" that this correlation contains is given by a ratio of the residual error over the pure error. The "lack of fit" for this correlation is 2.63, which tells us that the there is no significant "lack of fit" for this correlation. According to the statistical consultants at Stat-ease Inc., the designers of Design Expert® [25], if the "lack of fit" value is around 1, it can be said that the replications are correctly quantifying the error in the system.

To further quantify the fit of the transformed correlation and variation in data, the R-Squared, Adjusted R-Squared, and Predicted R-Squared can be investigated. As displayed in *Table 4-9*, the R-Square value for this correlation is 0.9517. Since the R-squared value will simply increase as the total number of factors increases, is not a very reliable judge of variation in the data. Therefore, the adjusted R-squared value is a much better judge of the variation within the correlation. The predicted R-squared value quantifies the variation in predictions by the correlation. According to the statistical consultants at Stat-ease Inc., the maximum acceptable difference between the adjusted and predicted R-squared values should be no more then about 0.2.

Table 4-9. Adhesion Correlation R-Squared Table

R-Squared	0.9517
Adj R-Squared	0.9348
Pred R-Squared	0.9079

Design Expert® supplies the ability to optimize the design space and will provide optimal solutions for the design. *Table 4-10* displays the top 10 solutions. Common themes found within these optimum solutions for the adhesion correlation are somewhat random loading, mid-ranged composition, high fabrication pressure, and a longer fabrication time.

Table 4-10. Top 10 Adhesion Solutions suggested by Design Expert

Solution Number	Loading (mg/cm^2)	Composition (wt.% PTFE)	Fabrication Pressure (PSI)	Fabrication Time (Minute)	Fracture Energy (J/m^2)
1	1.5	33.54	10.34	7.99	107.6
2	1.5	32.79	10.34	7.8	107.2
3	2.1	32.76	10.34	8	107.1
4	1.5	32.75	10.34	7.78	107.1
5	3.89	30.69	10.34	8	106.4
6	3.97	30.58	10.34	8	106.4
7	4	30.81	10.34	8	106.4
8	4	31.51	10.34	7.97	106.2
9	4	30.58	10.34	7.87	106.1
10	4	27.6	10.34	7.95	105.0

4.2.2 Effect of MSL Design/Fabrication Factors on Adhesion. As identified by the ANOVA table, Factor B and B^2 in *Table 4-8*, MSL composition can have a significant effect on the adhesion of the PEMFC. *Table 4-10* displays the top 10 optimum combinations of MSL design factors, in which composition is around 30 wt.% PTFE. *Figure 4-12* illustrates the effect of varying the composition on the predicted fracture energy. As displayed in *Figure 4-12*, the relationship between composition and fracture energy is best described by a quadratic fit. As noted in previous paragraphs, the main effect of composition could be somewhat masked by higher order interactions, a better idea of how composition interacts with the other correlation factors is illustrated in the following paragraphs.

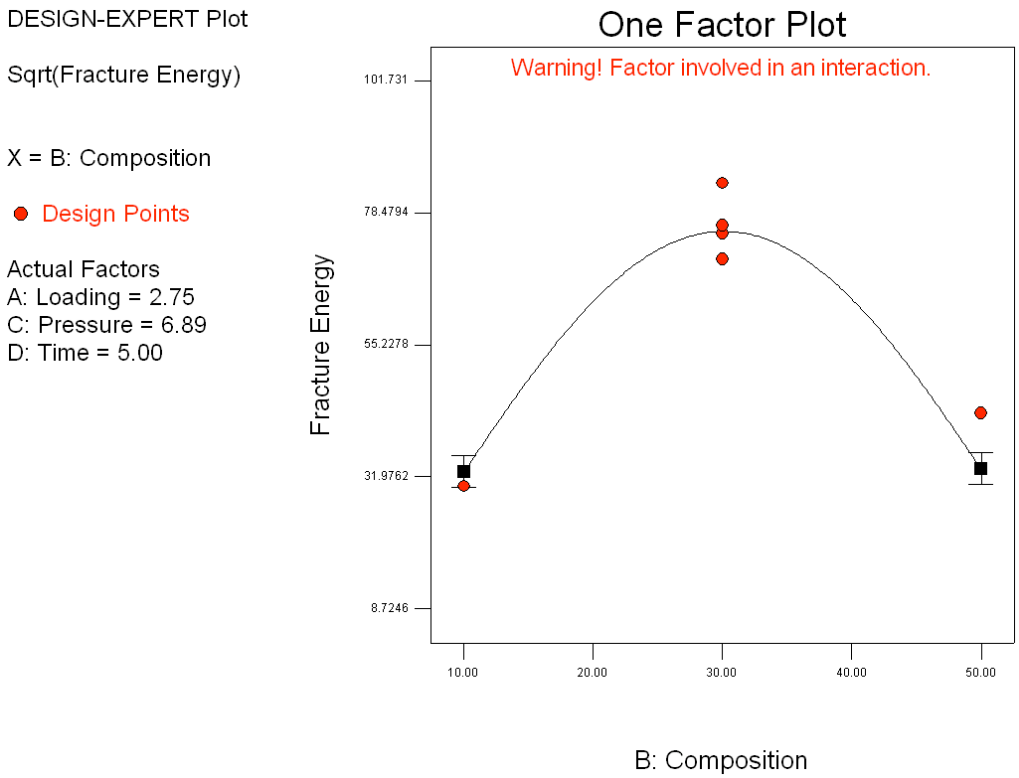

Figure 4-12. Fracture energy as a function of composition.

MSL loading, or factor A, was originally not included in the correlation, but added to satisfy higher order interactions. This doesn't necessarily mean that loading is insignificant; it could simply be masked by the higher order interactions. The top 10 optimal solutions, as displayed in *Table 4-10*, reveal a range of MSL loadings. However, the higher values for predicted fracture energy occur with a low MSL loading. Just as described in the performance study, a low loading reduces material cost. Also, since the MSL is applied in small layers, lower loadings mean less time is required to apply the desired amount. Therefore, when considering this process in a high speed manufacturing line, low loadings could save time and money. *Figure 4-13* displays the 3-D correlation of the fracture energy as a function composition and fabrication pressure, with a constant time of 8 minutes and a low MSL loading. This figure should be compared to *Figure 4-14*, where everything is the same as in *Figure 4-13*, except the constant value of loading has increased to the highest loading in the design space (4 mg/cm^2). Comparison between these two figures illustrates the concept that increasing the loading will decrease the fracture energy.

DESIGN-EXPERT Plot

Sqrt(Fracture Energy)
X = B: Composition
Y = C: Pressure

Actual Factors
A: Loading = 1.50
D: Time = 8.00

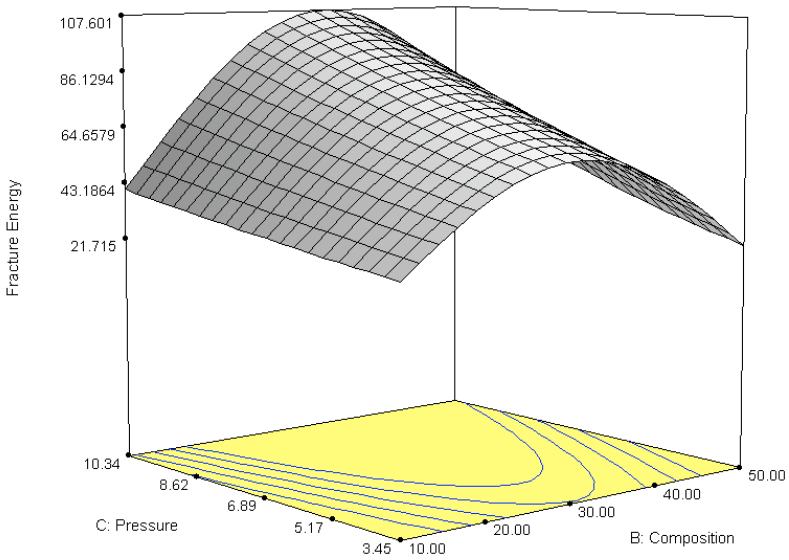

Figure 4-13. Fracture energy as a function of composition and pressure – Low loading

DESIGN-EXPERT Plot

Sqrt(Fracture Energy)
X = B: Composition
Y = C: Pressure

Actual Factors
A: Loading = 4.00
D: Time = 8.00

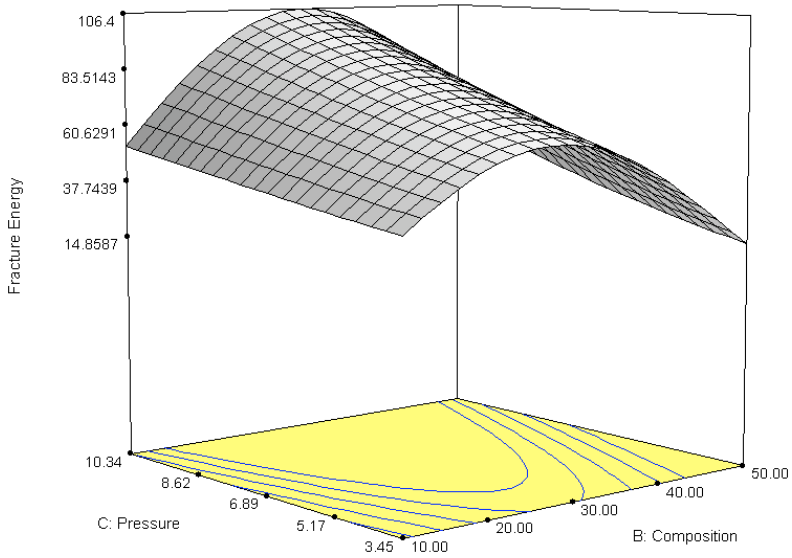

Figure 4-14. Fracture energy as a function of composition and pressure – High loading

Fabrication pressure is also recommended as a significant factor in the correlation. Inspection of the top 10 optimal solutions, *Table 4-10*, reveal 10 out of 10 of those optimal solutions recommend approximately 10.34 MPa of pressure, which is the high end of the design range (3.45-10.34 MPa). As illustrated by the difference between *Figure 4-15* and *Figure 4-16*, the fabrication pressure can have a large effect on the predicted fracture energy. *Figure 4-15* displays the fracture energy as a function of composition and loading, while holding fabrication time at 8 minutes, and fabrication pressure at the low range of the design space (3.45 MPa). *Figure 4-16* displays the same data as in *Figure 4-15*, except for the fabrication pressure, which is increased the highest value in the design space, 10.34 MPa.

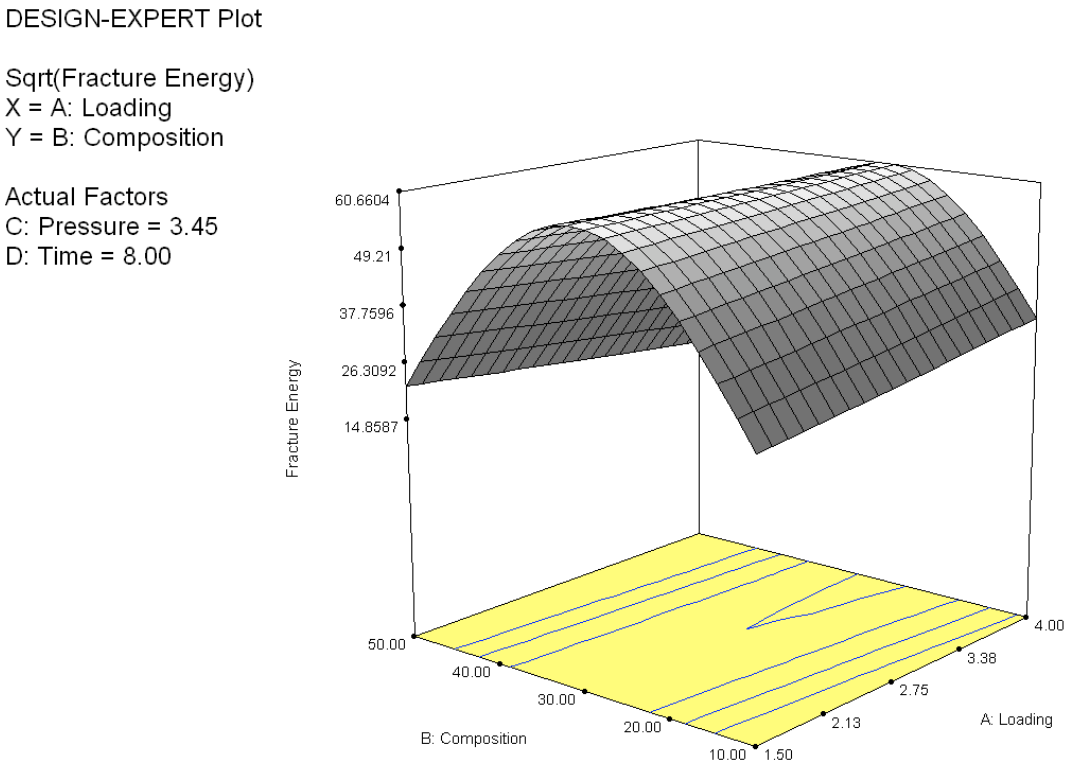

Figure 4-15. Fracture energy as a function of composition and loading – Low pressure

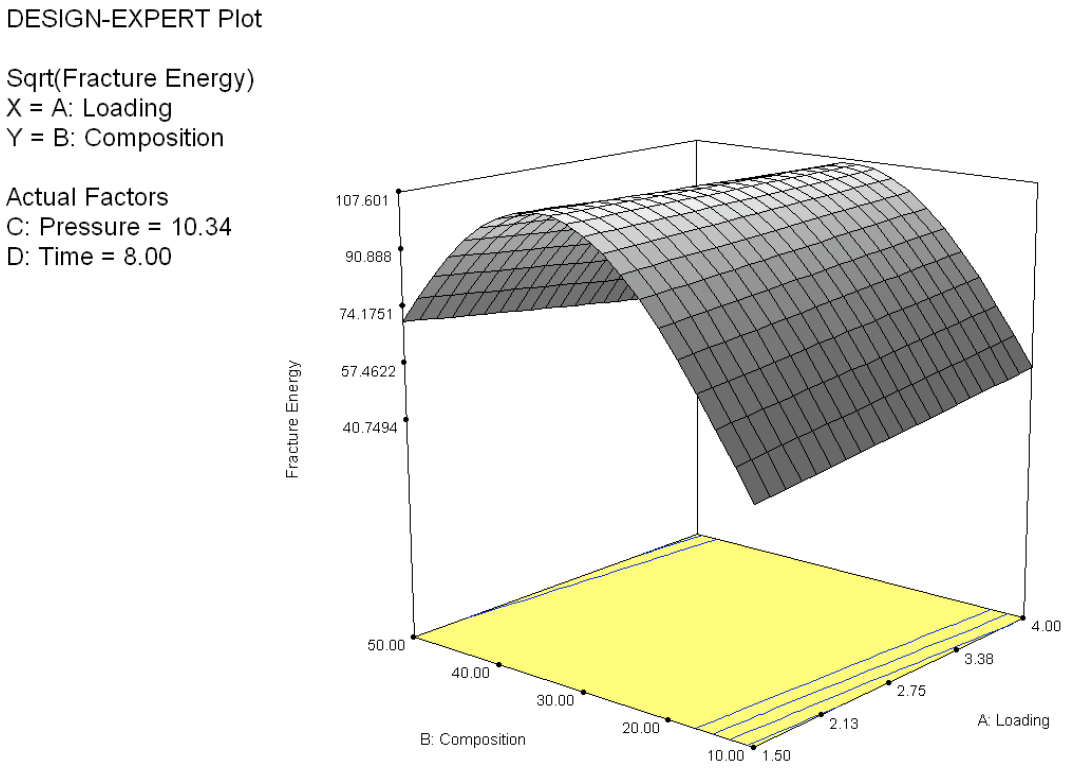

Figure 4-16. Fracture energy as a function of composition and loading – High pressure

As noted by the ANOVA table, *Table 4-8*, fabrication time is a very significant factor in the fracture energy correlation. The top 10 optimal solutions, display the highest predicted fracture energy is achieved with a higher value for fabrication time. *Figure 4-17* and *Figure 4-18* illustrate the significant effect of changing the fabrication time from the highest to the lowest, while holding fabrication pressure at 10.34 MPa (optimal value from *Table 4-10*). *Figure 4-17* displays fracture energy as a function of composition and loading, with the optimal fabrication pressure of 10.34 MPa and a low fabrication time (2 minutes). *Figure 4-18* displays fracture energy as a function of composition and loading, with the optimal fabrication pressure of 10.34 MPa and a high fabrication time (8 minutes).

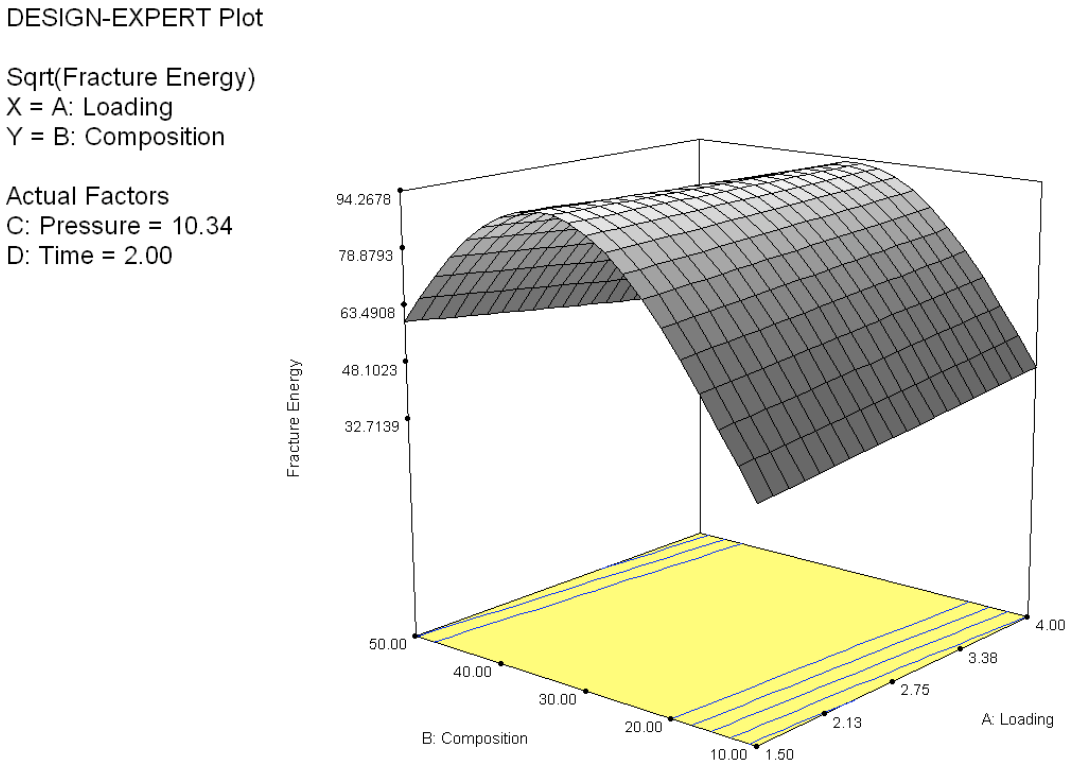

Figure 4-17. Fracture energy as a function of composition and loading – Low time

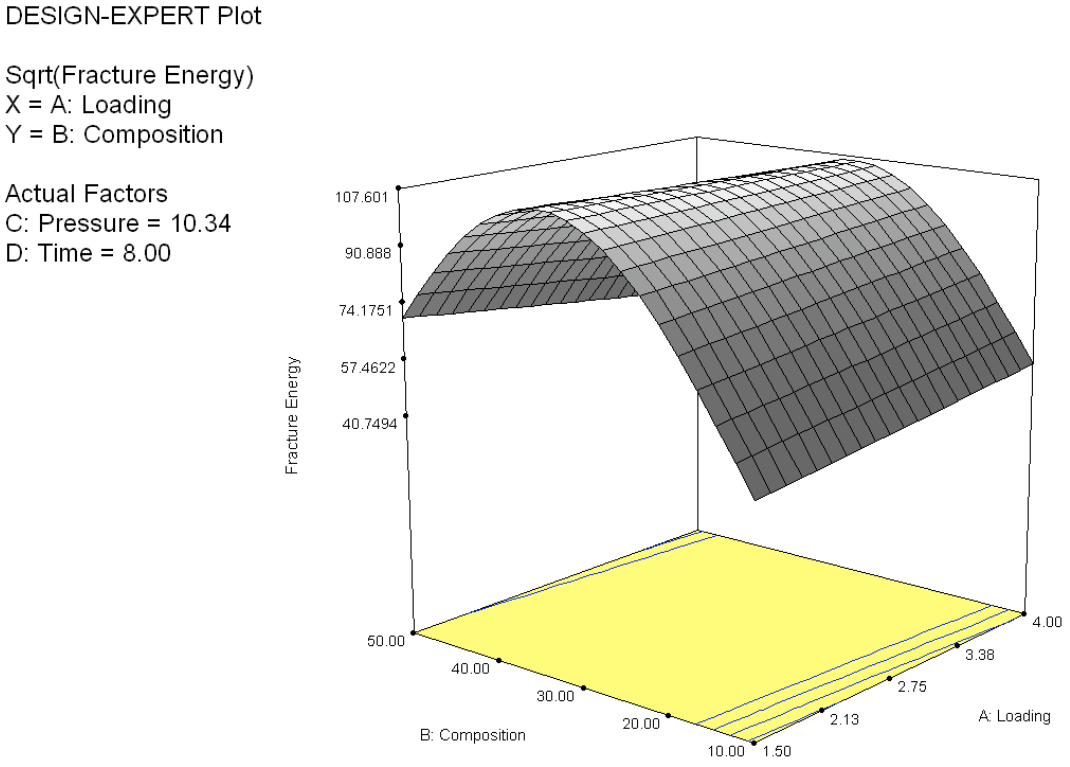

Figure 4-18. Fracture energy as a function of composition and loading – High time

4.2.3. Detailed Exploration of Results. Certain points in the design space produced unexpected and difficult to interpret results. For design points 15, 16, 19, and 20, it was difficult to identify an accurate value for fracture energy. The problem, as displayed in *Figure 4-19*, was the load recorded from the Instron load frame, which is directly related to fracture energy, never reached a plateau. It is interesting to note that the common elements in all of these problematic points are high fabrication pressure and a 50 wt.% PTFE MSL.

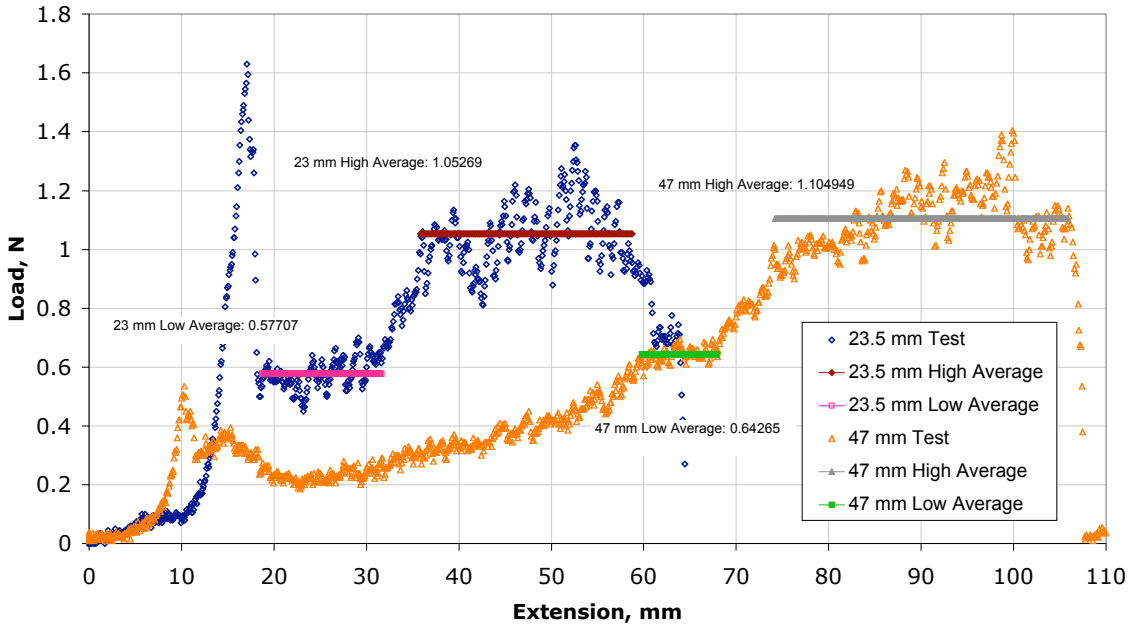

Figure 4-19. Load as a function of extension – Design point 20

One attempt at rectifying this problem was to create pseudo fuel cell assemblies with twice the length of catalyst and MSL layers. As displayed in *Figure 4-19*, the result was similar to the original length tests, the recorded load continued to drift as the extension increased, and the determination of a plateau in the data was still very difficult. *Figure 4-19* displays two averages for each test, an estimate of a high plateau and a low plateau. The lower averages where chosen as the results used to create the statistical correlation previously displayed. The rationale behind using the lower averages is that even though the value is low, it is the start of a fracture, and a fracture is a failure. Using the lower value, of about 0.61 Newtons (fracture energy of 61.0 J/m^2) for this particular

specimen falls within the range of results produced by the other similar design points 15, 16, and 19.

One possibility for the lack of a single obvious plateau in the data is due to the fracture propagating through the layers of the pseudo fuel cell assembly. *Figure 4-20* is an image of the specimen corresponding to design point 20 (point used to create response displayed in *Figure 4-19*). Inspection of this figure supports the idea of the fracture propagating through the layers, and displays how the fracture started in the catalyst-MSL interface and moved into the MSL-GDL interface. This locus of failure would explain the various levels of adhesion illustrated by *Figure 4-19*.

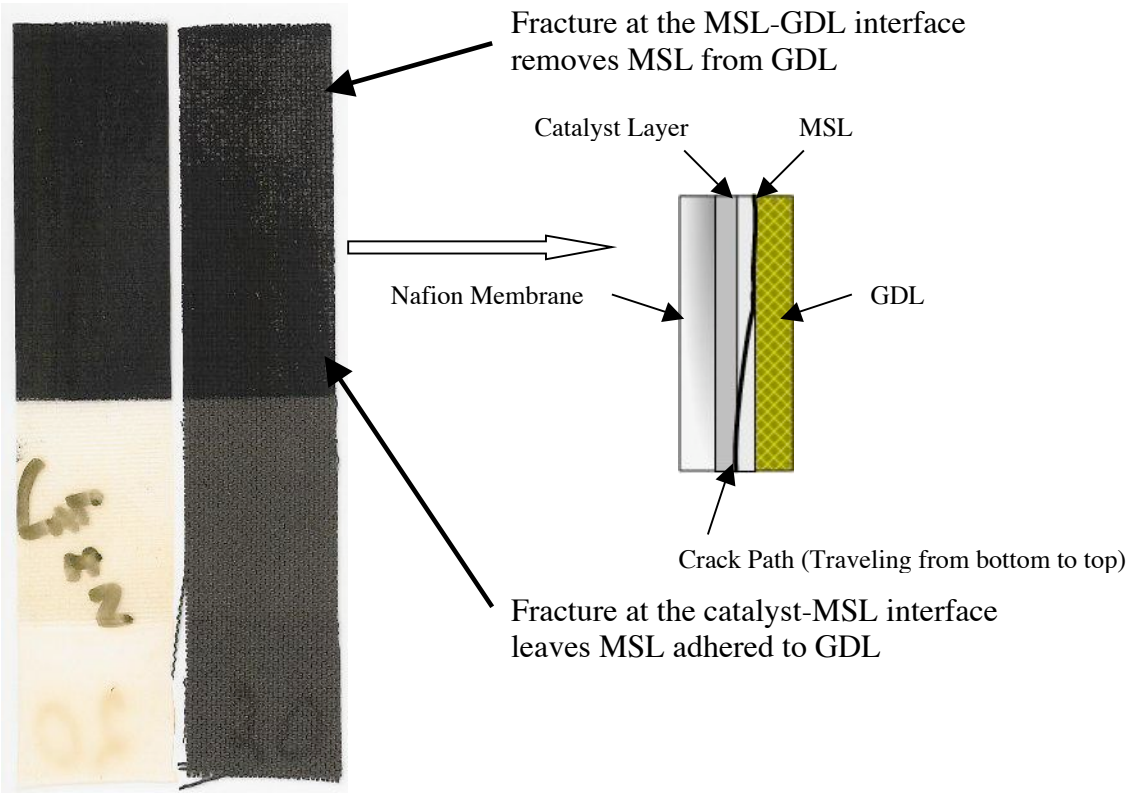

Figure 4-20. Actual extended pseudo fuel cell assemblies

Recall, from the Experimental Procedures section, the MSL is sintered to the GDL. The final temperature of the sintering process (350°C) is just high enough to reach the melting point of Teflon™. Therefore, the Teflon™ particles in the MSL will bond

with the Teflon™ particles in the GDL. On the other hand, during the fabrication process the MSL is pressed to the catalyst layer at much lower temperature (135°C). With this in mind, it is expected that the adhesion between the MSL and GDL will be higher than the adhesion between MSL and catalyst layer. To support this claim, *Figure 4-21* is a comparison between design point 9 (30 wt.% PTFE, 2.75 mg/cm^2, 6.89 MPa, and 5 minutes) and design point 17 (50 wt.% PTFE, 4 mg/cm^2, 3.45 MPa, and 8 minutes). As displayed in *Table 4-7*, the fracture energy for design point 9 is 70.3 J/m^2, and the fracture energy reported for design point 17 is 12.1 J/m^2. Thus, design point 9 corresponds to a higher fracture energy and its appearance is similar to the end of the fracture in *Figure 4-20*, indicating a failure at the MSL-GDL interface. On the other hand, design point 17 corresponds to a lower fracture energy and its appearance is similar to the start of the fracture in *Figure 4-20*, indicating a failure at the catalyst-MSL interface.

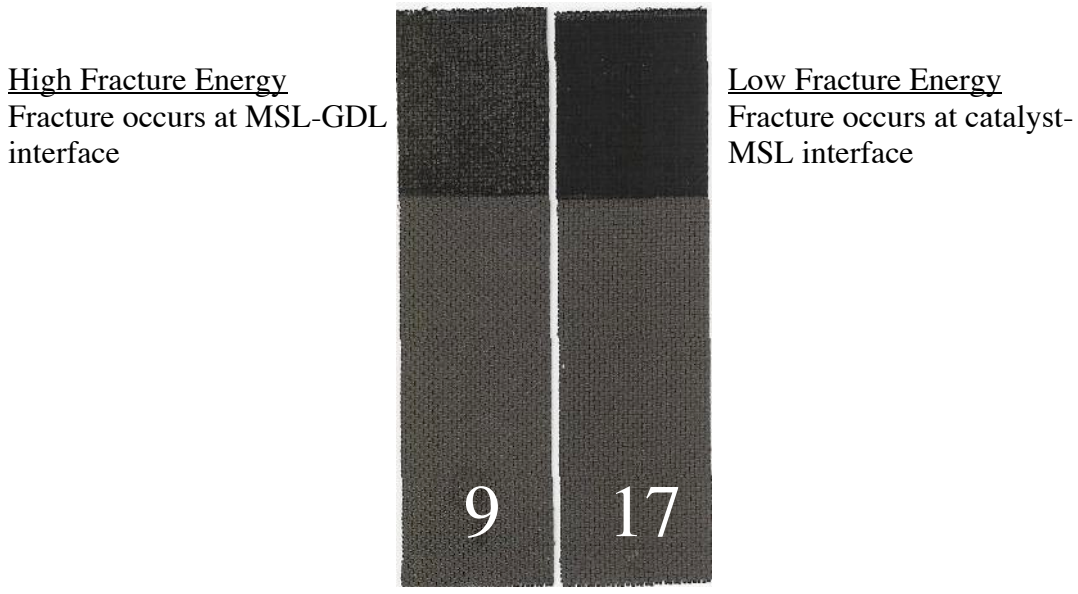

Figure 4-21. Comparison between the fracture interface of design point 9 & 17

After identifying the locus of failure, the question becomes why would the growing crack move into an area of higher adhesion. Ideally, during a T-Peel test, the adhered section should be perpendicular to the adherends, as illustrated by *Chapter 3, Figure 3-8.* As displayed in *Figure 4-22*, this was rarely the case for the actual tests, the

adhered sections would "lean" towards the stiffer GDL. Chen [22] report that the crack will grow perpendicular to the largest tensile stress or strain. Using the following equation, the maximum strain can be estimated from the radius of curvature.

$$\varepsilon = \frac{t/2}{\rho} \tag{4-5}$$

where ρ is the radius of curvature and t is the thickness of the adherend. *Figure 4-23* provides an analysis used to estimate the radius of curvature for each of the adherends. From *Figure 4-23*, it can be concluded that the radius of curvature of the membrane is approximately 7 times the radius of curvature of the GDL. From *Equation 4-5* the strain of the GDL is calculated to be about 16 times the strain of the membrane.

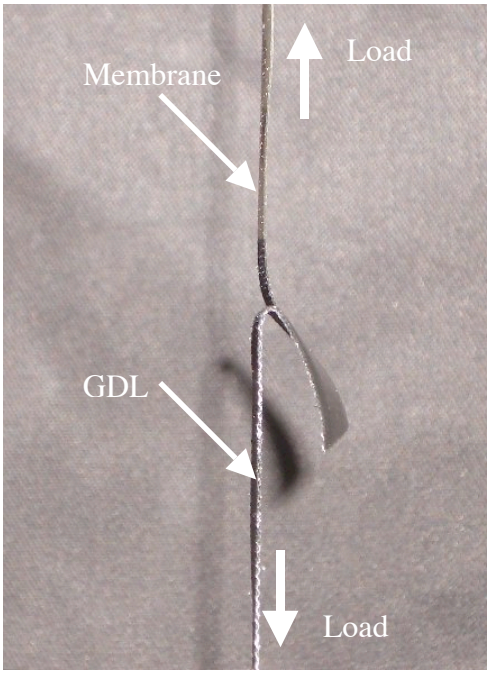

Figure 4-22. Actual T-peel test

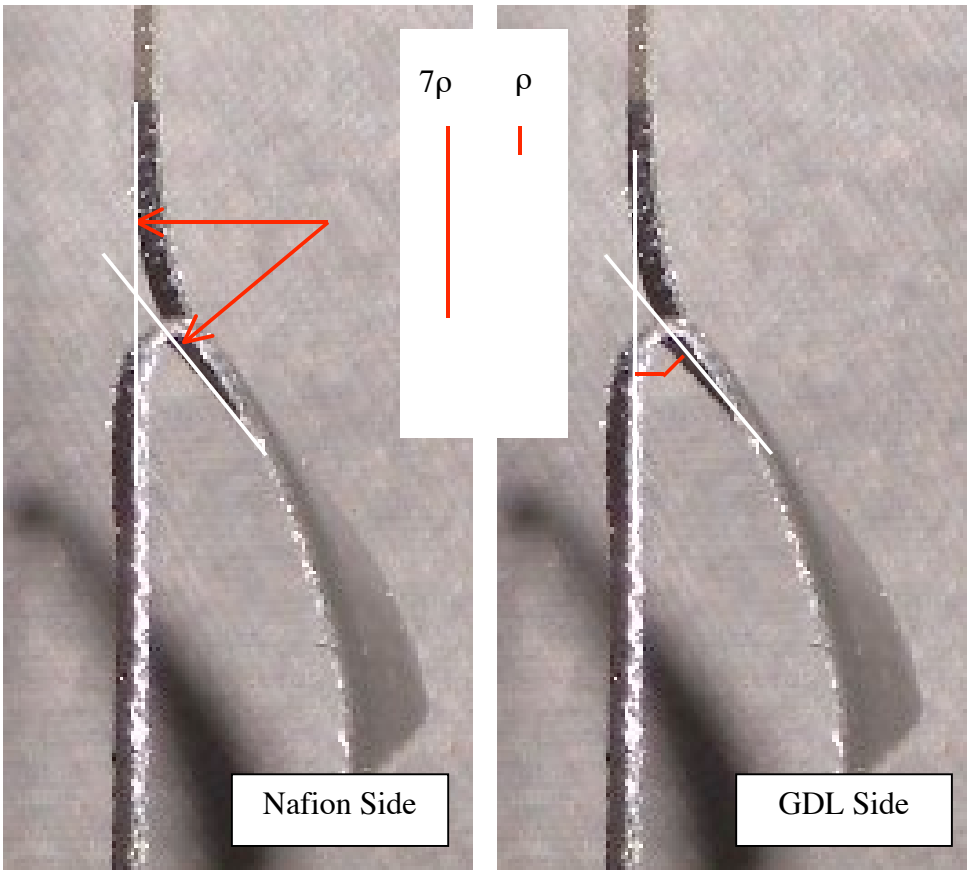

Figure 4-23. Radius of curvature analysis

Figure 4-24 illustrates the effect of the increased strain on a discrete element that would be found at the crack tip. This figure demonstrates how the perpendicular (with respect to the highest strain) movement of the crack causes it to move through the MSL to the GDL. This is noteworthy in that the crack migrates from a less tough to a tougher region within the specimen.

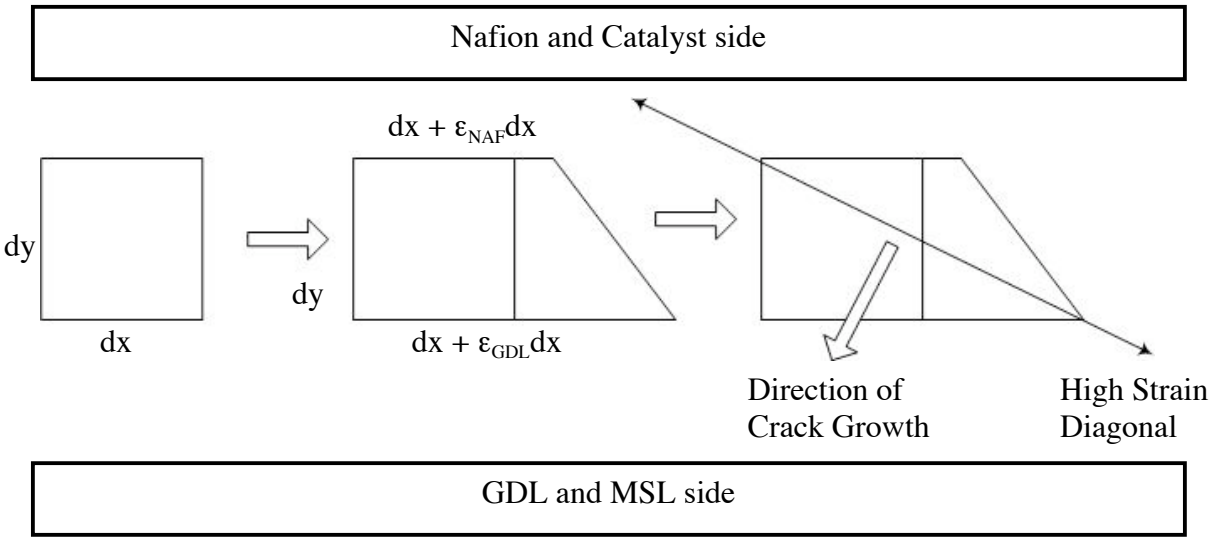

Figure 4-24. Crack tip discrete element analysis

Using the knowledge provided by Chen [22], identifying the GDL as the more highly strained adherend (*Figure 4-22 - 4-23*), and the actual test specimen image (*Figure 4-20*), it can be concluded that the propagation of the crack through the various layers of the fuel cell can be expected, and is not due to poor test specimen construction or testing procedures.

An independent study was done to investigate the level of adhesion that could be expected from one of these pseudo fuel cell assemblies that did not have any MSL applied to its GDL. Five tests were run, exploring various fabrication pressures and times. As illustrated in *Table 4-11*, all tests produced fracture energies close to zero. In fact, one of the design points (No MSL – 3.45 MPa – 2 minutes) did not even have a high enough level of adhesion to survive trimming the sides to a 20 mm width. From this study, it is concluded that any amount of MSL is helpful to the level of adhesion between the various layers within the PEMFC.

Table 4-11. Adhesion Results for No MSL Specimens

Fabrication Pressure (MPa)	Fabrication Time (Minutes)	Fracture Energy (J/m^2)
3.45	2	Not strong enough to withstand trimming
3.45	8	0.0
6.89	5	3.4
10.34	2	4.1
10.34	8	2.4

5 Conclusions and Recommendations

5.1 Performance and Adhesion Correlation Conclusions

As noted in *Chapter 4*, the addition of the MSL is essential for architectures requiring adhesion within the assembly, and the incorporation of an MSL always leads to a better bond between the GDL and catalyzed membrane. However, with regard to performance, this is not the case and the MSL, if not carefully designed, can have an adverse affect on the performance of the PEMFC. This highlights the need for careful design of the MSL and the usefulness of a correlation that can explain the effect of MSL design and fabrication parameters on performance and adhesion in PEM fuel cells.

The performance correlation, as presented in *Chapter 4*, includes MSL loading, MSL composition, fuel cell fabrication pressure, and an interaction between MSL loading and composition. This correlation suggests that the optimal PEMFC performance is achieved with low MSL loadings, low MSL PTFE content, and a low fabrication pressure. Detailed examination of the individual polarization curves (See *Appendix C*) illustrates how increasing the MSL loading tends to increase the mass transport limitations and in-turn create more diffusion losses. It was also observed that with a low MSL loading the PTFE content could affect the ohmic region of the polarization curves. This suggests that as the PTFE content increases and the corresponding carbon content decreases, the conductivity of the MSL is reduced, therefore decreasing the performance of the fuel cell.

The adhesion correlation, also presented in *Chapter 4*, includes MSL loading, MSL composition, fuel cell fabrication pressure, fuel cell fabrication time, a quadratic expression for composition, an interaction between loading and composition, and an interaction between composition and fabrication pressure. The adhesion correlation suggests a mid-ranged MSL PTFE content, high fuel cell fabrication pressure, and high fuel cell fabrication time. Although MSL loading is in the correlation, the fact that it varies at random across the top 10 solutions, suggests that it is not highly significant as an

individual factor, but is more critical when interacting with other factors. Typically, better adhesion was observed between the MSL-GDL interface than between the catalyst layer-MSL interface. The higher level of adhesion between the MSL and GDL is most likely attributed to the sintering of the MSL to the GDL at a high enough temperature to reach the melting point of the PTFE (350ºC) found within both layers. On the other hand, the MSL is pressed to the catalyst layer at a much lower temperature (135ºC). With this in mind, it suggested that one of the keys to in increasing the adhesion within the layers of the fuel cell is to increase the bond between the catalyst layer and the MSL.

The contradicting terms between the performance and adhesion correlations are the fuel cell fabrication time and pressure. Better adhesion is expected when the assembly is fabricated at higher pressure and longer periods of time, but as identified by the performance correlation, the structure of the fuel cell does not respond well to such conditions. As noted in previous sections, due to the temperature of the fabrication process, a longer fabrication time increases the risk of damaging the Nafion membrane. Similarly, as the fabrication pressure is increased, so does the risk of permanently compacting the GDL and reducing PEMFC performance due to mass transport limitations. Thus, the selection of fabrication pressure and time must involve a compromise between the objectives of high performance and high adhesion.

5.2 Recommendations for Future Research

As identified in *Chapter 4* the performance correlation contains a significant amount of curvature. In order to explore this curvature it is recommended that the full factorial performance experiment be augmented to a central composite design. As displayed in *Table 4-6*, it requires an additional 8 design points to augment the design. Augmenting the design to provide a correlation that is applicable across the entire design space, will allow for evaluation of designs that lead to sub-optimal performance but that have better adhesion. These types of compromises will be essential for identifying the best overall set of design and fabrication parameters for the MSL.

It is also recommended that the design of the MSL be undertaken in conjunction with the design and/or selection of the GDL. In other words, as the material specifications for the GDL become better defined, the work presented here may need to be repeated to evaluate the best MSL for a specific GDL material. For example, if a coarsely woven fabric is used, instead of the B-1/A fabric used during this study, it may be necessary to increase the MSL loading to compensate for the rough fabric surface. Preliminary studies have demonstrated significant improvements for coarse weaves with MSL loadings higher than those recommended here.

Similarly, conclusions regarding the best MSL are likely to be different for carbon paper than for the carbon cloth evaluated here. This is thought to be true due to the differences between the structure of carbon paper and carbon weave. The carbon cloth may be less porous and resist penetration by the MSL thus requiring a lower loading. On the other hand carbon paper may require more "leveling" than a tightly woven cloth to maintain good surface contact with the catalyzed membrane. Work is currently underway to extend this research to address these related questions.

6 References

1. Qi, Z. G., and Kaufman, A. (2002). "Improvement of water management by a microporous sublayer for PEM fuel cells." *Journal of Power Sources*, 109(1), 38-46.

2. Song, J. M., Cha, S. Y., and Lee, W. M. (2001). "Optimal composition of polymer electrolyte fuel cell electrodes determined by the AC impedance method." *Journal of Power Sources*, 94(1), 78-84.

3. Chen, J., Matsuura, T., and Hori, M. (2004). "Novel gas diffusion layer with water management function for PEMFC." *Journal of Power Sources*, 131(1-2), 155-161.

4. Lee, H. K., Park, J. H., Kim, D. Y., and Lee, T. H. (2004). "A study on the characteristics of the diffusion layer thickness and porosity of the PEMFC." *Journal of Power Sources*, 131(1-2), 200-206.

5. Nam, J. H., and Kaviany, M. (2003). "Effective diffusivity and water-saturation distribution in single- and two-layer PEMFC diffusion medium." *International Journal of Heat and Mass Transfer*, 46(24), 4595-4611.

6. Pasaogullari, U., and Wang, C. Y. (2004). "Two-phase transport and the role of micro-porous layer in polymer electrolyte fuel cells." *Electrochimica Acta*, 49(25), 4359-4369.

7. Thoben, B., and Siebke, A. (2004). "Influence of different gas diffusion layers on the water management of the PEFC cathode." *Journal of New Materials for Electrochemical Systems*, 7(1), 13-20.

8. Lim, C., and Wang, C. Y. (2004). "Effects of hydrophobic polymer content in GDL on power performance of a PEM fuel cell." *Electrochimica Acta*, 49(24), 4149-4156.

9. Park, G. G., Sohn, Y. J., Yang, T. H., Yoon, Y. G., Lee, W. Y., and Kim, C. S. (2004). "Effect of PTFE contents in the gas diffusion media on the performance of PEMFC." *Journal of Power Sources*, 131(1-2), 182-187.

10. Jordan, L. R., Shukla, A. K., Behrsing, T., Avery, N. R., Muddle, B. C., and Forsyth, M. (2000). "Diffusion layer parameters influencing optimal fuel cell performance." *Journal of Power Sources*, 86(1-2), 250-254.

11. Paganin, V. A., Ticianelli, E. A., and Gonzalez, E. R. (1996). "Development and electrochemical studies of gas diffusion electrodes for polymer electrolyte fuel cells." *Journal of Applied Electrochemistry*, 26(3), 297-304.

12. Passalacqua, E., Squadrito, G., Lufrano, F., Patti, A., and Giorgi, L. (2001). "Effects of the diffusion layer characteristics on the performance of polymer electrolyte fuel cell electrodes." *Journal of Applied Electrochemistry*, 31(4), 449-454.

13. Giorgi, L., Antolini, E., Pozio, A., and Passalacqua, E. (1998). "Influence of the PTFE content in the diffusion layer of low-Pt loading electrodes for polymer electrolyte fuel cells." *Electrochimica Acta*, 43(24), 3675-3680.

14. Passalacqua, E., Lufrano, F., Squadrito, G., Patti, A., and Giorgi, L. (1998). "Influence of the structure in low-Pt loading electrodes for polymer electrolyte fuel cells." *Electrochimica Acta*, 43(24), 3665-3673.

15. Larminie, J., and Dicks, A. (2003). *Fuel Cell Systems Explained*, John Wiley and Sons, West Sussex, England.

16. Ticianelli, E. A., Derouin, C. R., Redondo, A., and Srinivasan, S. (1988). "Methods to Advance Technology of Proton-Exchange Membrane Fuel-Cells." *Journal of the Electrochemical Society*, 135(9), 2209-2214.

17. de Almeida, S. H., and Kawano, Y. (1999). "Thermal behavior of Nafion membranes." *Journal of Thermal Analysis and Calorimetry*, 58(3), 569-577.

18. Bevers, D., Rogers, R., and vonBradke, M. (1996). "Examination of the influence of PTFE coating on the properties of carbon paper in polymer electrolyte fuel cells." *Journal of Power Sources*, 63(2), 193-201.

19. Gamburzev, S., and Appleby, A. J. (2002). "Recent progress in performance improvement of the proton exchange membrane fuel cell (PEMFC)." *Journal of Power Sources*, 107(1), 5-12.

20. Springer, T. E., Zawodzinski, T. A., Wilson, M. S., and Gottesfeld, S. (1996). "Characterization of polymer electrolyte fuel cells using AC impedance spectroscopy." *Journal of the Electrochemical Society*, 143(2), 587-599.

21. Mathias, M., Roth, J., Fleming, J., and Lehnert, W. (2003). "Chapter 46 - Diffusion media materials and characterisation." Handbook of Fuel Cells: Volume 3 - Fuel Cell Technology and Applications, W. Vielstich, H. Gasteiger, and A. Lamm, eds., John Wiley & Sons, Ltd, New York.

22. Chen, B., Dillard, D. A., Dillard, J. G., and Clark, R. L. (2002). "Crack path selection in adhesively bonded joints: the roles of external loads and speciment geometry." *International Journal of Fracture*, 114(2), 167-190.

23. Wilson, M. S., and Gottesfeld, S. (1992). "Thin-Film Catalyst Layers for Polymer Electrolyte Fuel-Cell Electrodes." *Journal of Applied Electrochemistry*, 22(1), 1-7.

24. Li, X., and Sabir, I. (2005). “Review of bipolar plates in PEM fuel cells: Flow-field designs.” *International Journal of Hydrogen Energy*, 30(4), 359-371.

25. Stat-Ease, Inc. 2005, “Design Expert, Version 6.0”, http://www.statease.com/software.html

Appendix A. Expanded Literature Review

Article Name	Author	Sublayer Material	Sublayer Composition	Sublayer Loading/ Thickness	Claims
Improvement of water management by a microporous sublayer for PEMFC	Zhigang Qi	PTFE and Carbon Black (Vulcan XC-72)	25, 35, and 45 % PTFE Also varied loadings from 0 MSL to around 4 mg/cm2	Reflected by carbon loading in layer	MSL controls water management - "not only makes the carbon paper morphology itself less critical, but also improved its capacity to manage water" - "The paper essentially became a support for the sublayer" - Prevents catalysts from getting into carbon paper - **35% was optimal with a loading of 2 mg/cm2**
Optimal composition of polymer electrolyte fuel cell electrodes determined by AC impedance method	J.M. Song	PTFE and Carbon Black **In an alcoholic Suspension - 2-Propanol**	1,5, 3.5, and 10 mg/cm2 and 10, 20, 30, 40% (wt) of PTFE	3.5 mg/cm2 and 30% (wt) about 50 MicroM for the MSL, and about 30 MircoM for the Cat Layer	MSL controls water management - Prevents catalysts from getting into carbon paper - Acts as diffusion control for the reacting species - Claims it is not necessary to place catalyst layer directly on membrane, they actually got better performance out of placing it on MSL - **30% (wt) was optimal**
Novel gas Diffusion layer	Jinhua Chen	PTFE and Carbon Black (Vulcan XC-72R)	NA	20, 50, and 100 MicroM	MSL controls water management - Prevents catalysts from getting into carbon paper
A study of the characteristics of the diffusion layer thickness and porosity of the PEMFC	Han-Kyu Lee	PTFE and Carbon Black (Vulcan XC-72)	30%(wt) - 10:3 ratio for carbon & PTFE	123 microM and a carbon loading of 4.12 mg/cm2	They tested a range of electrode thickness and concluded that an intermediate thickness was optimal
Effective Diffusivity and water-saturation distribution in single and two-layer PEMFC diffusion Media	Jin Hyun Nam	PTFE and Carbon Black	NA	Optimal = 1/3 total GDL + MSL	This thickness is based upon Network Model for species diffusion UFT - Unsaturated Flow Theory

Two-Phase transport and the role of micro-porous layer in polymer electrolyte fuel cells	U. Pasaogullari	PTFE and Carbon Black	NA	Optimal = .1 to .15 total GDL + MSL	This thickness is based upon M2 theory for species diffusion
Influence of different Gas diffusion Layers on the water management of the PEFC Cathode	B. Thoben	PTFE and Carbon Black	ELAT wont tell me!	ELAT wont tell me! We measured about 25% of total thickness being MSL for LT 1200	Single Sided performed better than double sided, and double sided performed better then having nothing
Effects of hydrophobic polymer content in the GDL on the power performance of a PEM fuel cell	Chan Lim	PTFE and Carbon Black	40 wt% carbon loading of 1.5 mg/cm2	NA	MSL did not improve performance - at higher current densities it appears that MSL imposes an additional diffusion resistance to oxygen transport into the catalyst layer, making the mass transport limiting current smaller - They also say "NOTE: when properly designed and fabricated, MSL should be also beneficial at high current densities
Effect of PTFE contents in the gas diffusion media on the performance of PEMFC	Gu-Gon Park	NA	NA	NA	When an MSL is applied there was no severe flooding, even at relative humidity's of 190% - "MSL plays an important role in water management in regard to stability as well as electrical conductivity"

Diffusion layer parameters influencing optimal fuel cell performance	L.R. Jordan	PTFE and Carbon Black (Vulcan XC-72R) OR Acetylene Black Susoended ins Cyclohexane	19, 15, 29, 39, 49 (wt%) PTFE	15, 25, 35, 50, 60 micro meters	Acetylene black gave ~15% improvement in maximum power density when campared to Carbon Black
Development and Electrochemical studies of gas Diffusion Electrodes of Polymer Electrolyte Fuel Cells	V. A. Paganin	PTFE and Carbon Black (Vulcan XC-72)	10, 15 20, 30, 40 (wt%) PTFE with a constant thickness of 50um	15, 25, 35, 50, 65 um with constant comp of 40 (wt%), thickness is sum of GDL and MSL	beteen 35 and 50 icrons thick, and a composition of about 15
Effects of the Diffusion Layer Characteristcs on the performance of polymer electrolyte fuel cell electrodes	E. Passalacqua	explored Vulcan XC-72, Acetylene Black (SAB), and L and Asbury 850	20 wt %	2.5 - 5 mg/cm2	Suggests the use of SAB - Claims the larger pore size of SAB helps with diffusion limititation
Influence of the PTFE Content in the Diffusion Layer of low-PT loading electrodes for polymer electrolyte fuel cellss	L. Giorgi	Vulcan XC-72	Varied from 10-60 wt PTFE	Constant at 2 mg/cm2	

Appendix B. MSL Application Optimization Images

Example of Good MSL Application

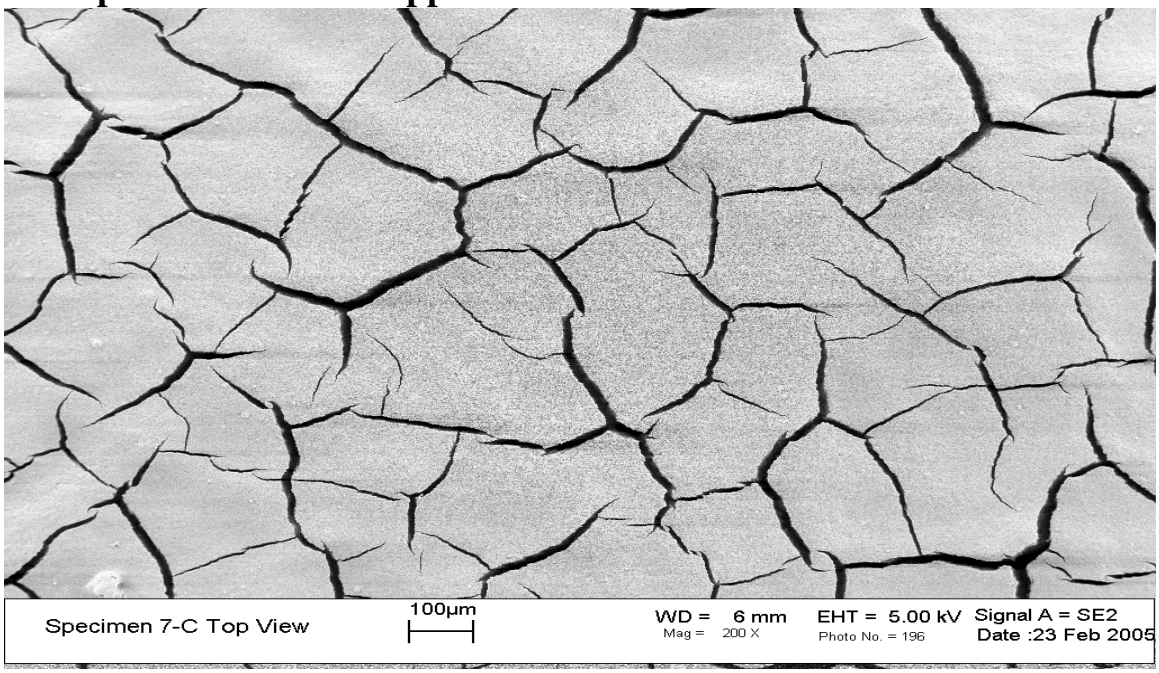

Figure B-1. 200X SEM from the top-center of Specimen 7

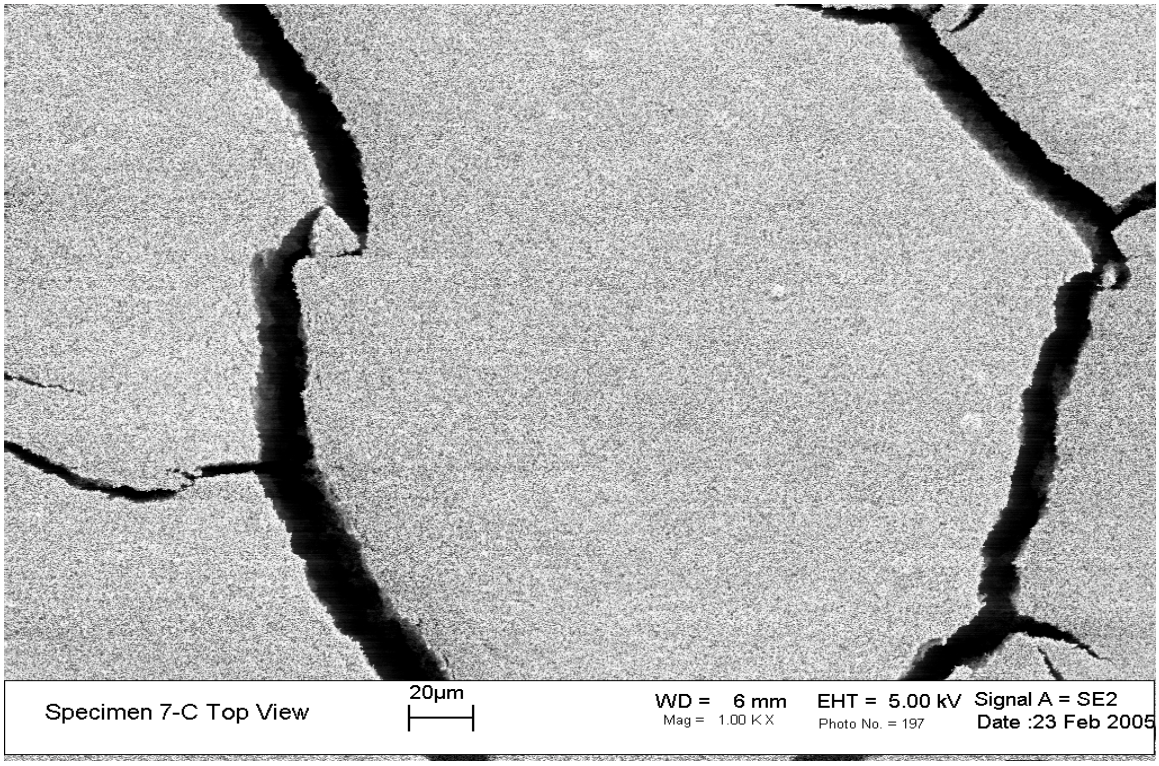

Figure B-2. 1000X SEM from the top-center of Specimen 7

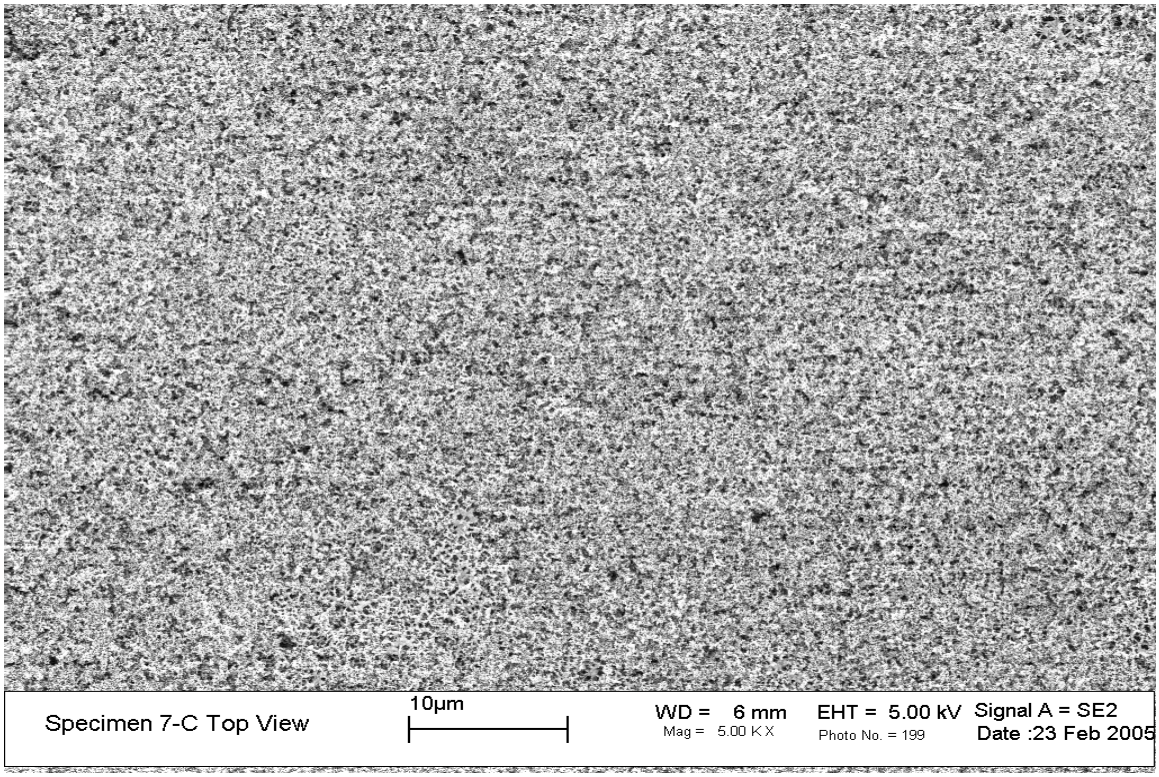

Figure B-3. 5000X SEM from the top-center of Specimen 7

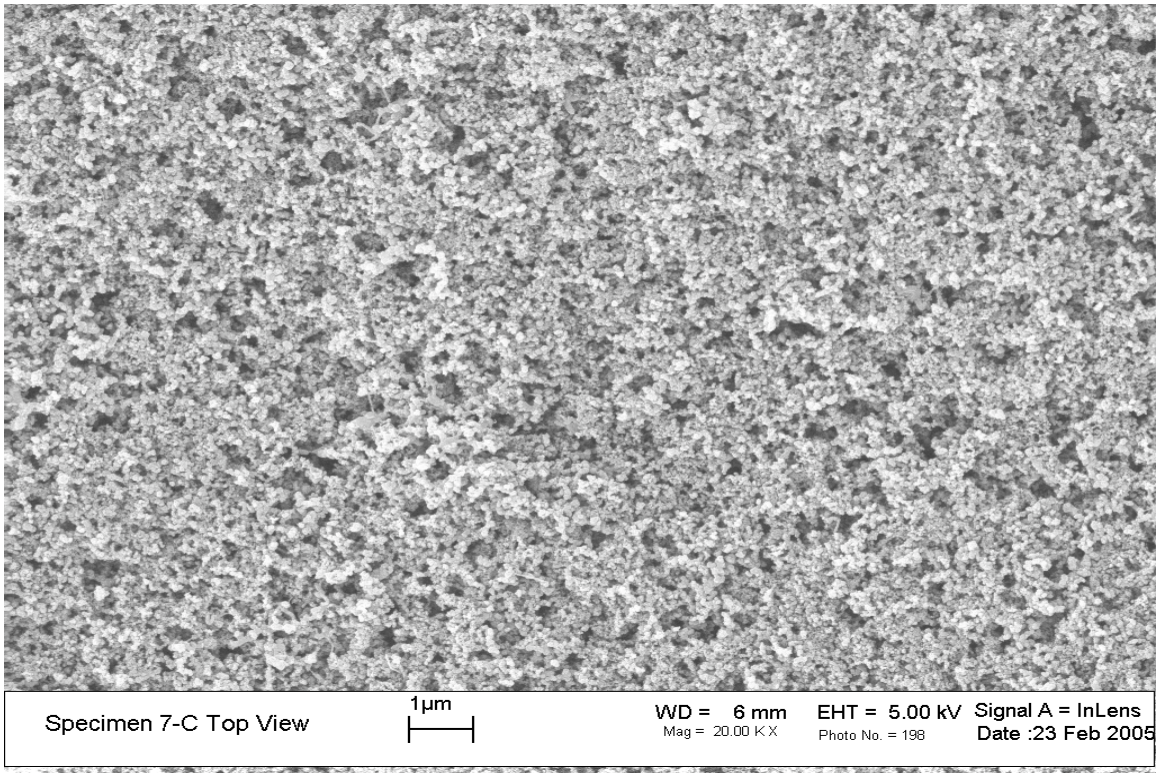

Figure B-4. 20000X SEM from the top-center of Specimen 7

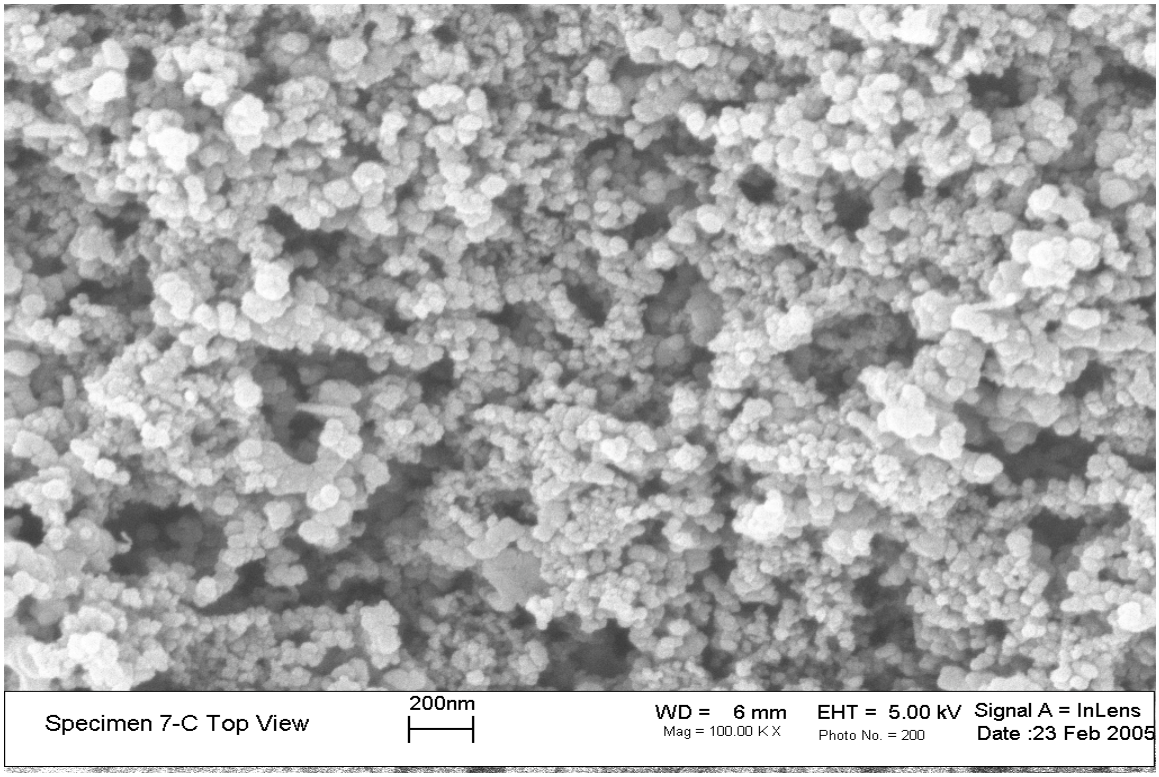

Figure B-5. 100000X SEM from the top-center of Specimen 7

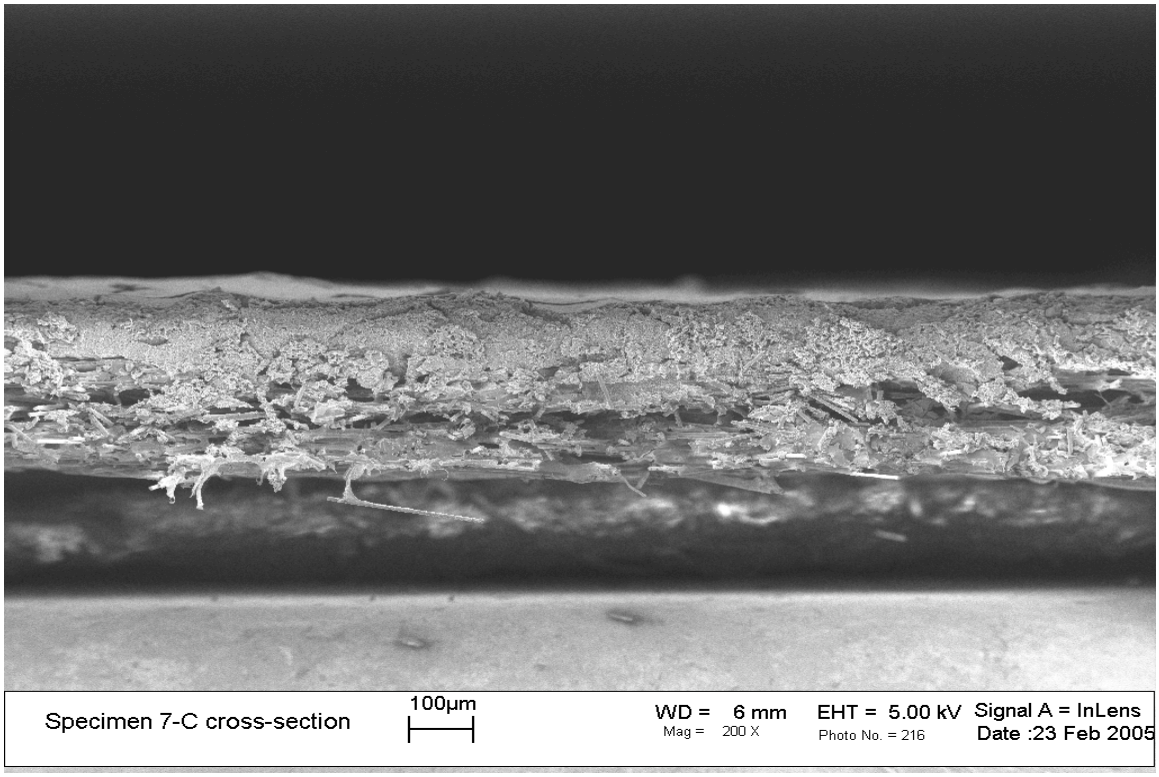

Figure B-6. 200X SEM cross-section from center of Specimen 7

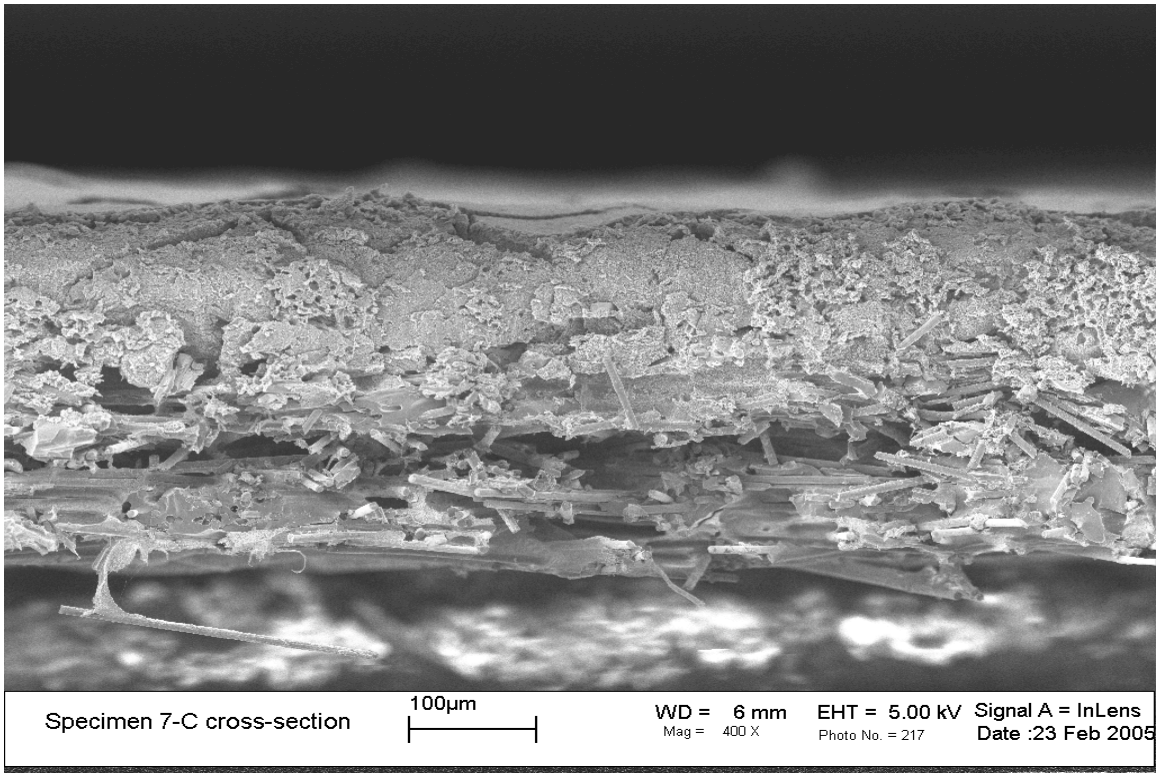

Figure B-7. 400X SEM cross-section from center of Specimen 7

Example of Poor MSL Application

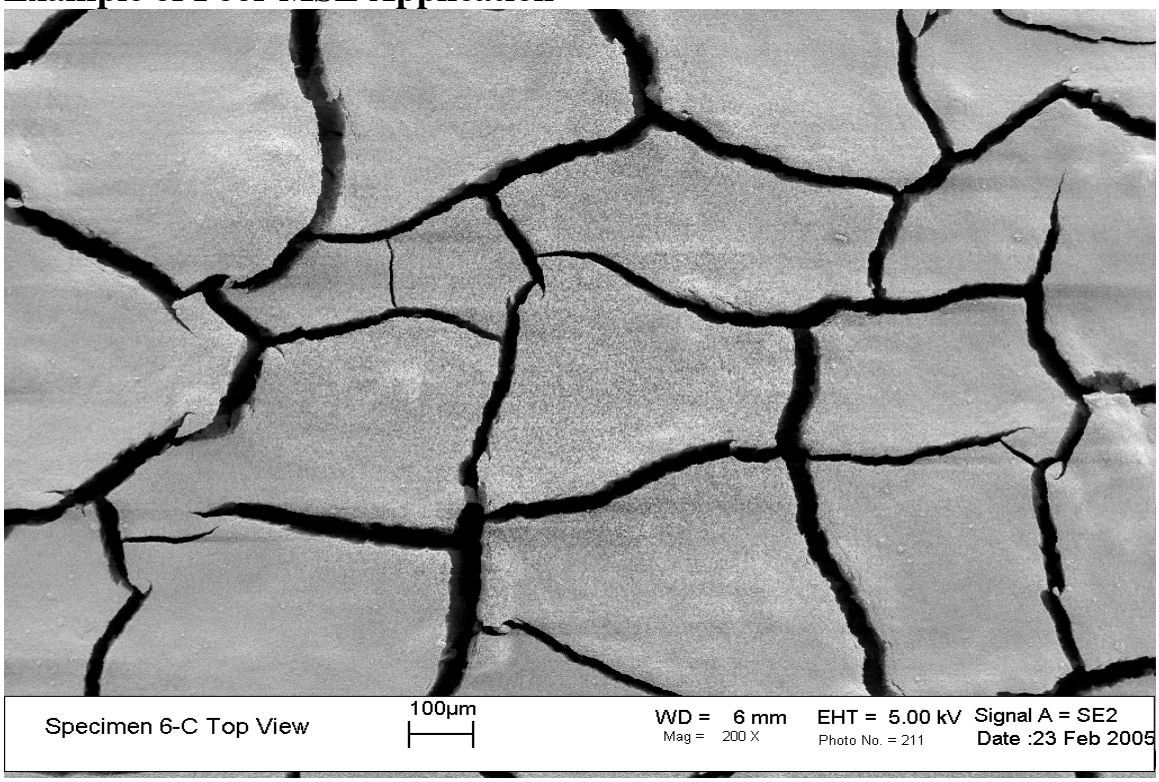

Figure B-8. 200X SEM from the top-center of Specimen 6

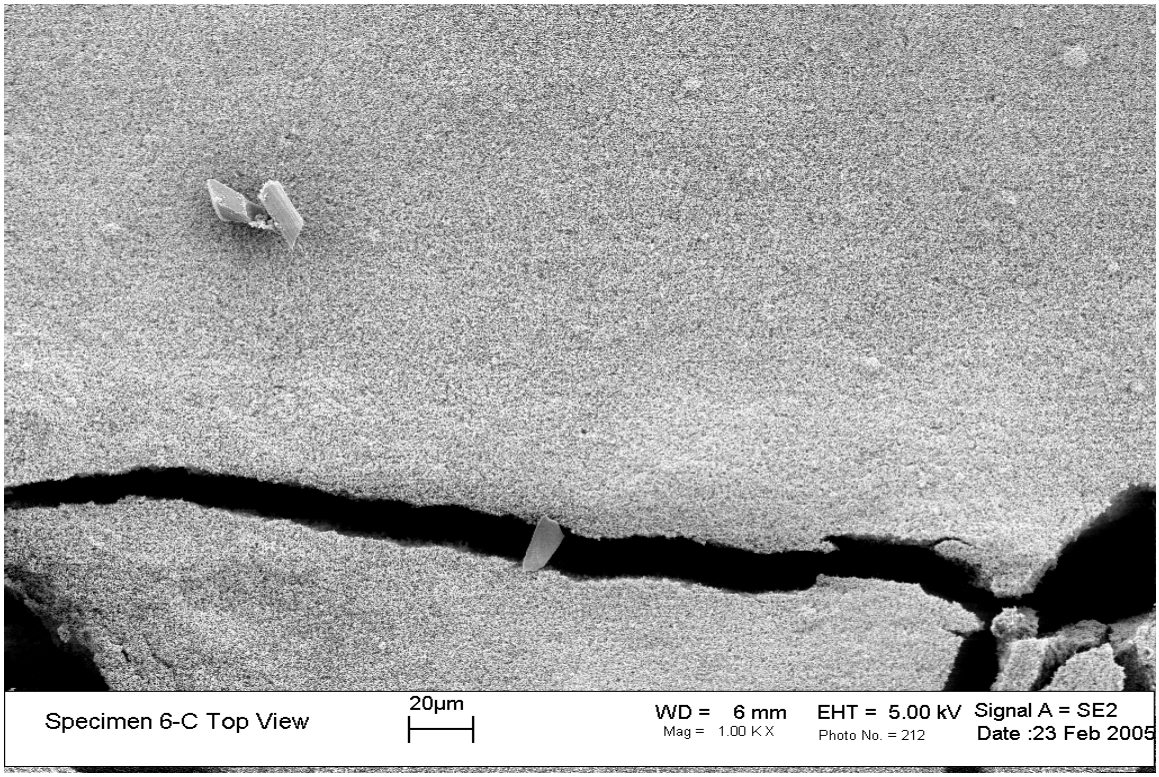

Figure B-9. 1000X SEM from the top-center of Specimen 6

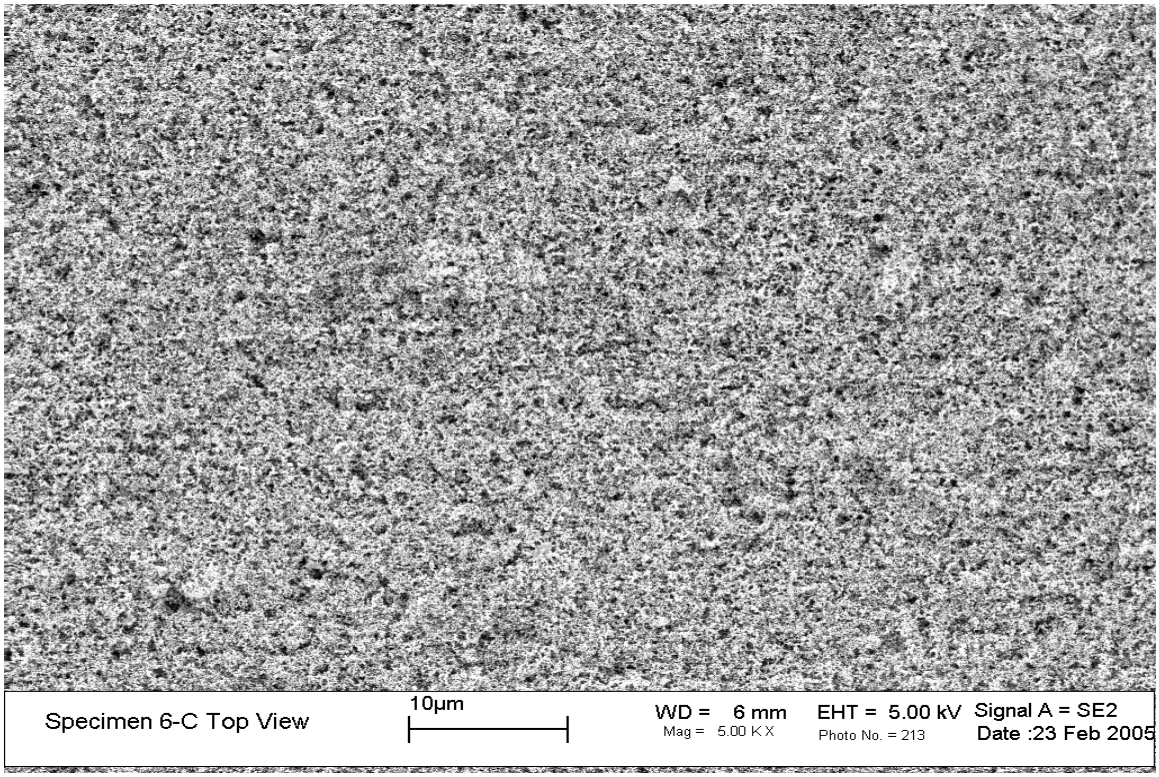

Figure B-10. 5000X SEM from the top-center of Specimen 6

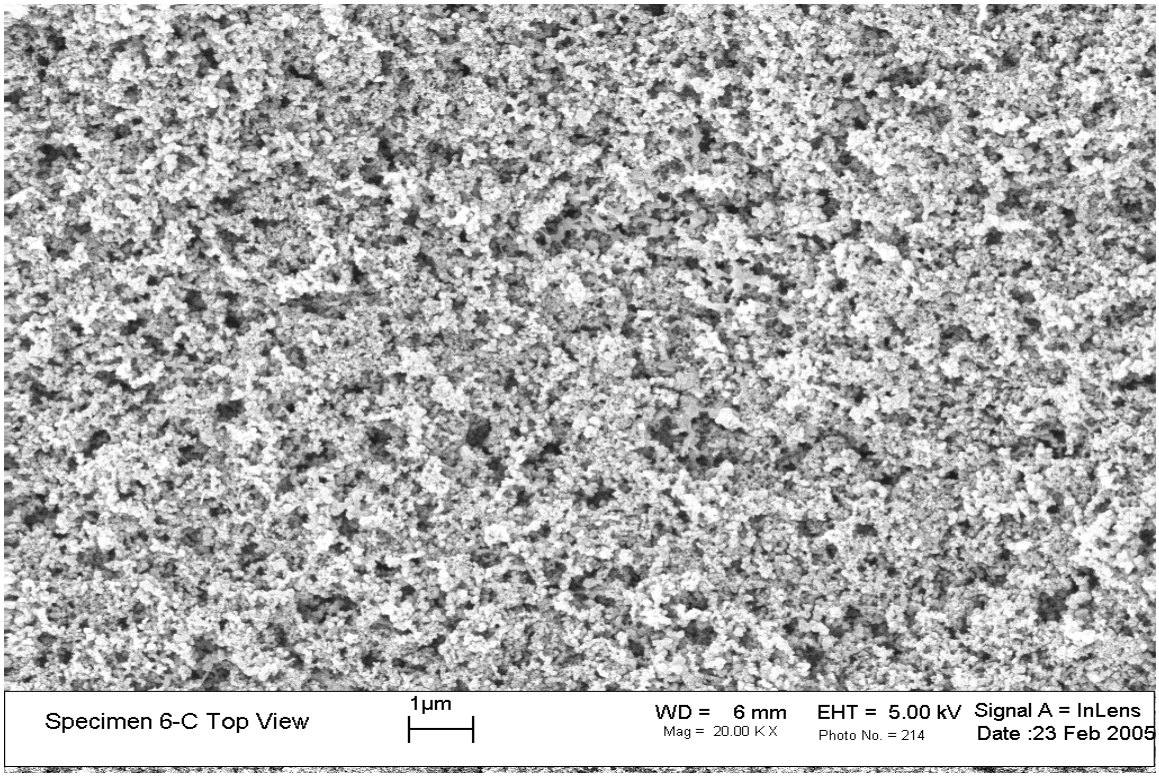

Figure B-11. 20000X SEM from the top-center of Specimen 6

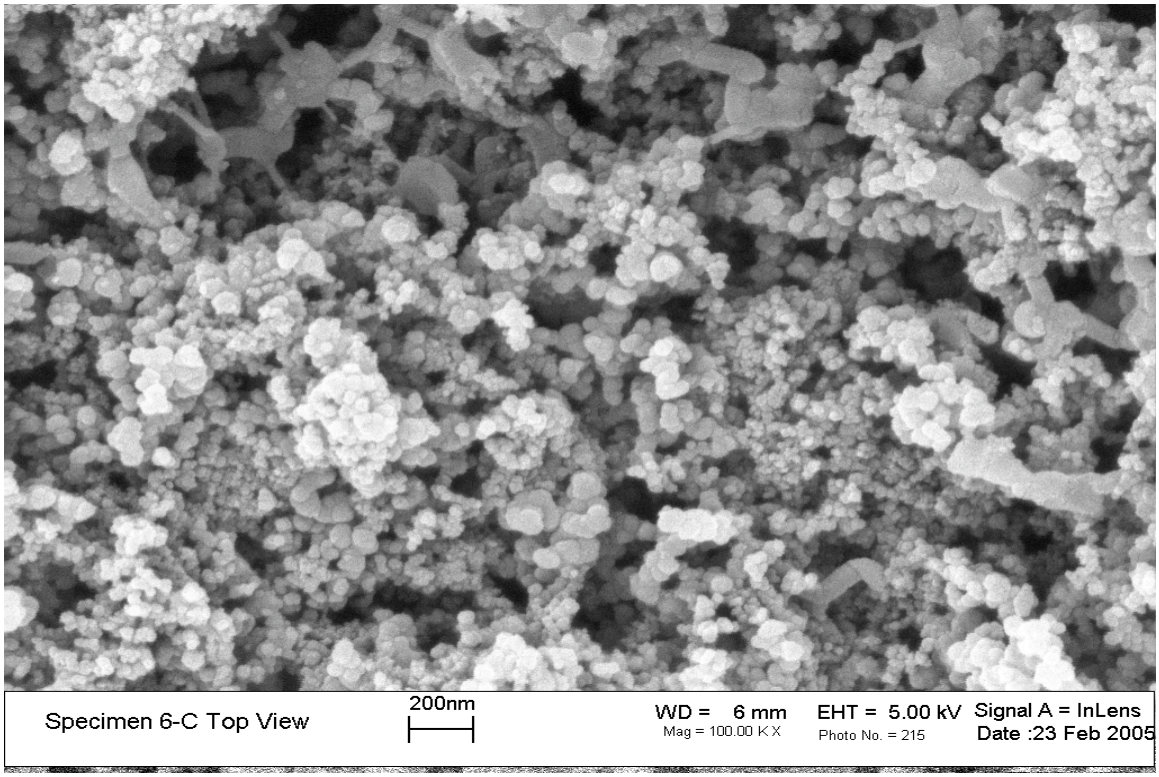

Figure B-12. 100000X SEM from the top-center of Specimen 6

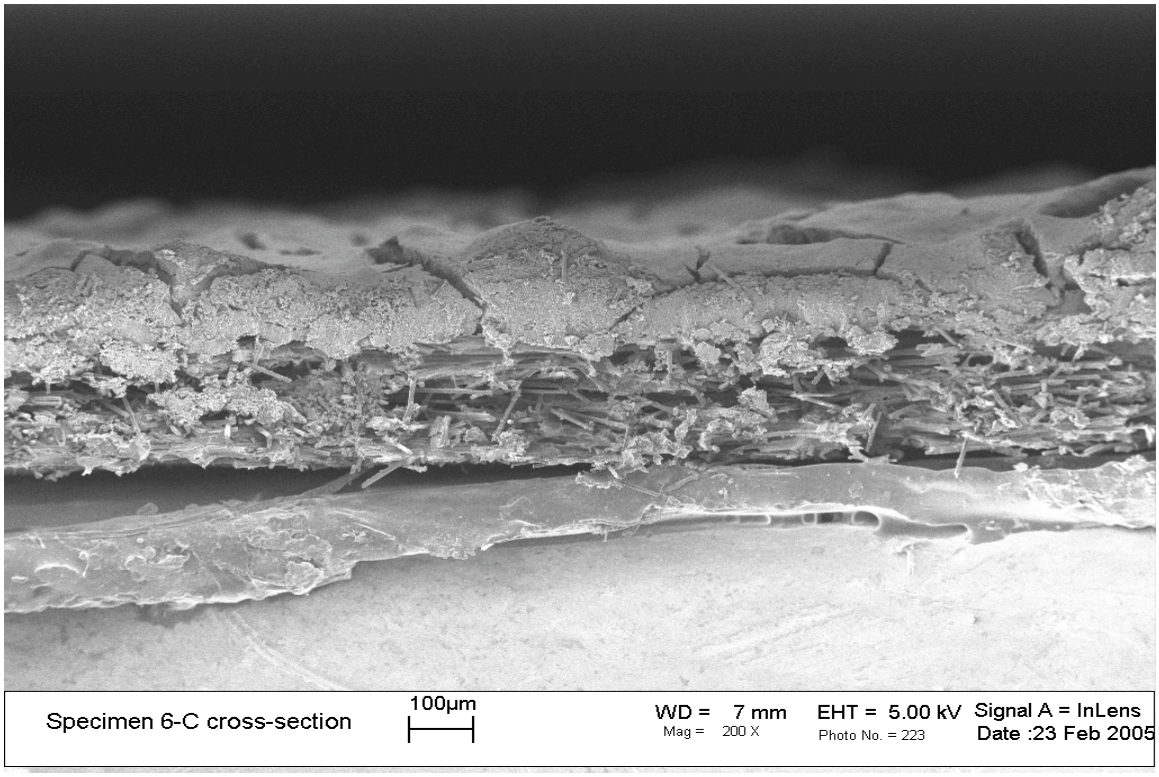

Figure B-13. 200X SEM cross-section from center of Specimen 6

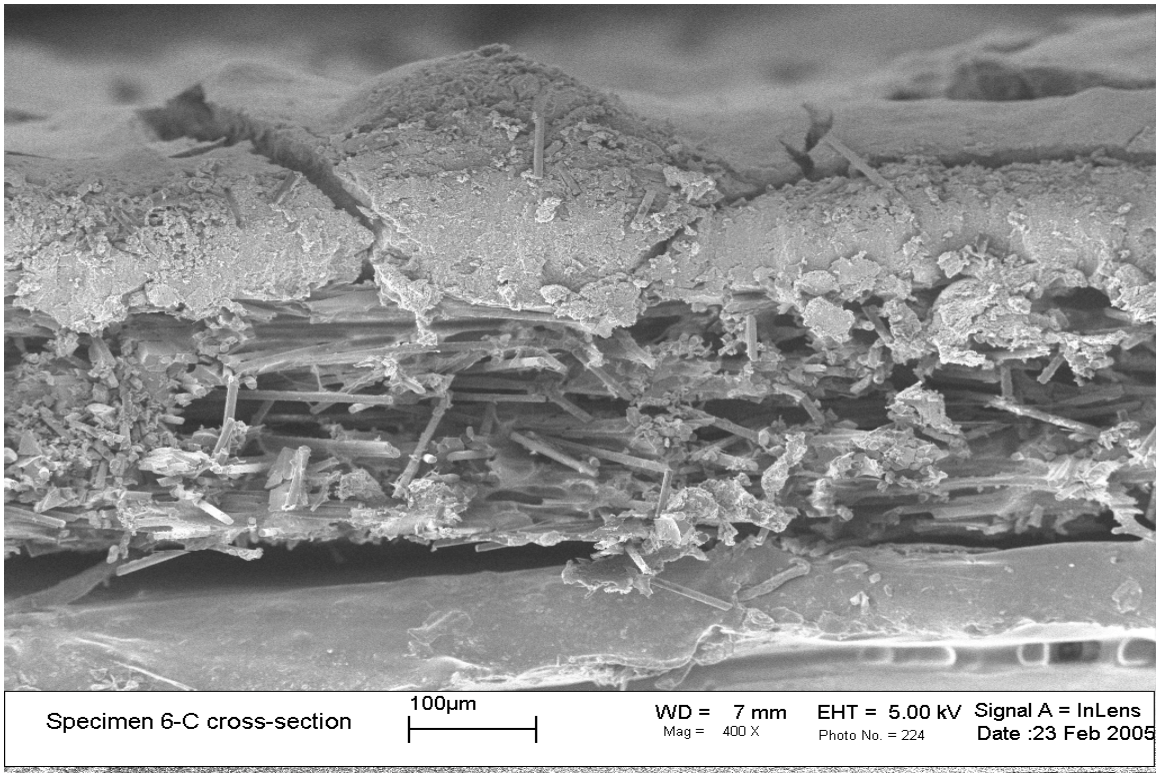

Figure B-14. 400X SEM cross-section from center of Specimen 6

Appendix C. Performance Design Point Plots

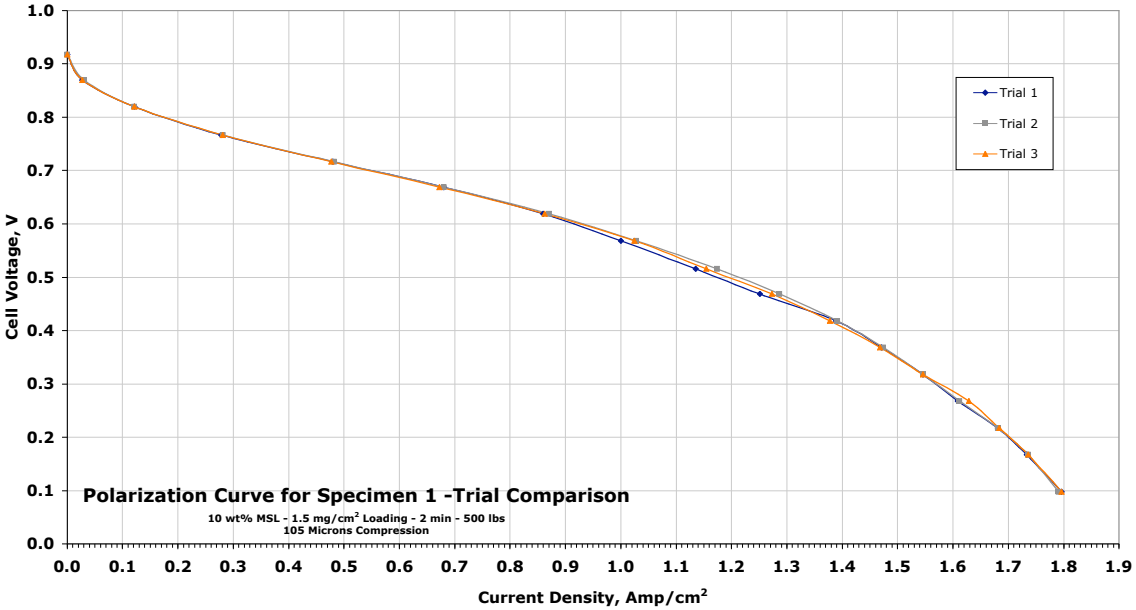

Figure C-1. Performance results for design point 1

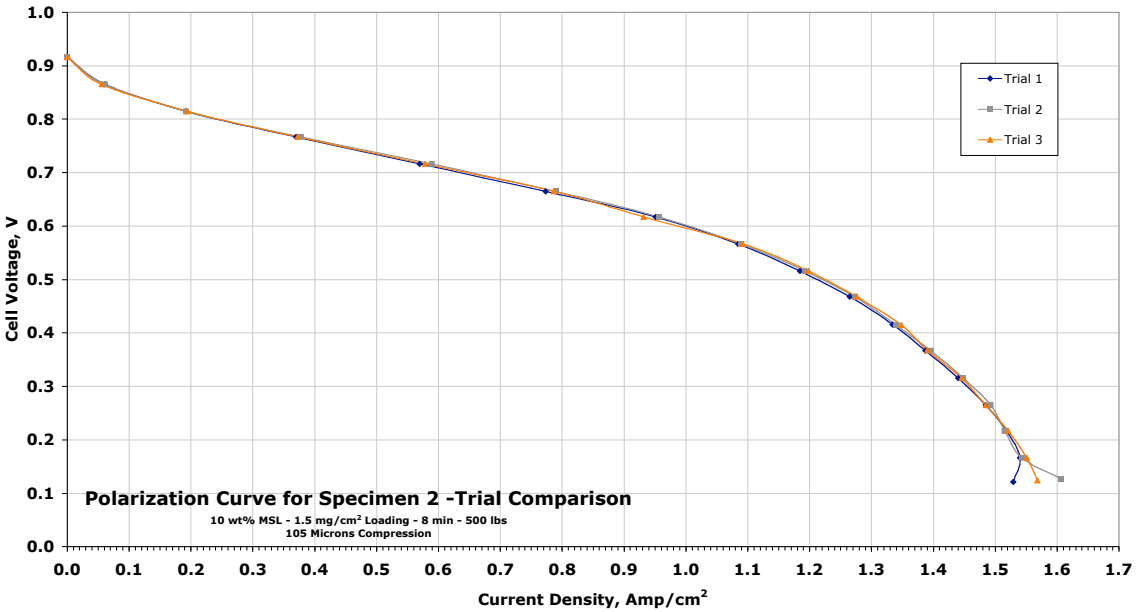

Figure C-2. Performance results for design point 2

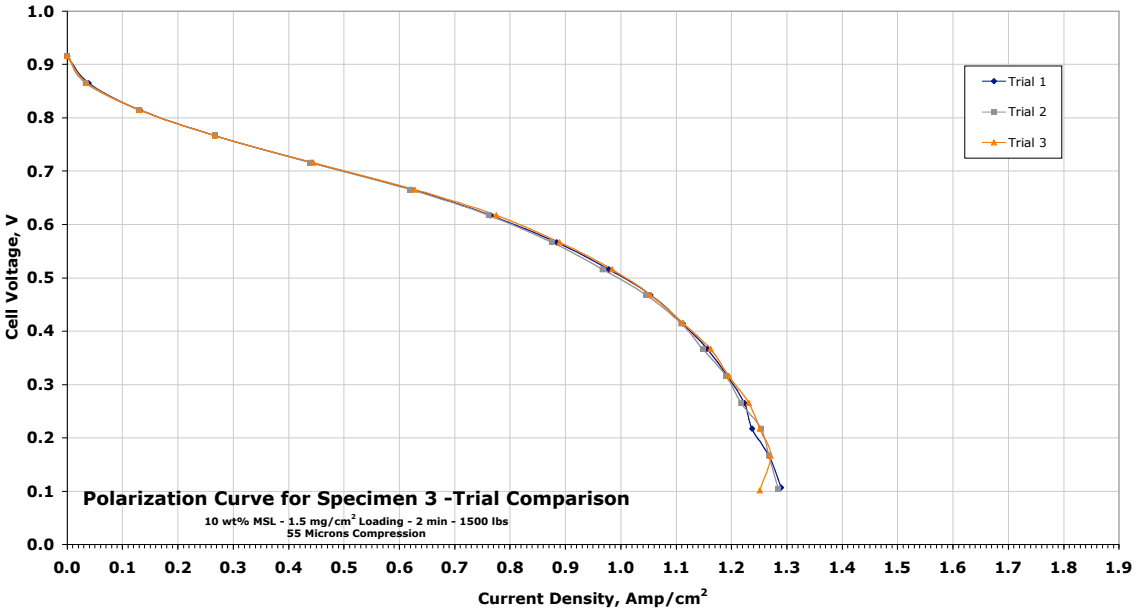

Figure C-3. Performance results for design point 3

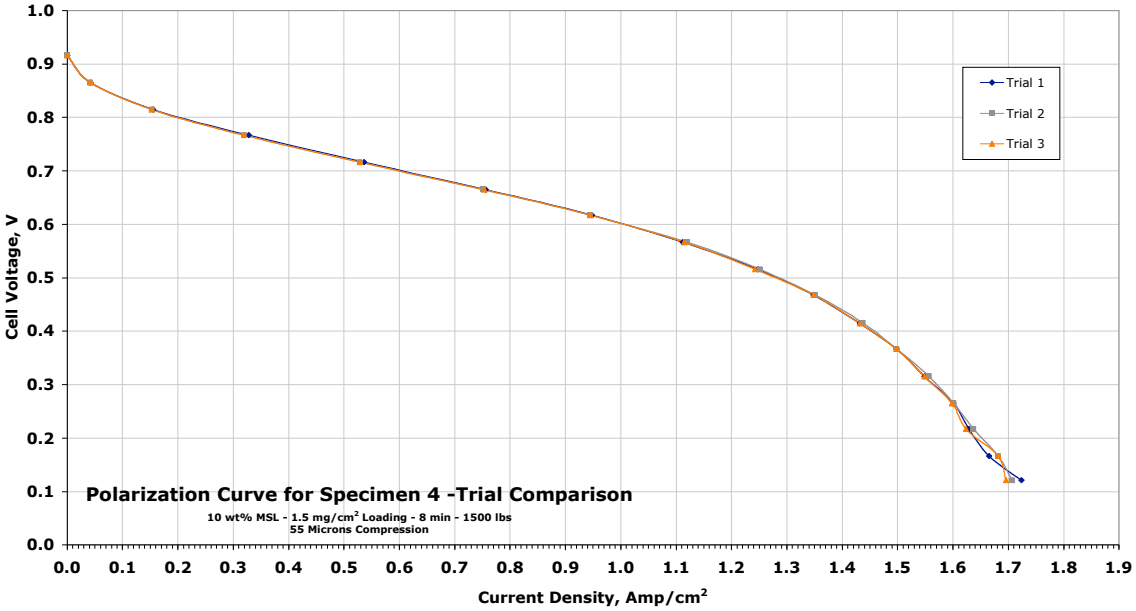

Figure C-4. Performance results for design point 4

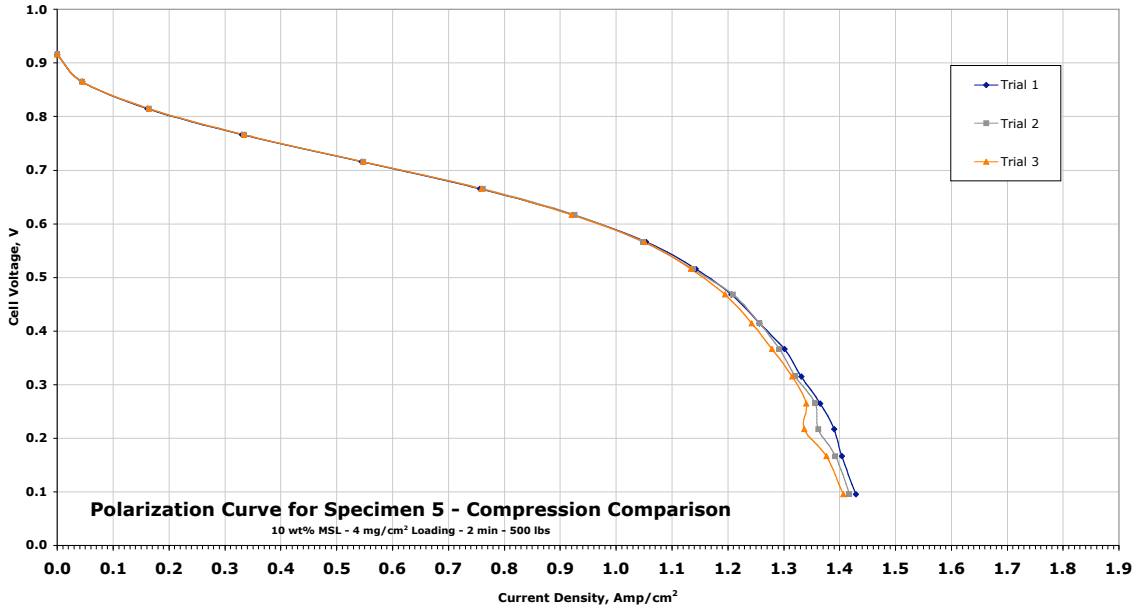

Figure C-5. Performance results for design point 5

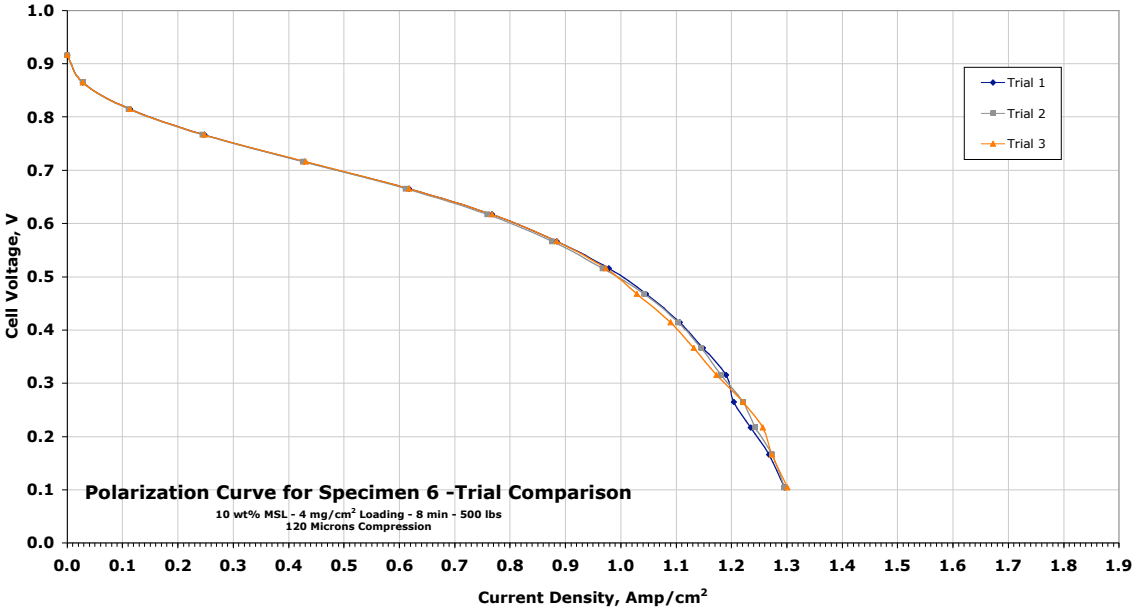

Figure C-6. Performance results for design point 6

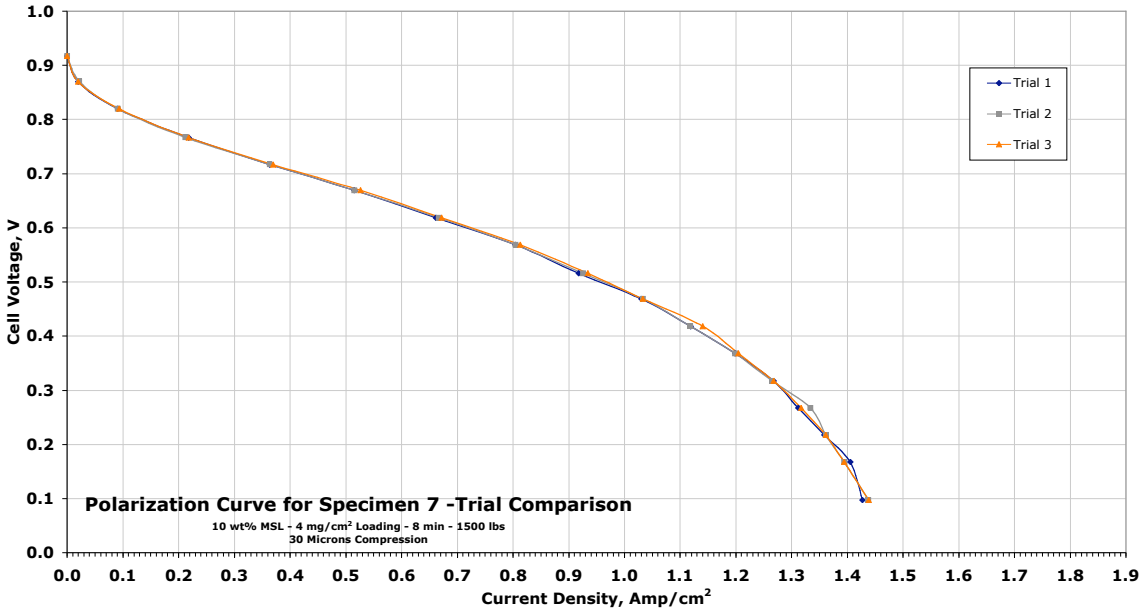

Figure C-7. Performance results for design point 7

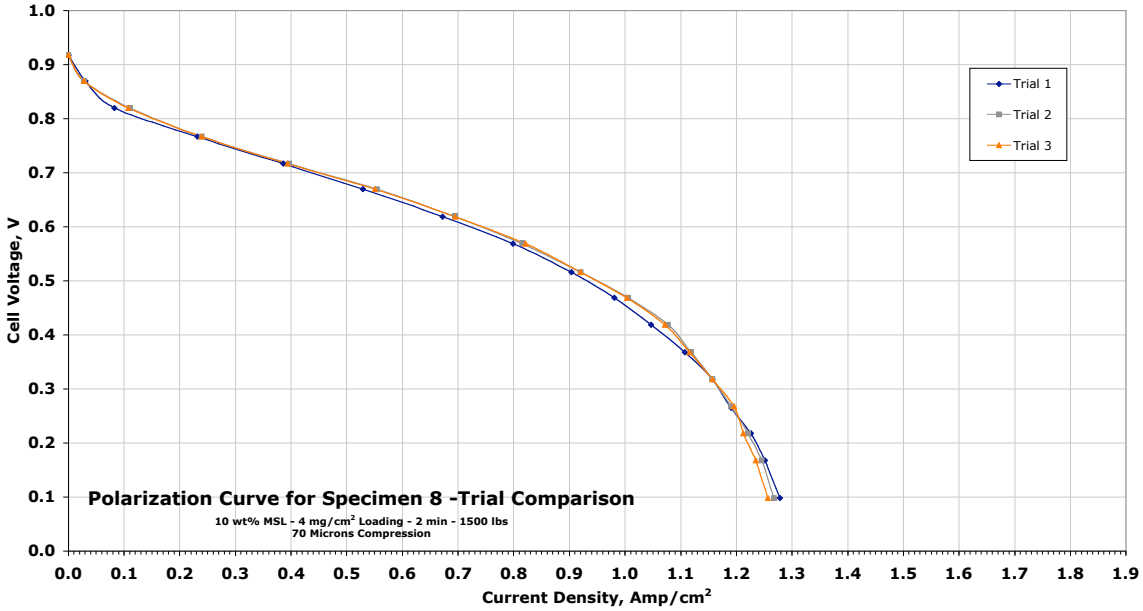

Figure C-8. Performance results for design point 8

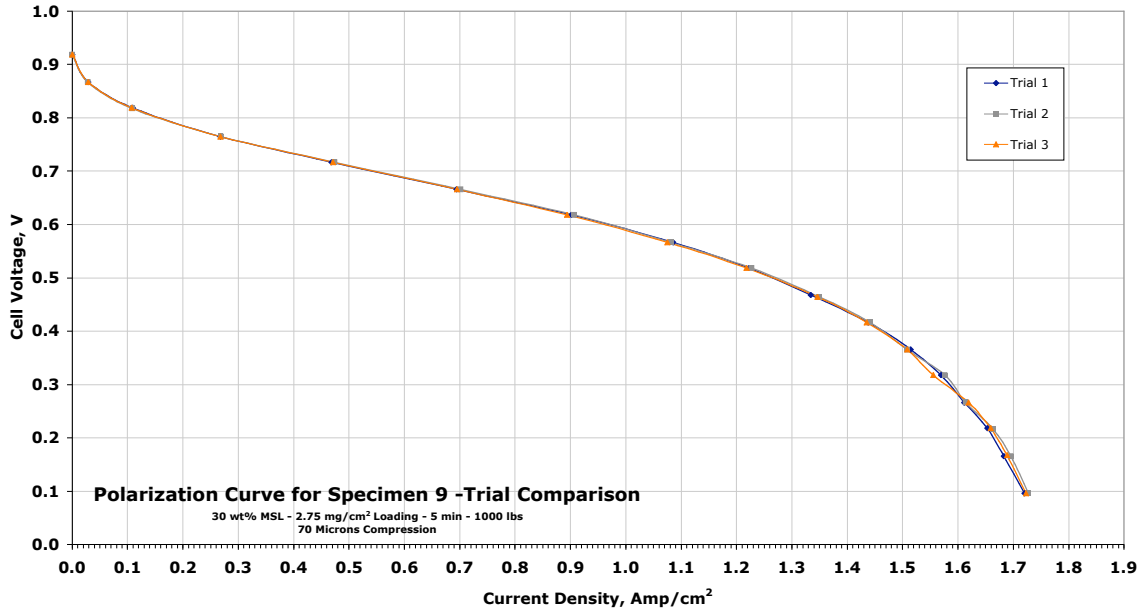

Figure C-9. Performance results for design point 9

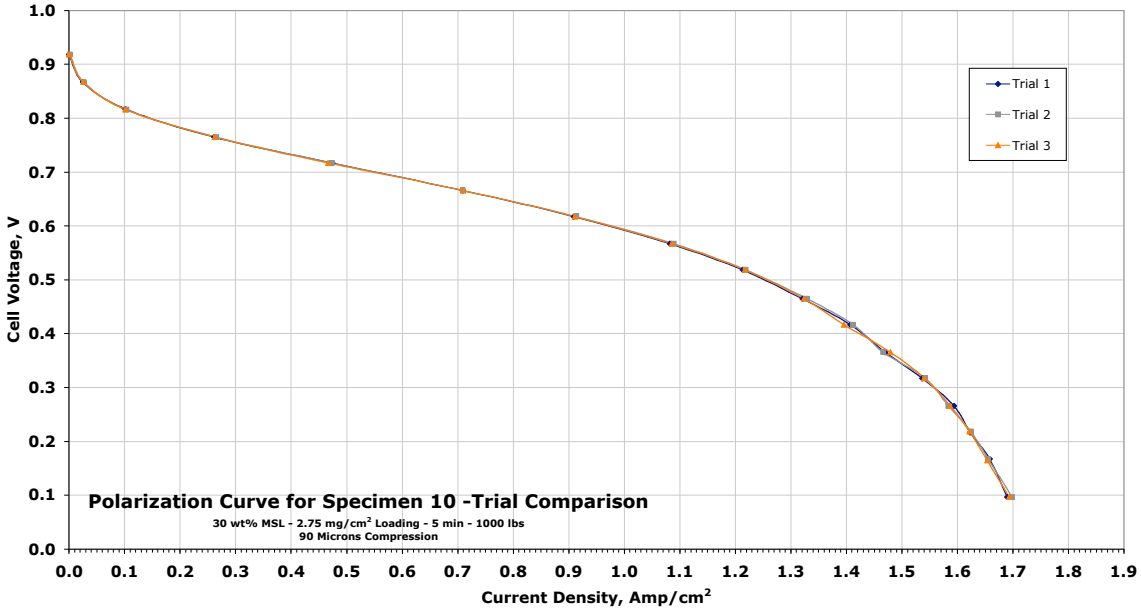

Figure C-10. Performance results for design point 10

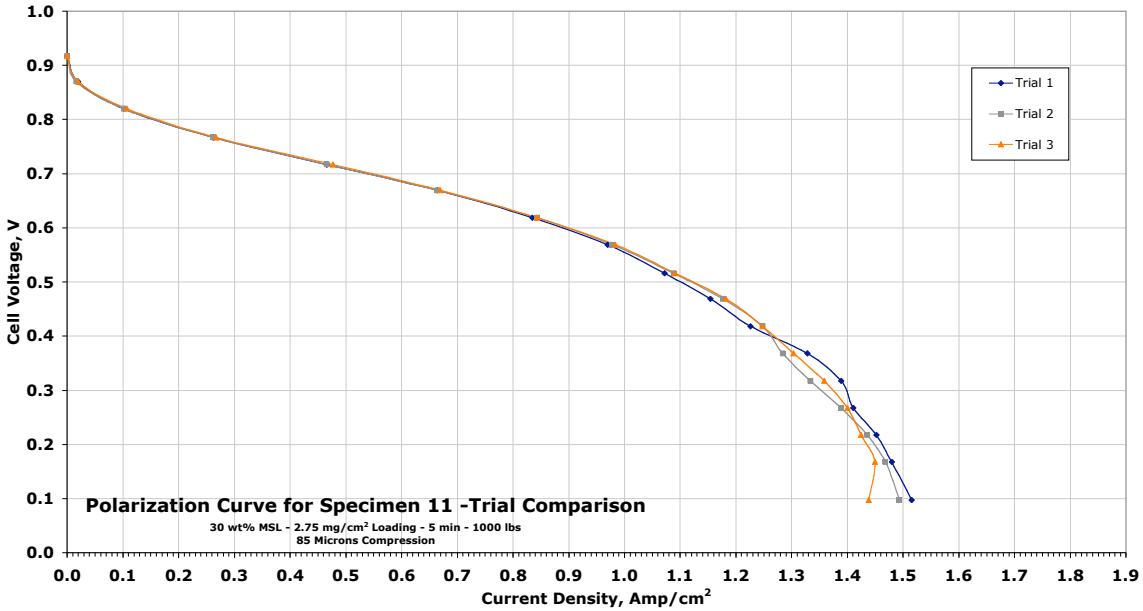

Figure C-11. Performance results for design point 11

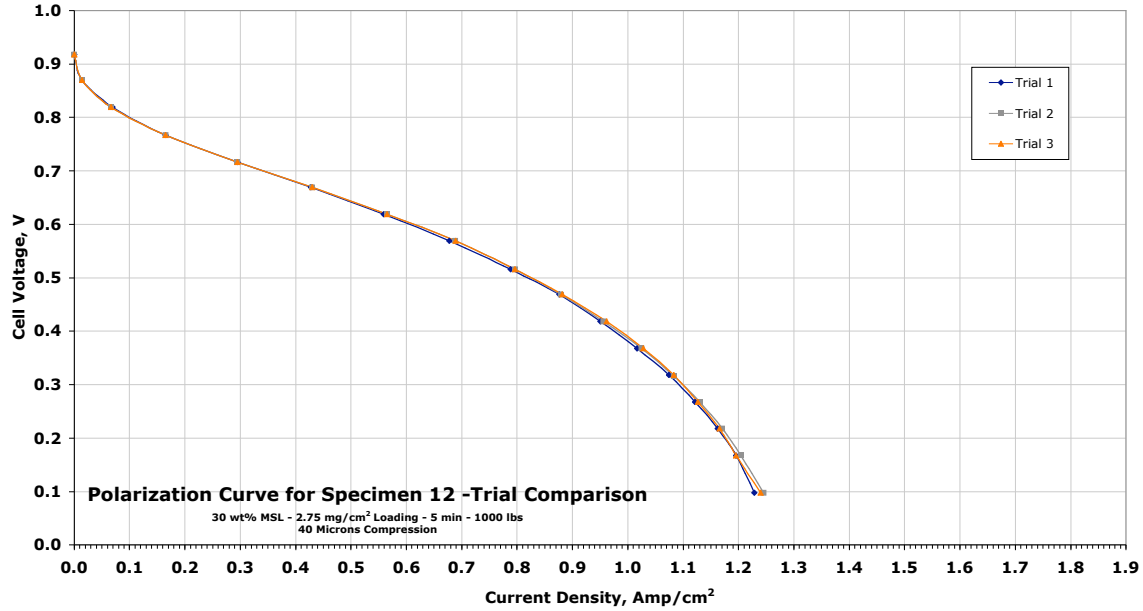

Figure C-12. Performance results for design point 12 (Deleted from matrix)

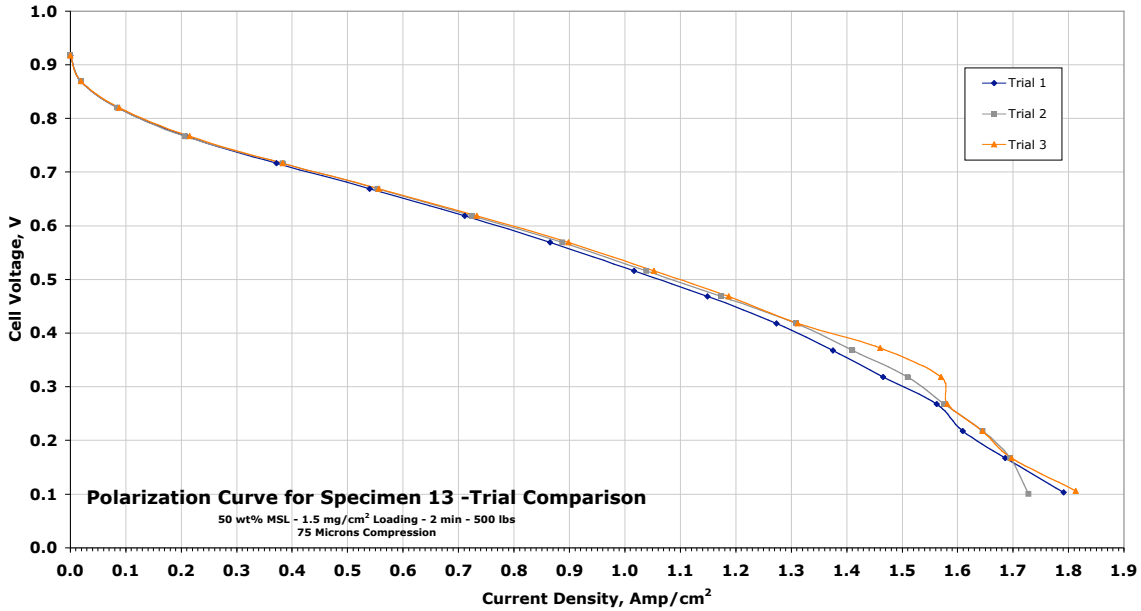

Figure C-13. Performance results for design point 13

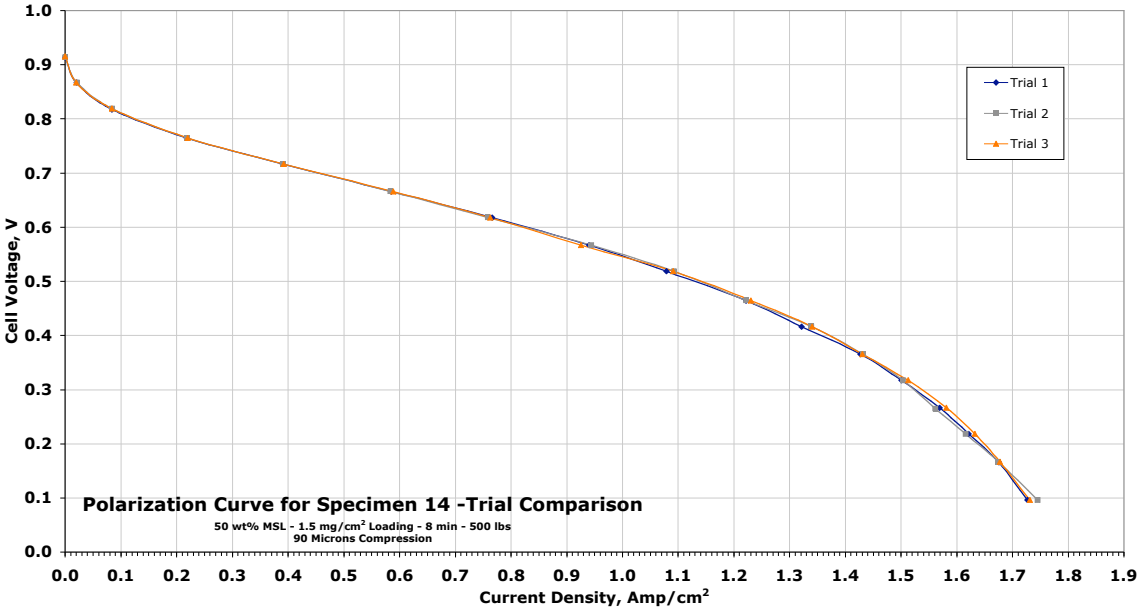

Figure C-14. Performance results for design point 14

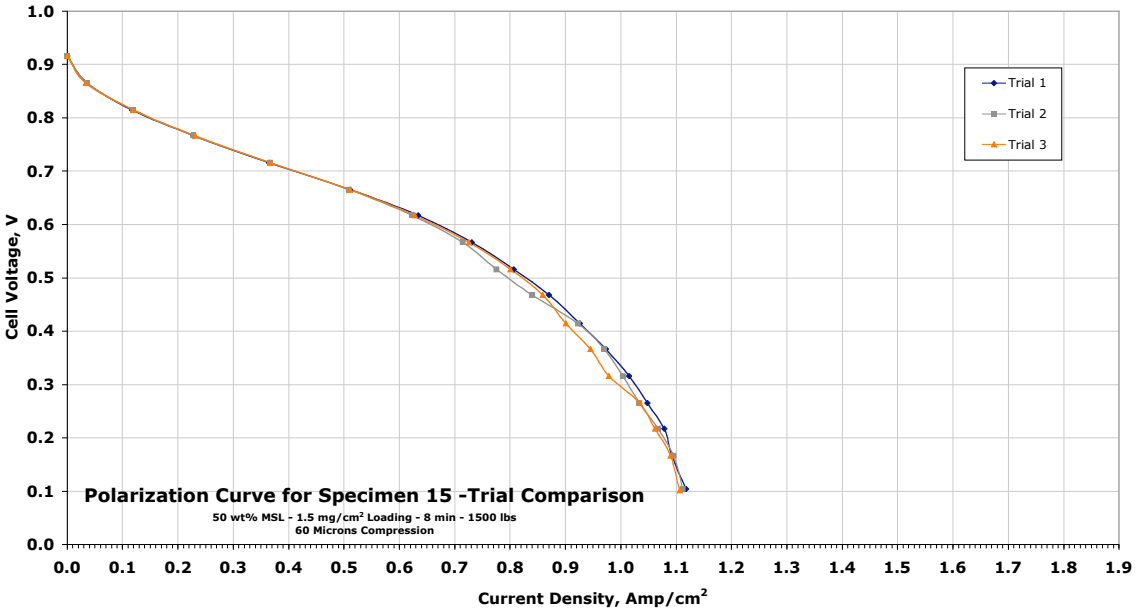

Figure C-15. Performance results for design point 15

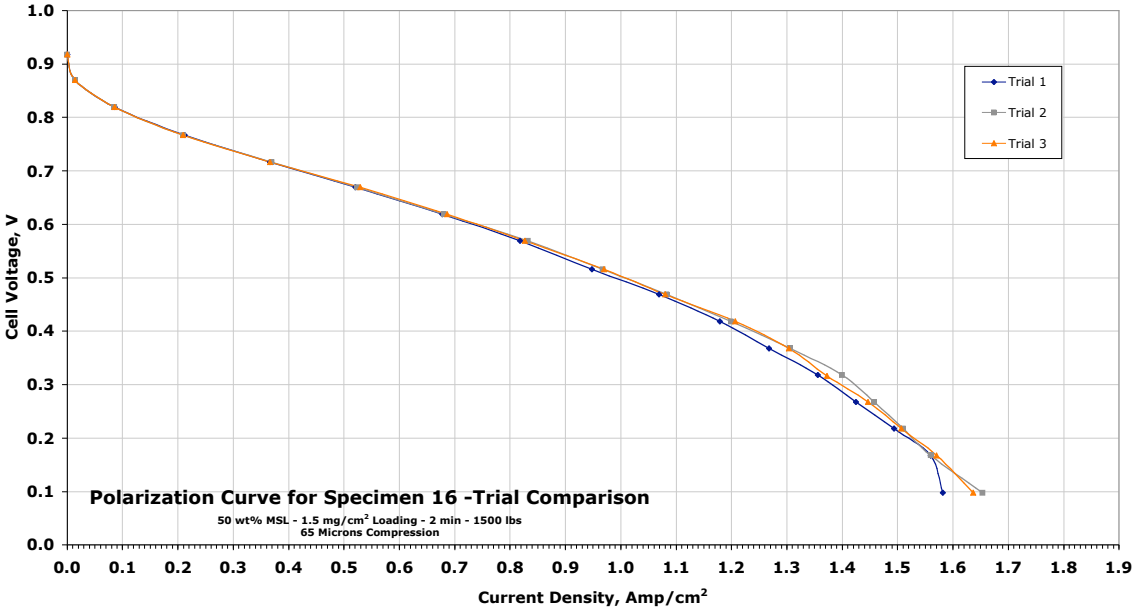

Figure C-16. Performance results for design point 16

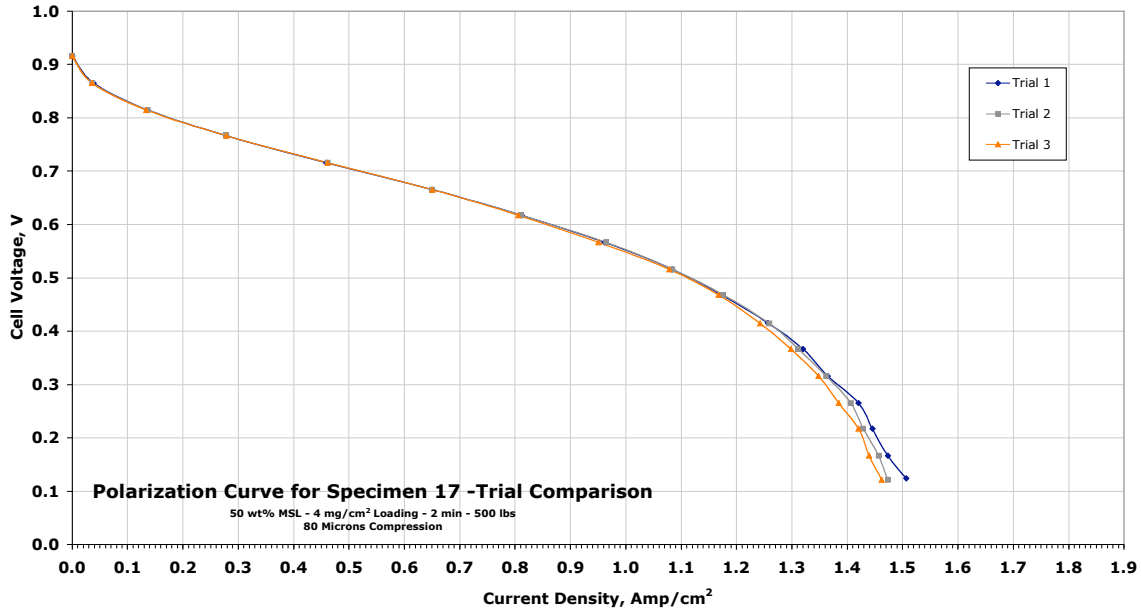

Figure C-17. Performance results for design point 17

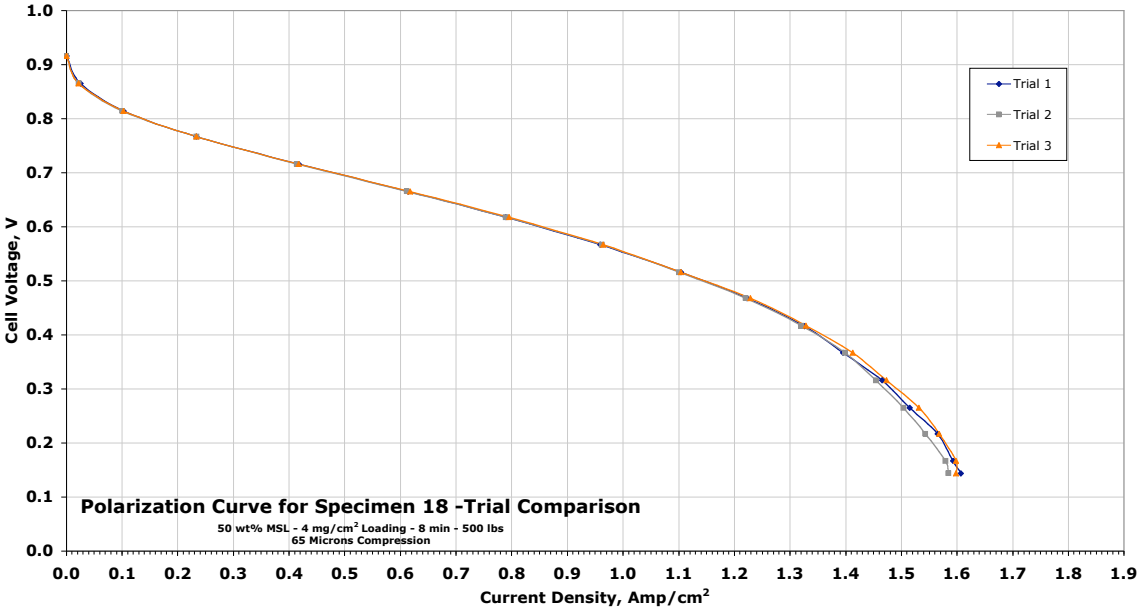

Figure C-18. Performance results for design point 18

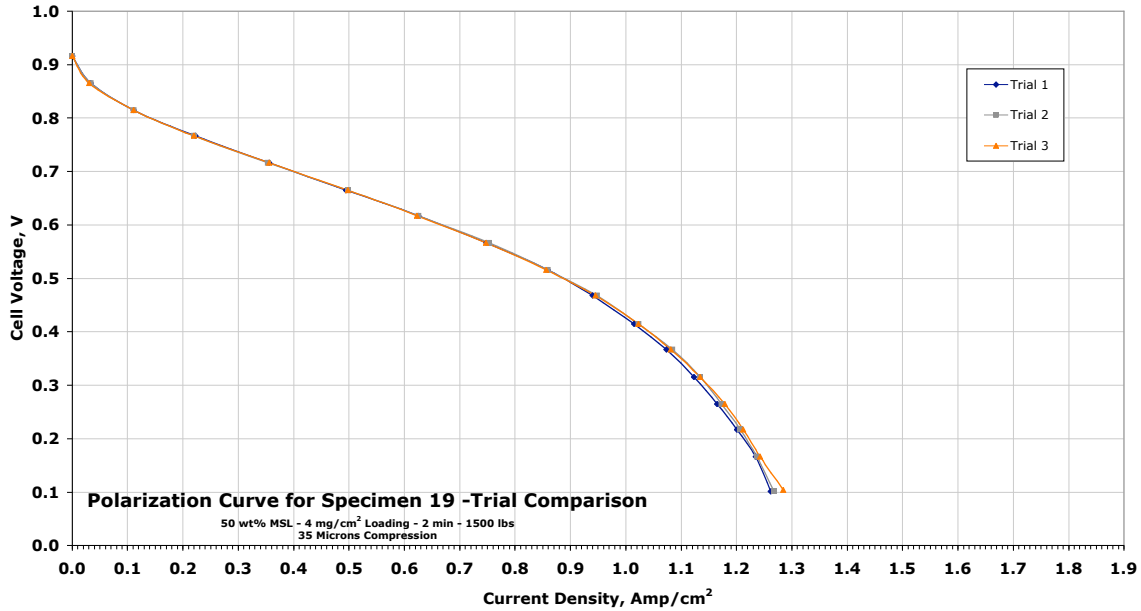

Figure C-19. Performance results for design point 19

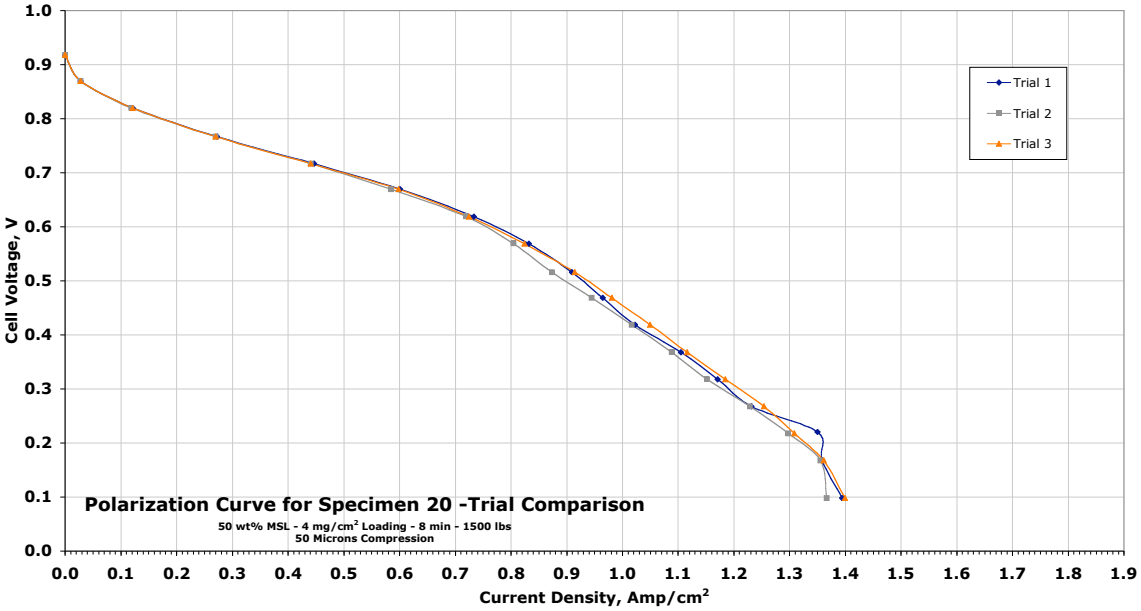

Figure C-20. Performance results for design point 20

Appendix D. Adhesion Design Point Plots

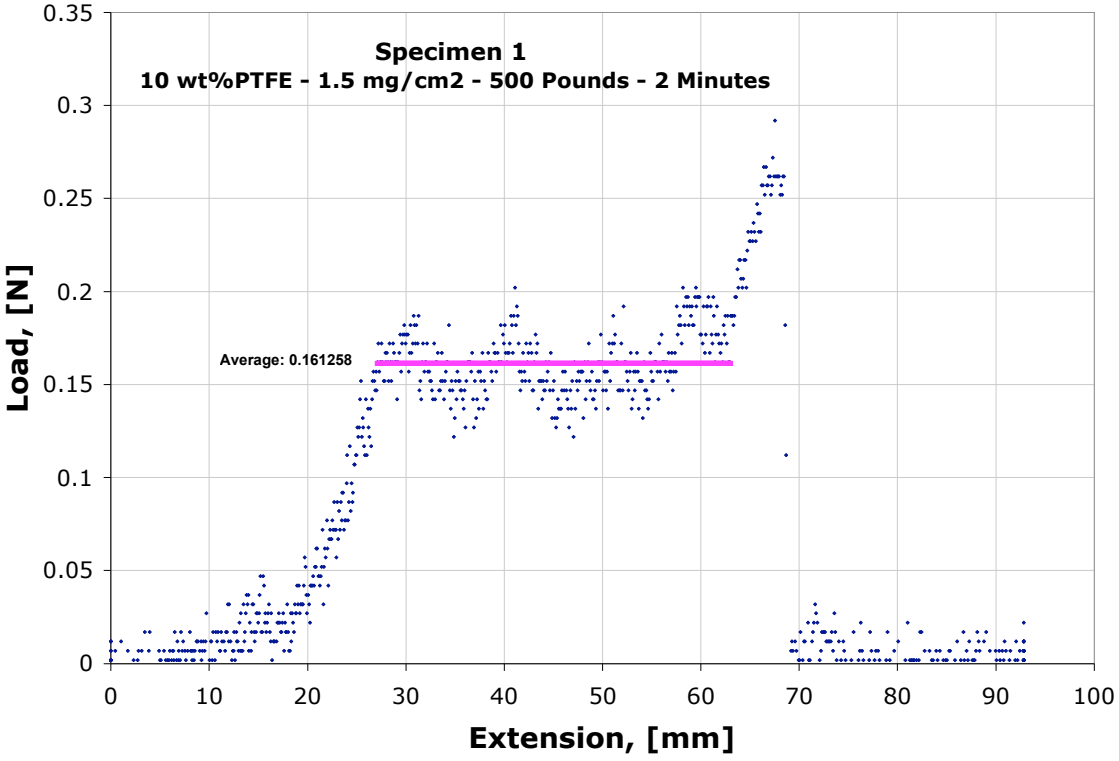

Figure D-1. Adhesion results for design point 1

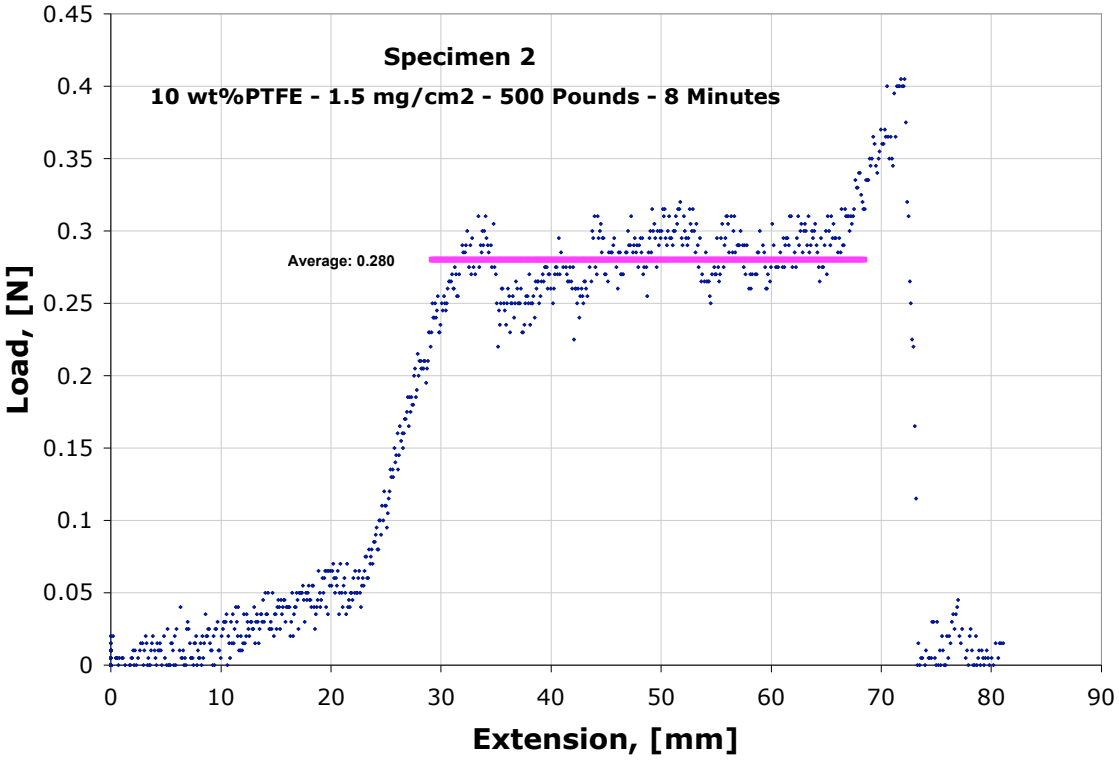

Figure D-2. Adhesion results for design point 2

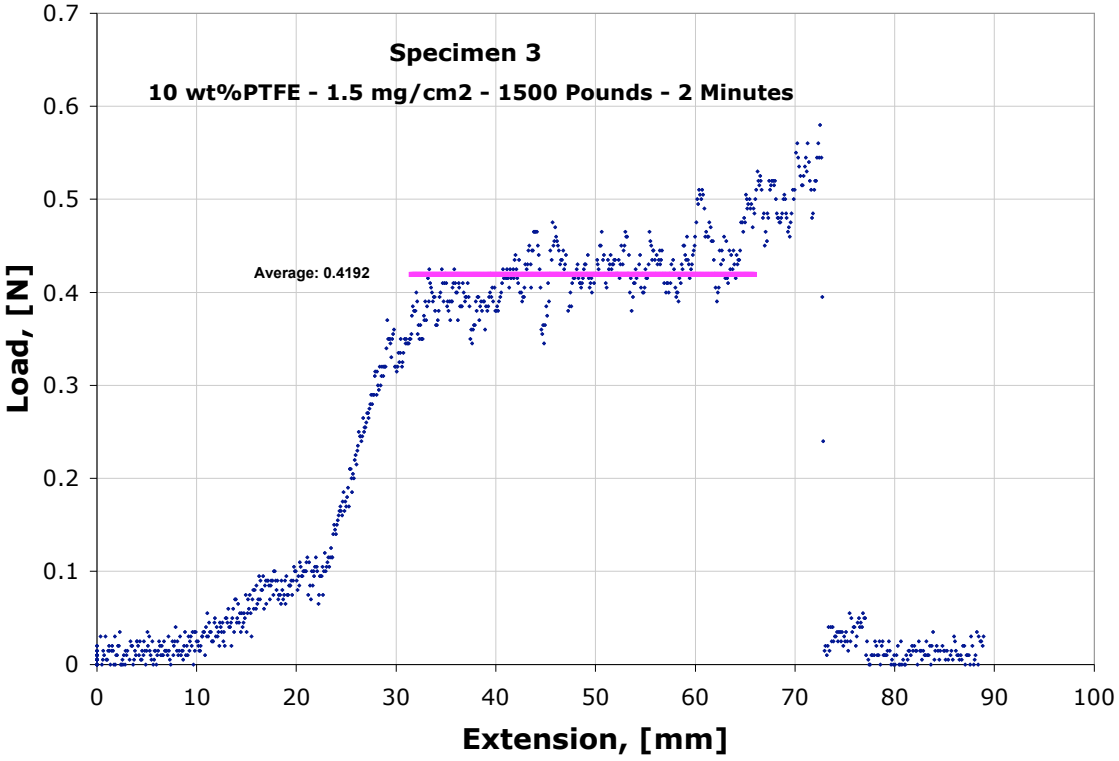

Figure D-3. Adhesion results for design point 3

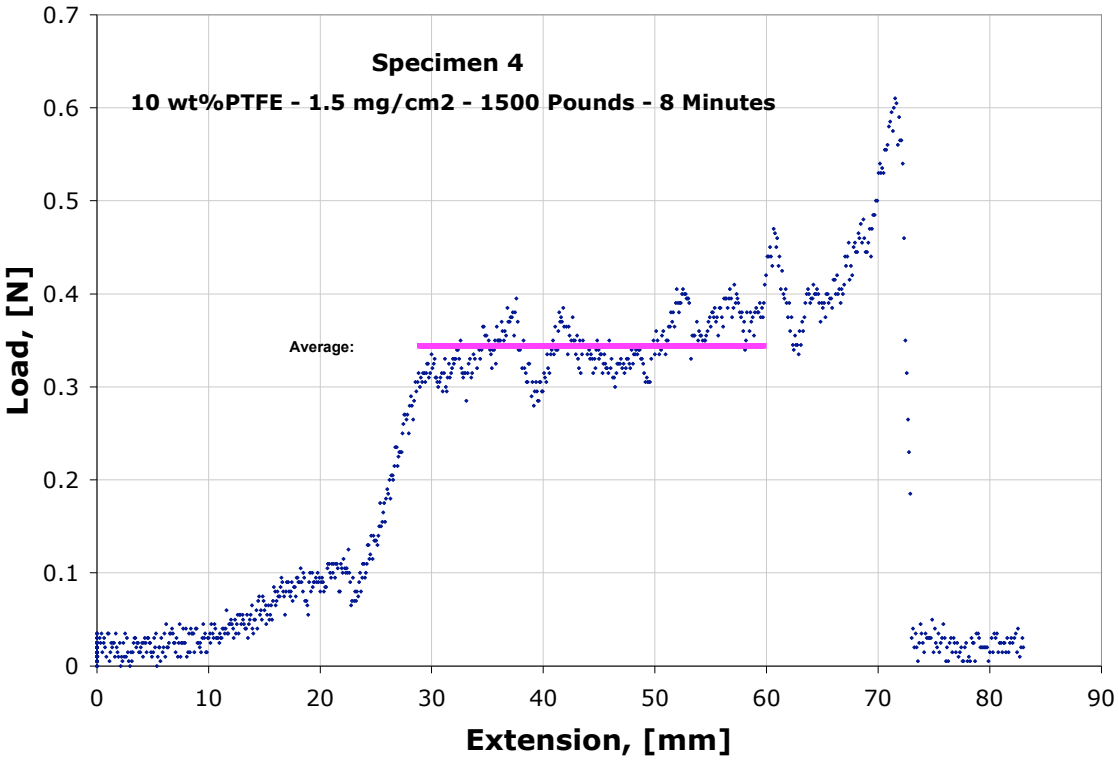

Figure D-4. Adhesion results for design point 4

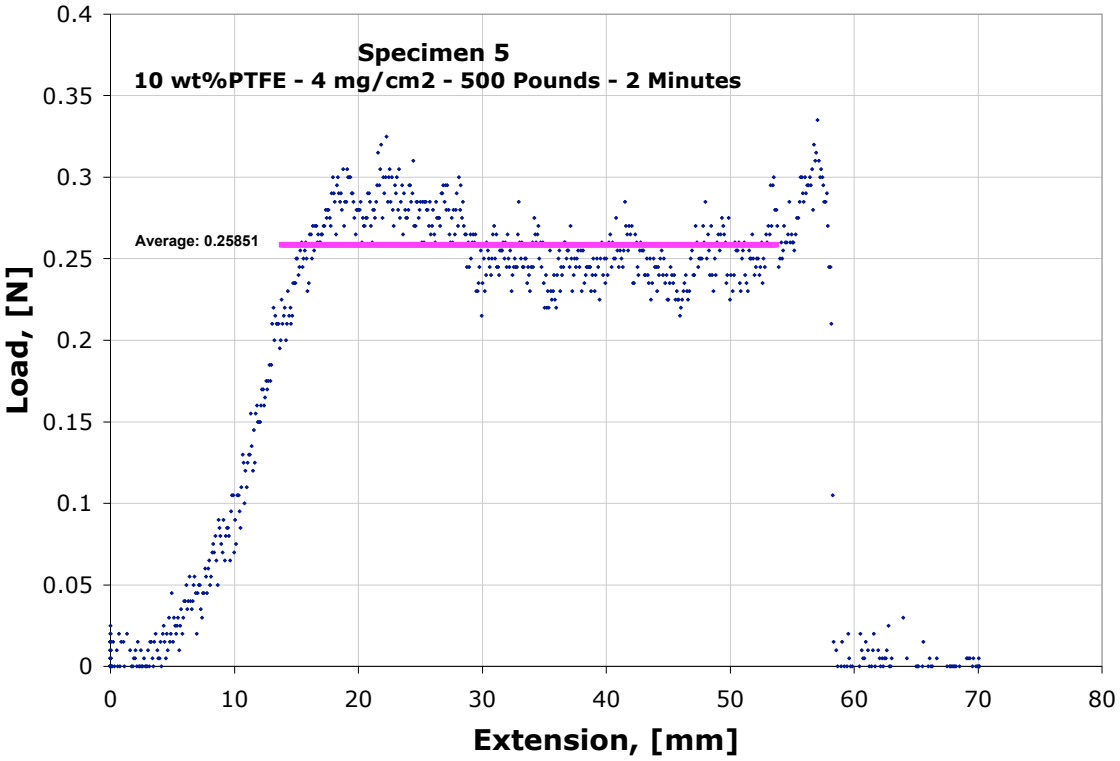

Figure D-5. Adhesion results for design point 5

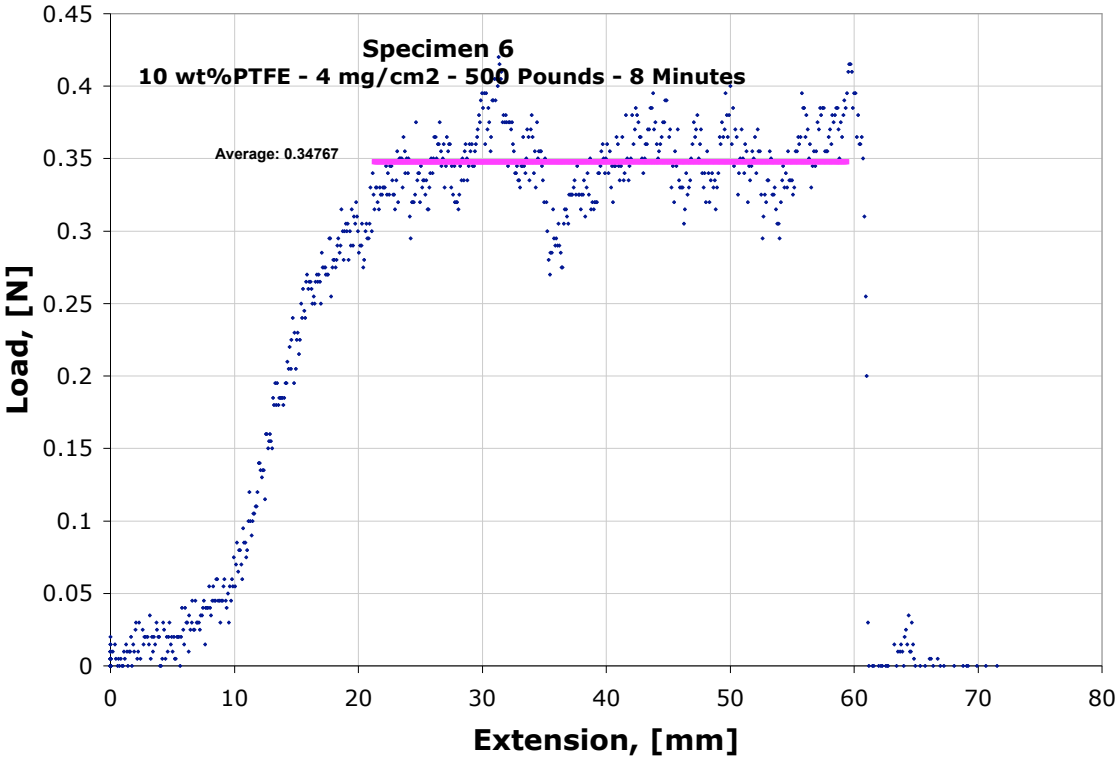

Figure D-6. Adhesion results for design point 6

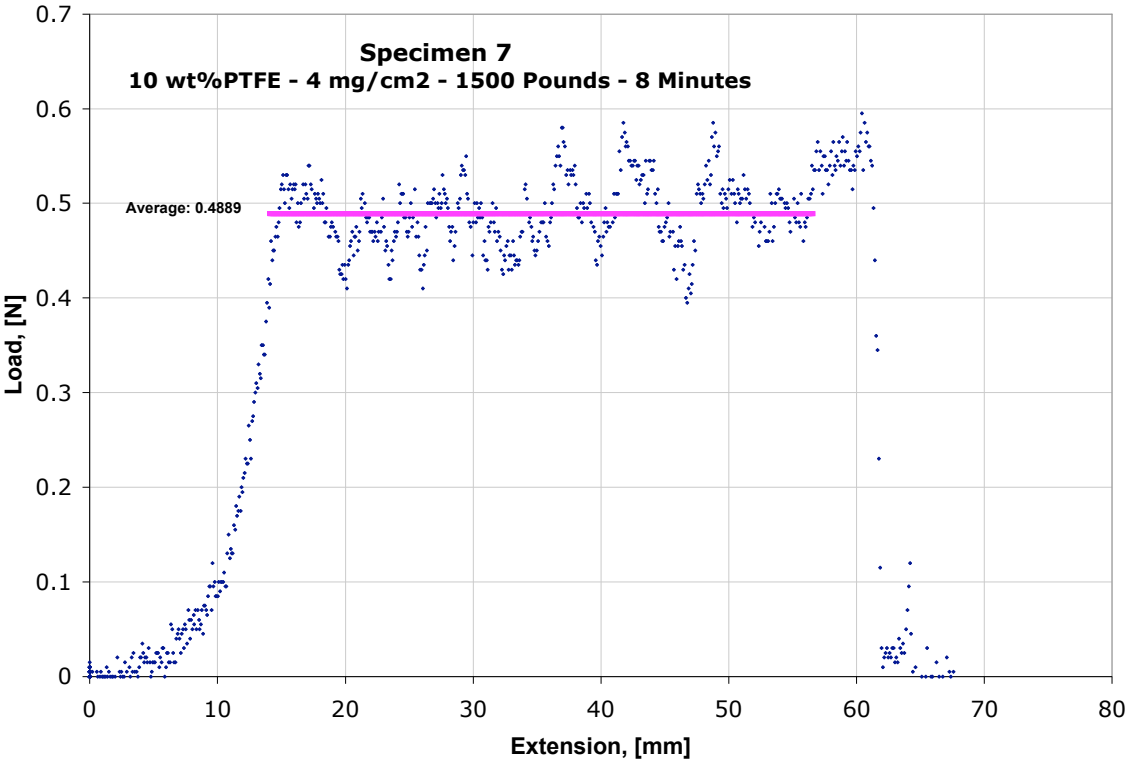

Figure D-7. Adhesion results for design point 7

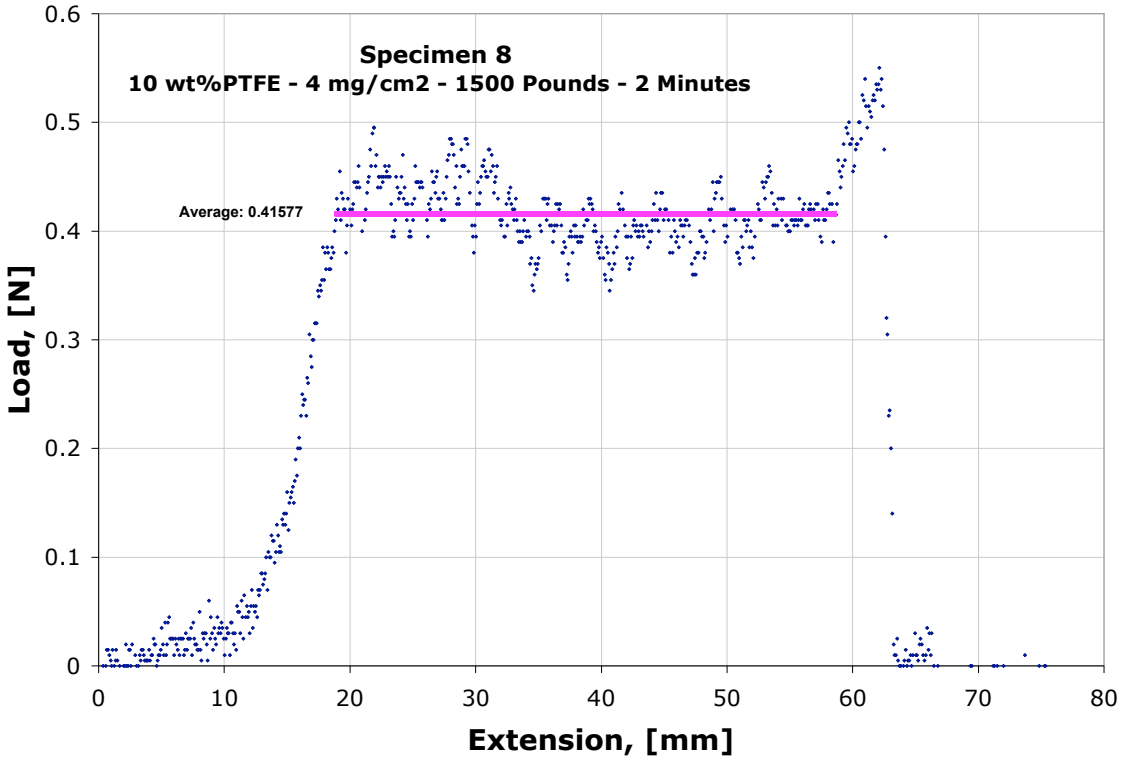

Figure D-8. Adhesion results for design point 8

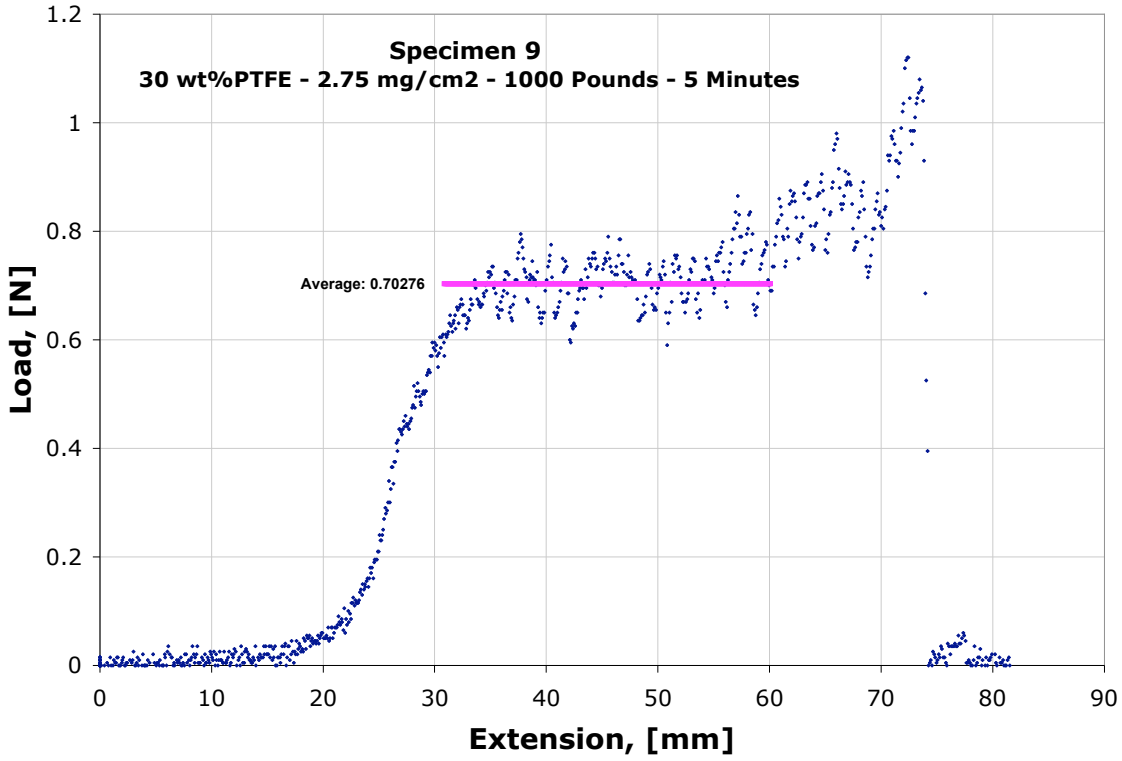

Figure D-9. Adhesion results for design point 9

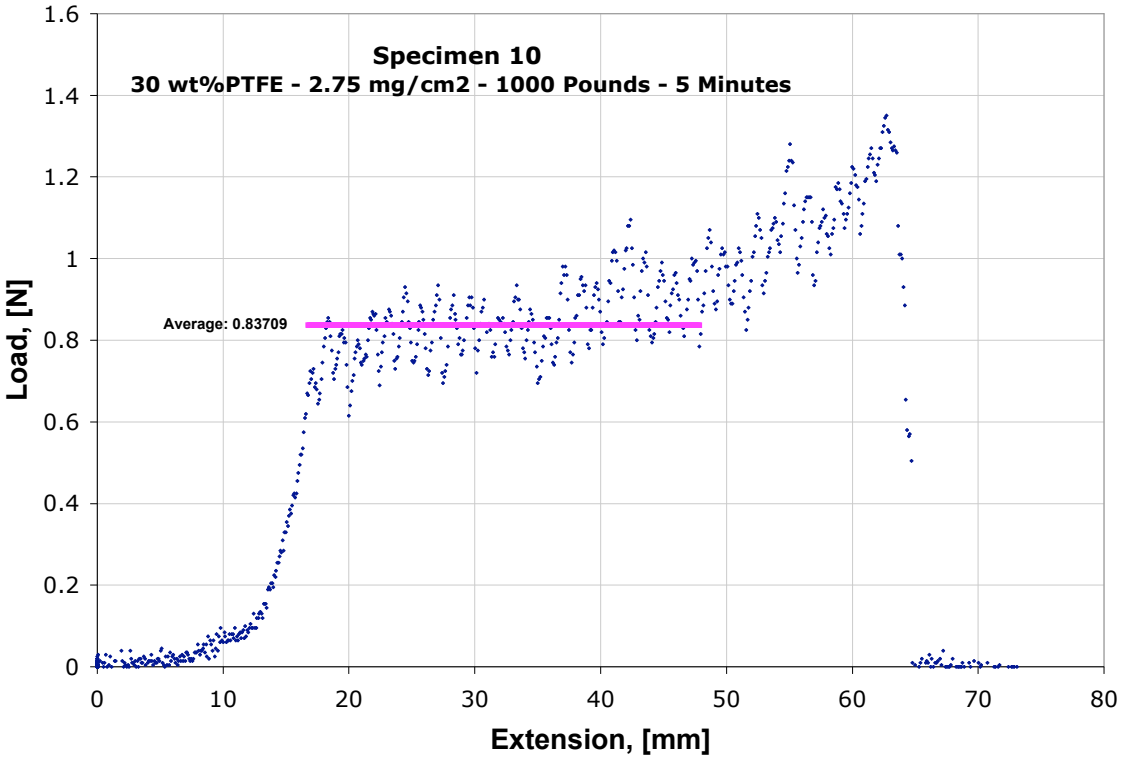

Figure D-10. Adhesion results for design point 10

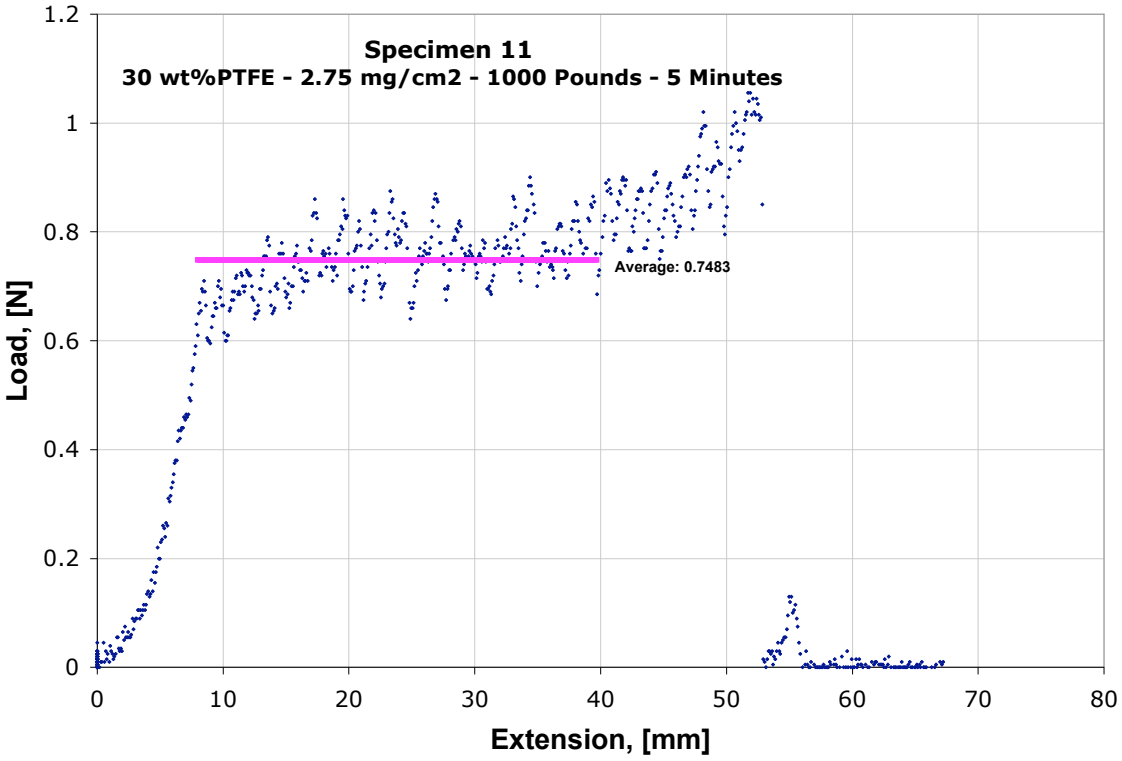

Figure D-11. Adhesion results for design point 11

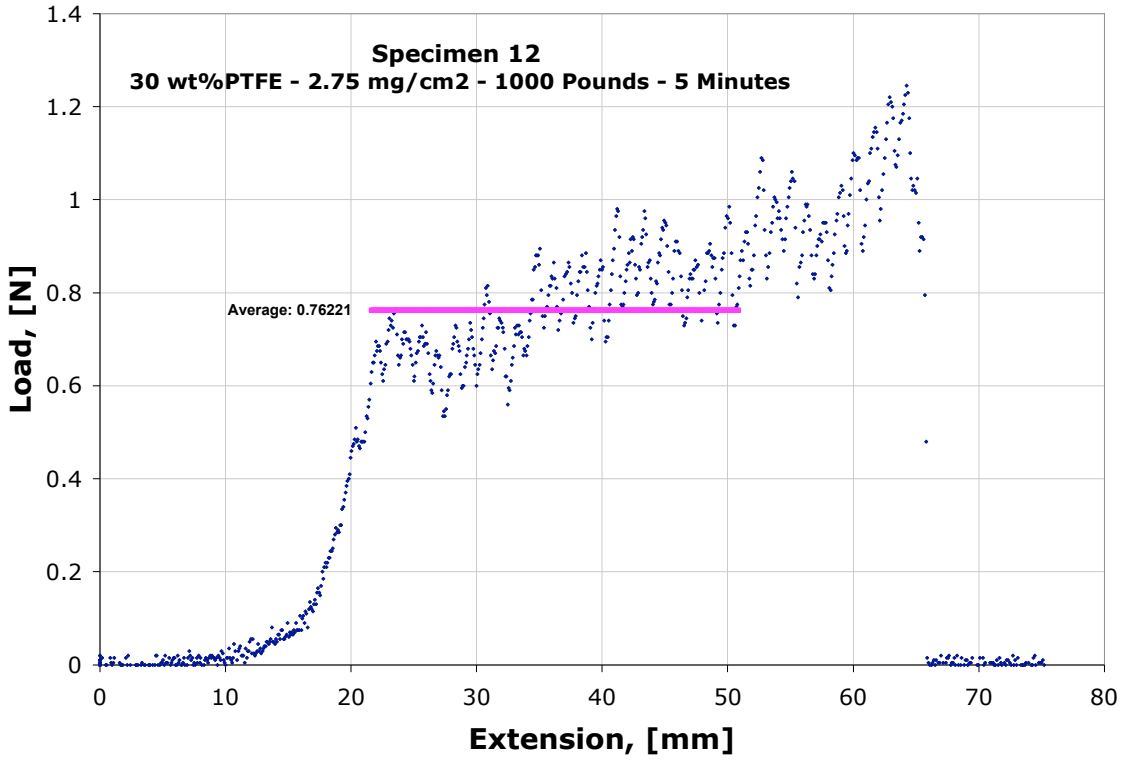

Figure D-12. Adhesion results for design point 12

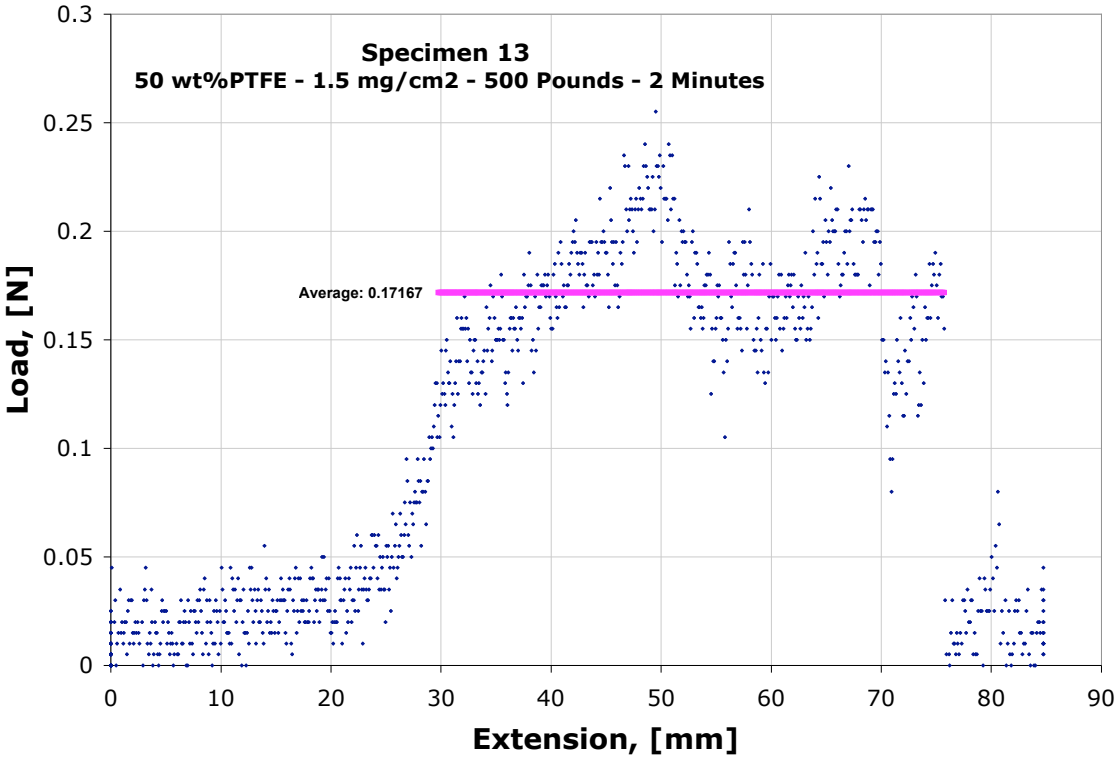

Figure D-13. Adhesion results for design point 13

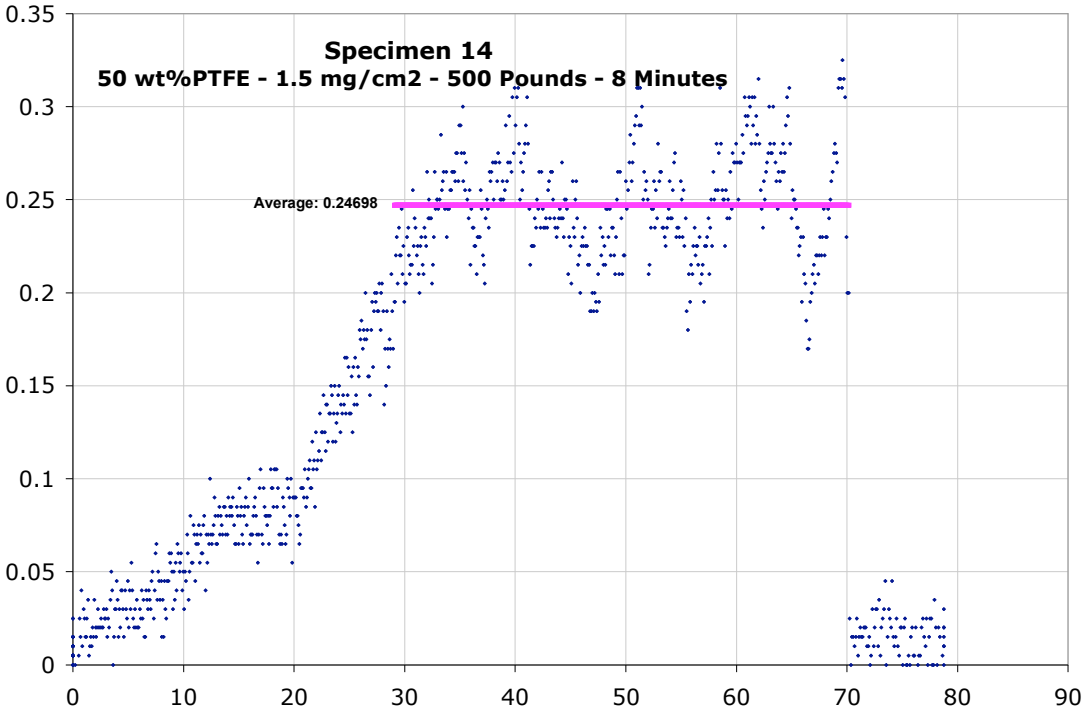

Figure D-14. Adhesion results for design point 14

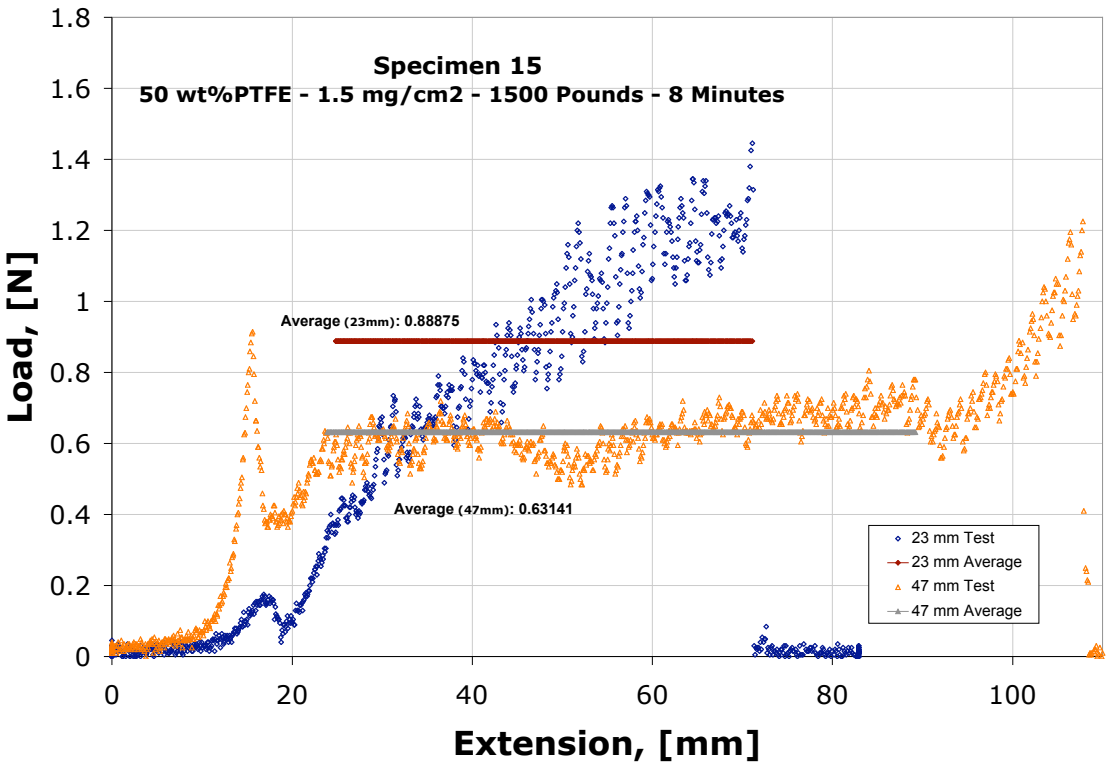

Figure D-15. Adhesion results for design point 15

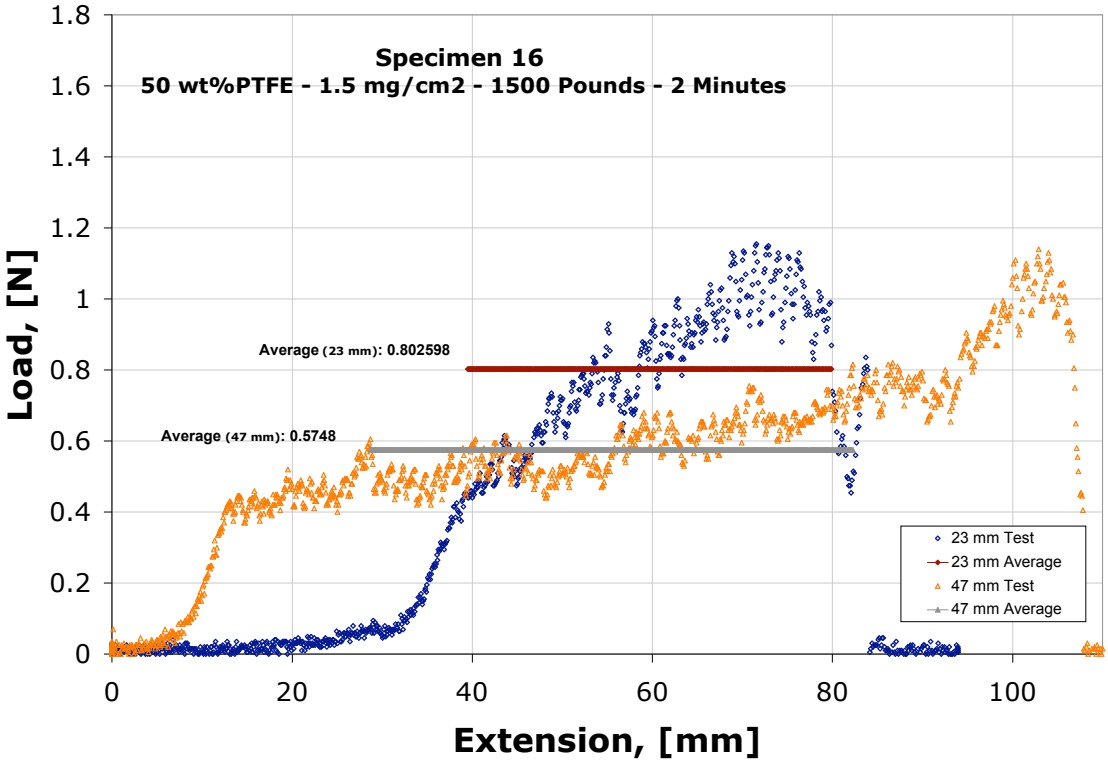

Figure D-16. Adhesion results for design point 16

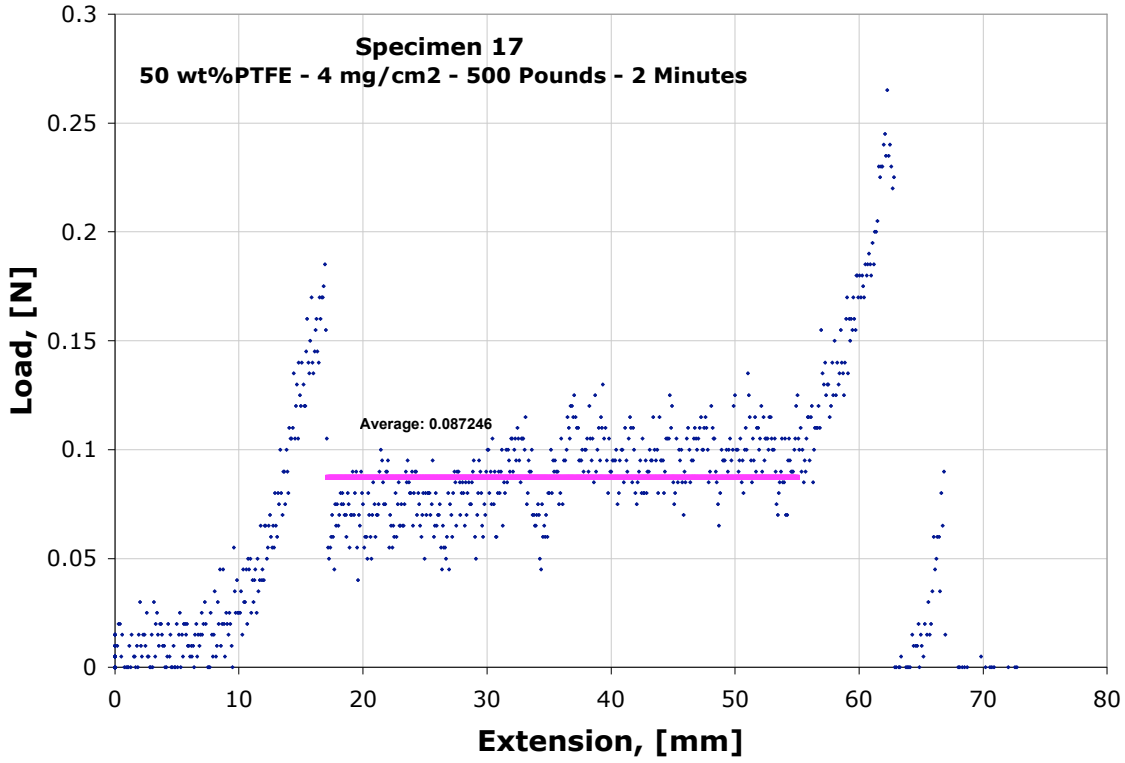

Figure D-17. Adhesion results for design point 17

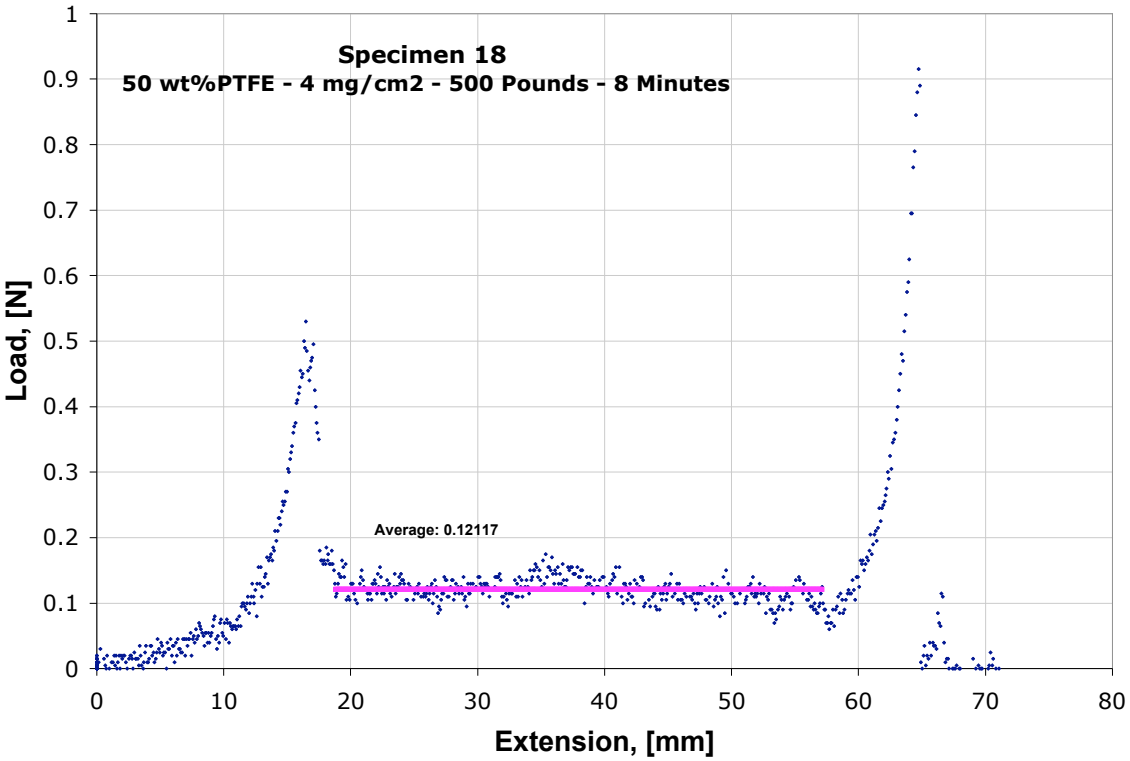

Figure D-18. Adhesion results for design point 18

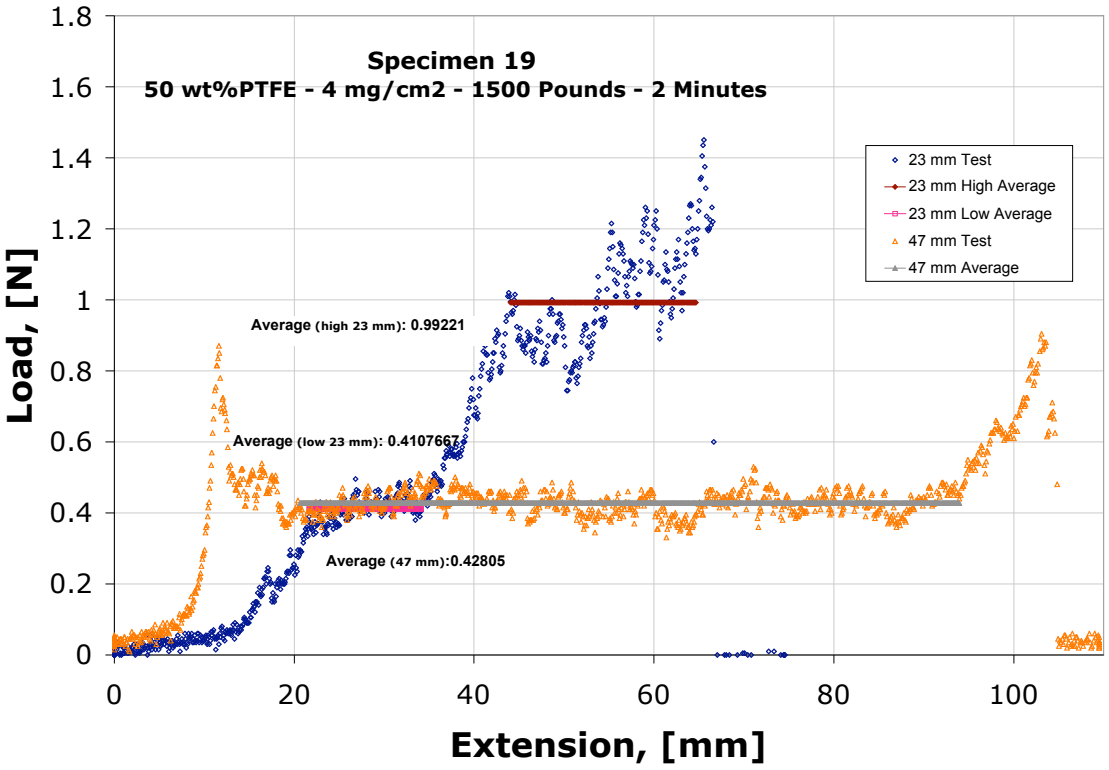

Figure D-19. Adhesion results for design point 19

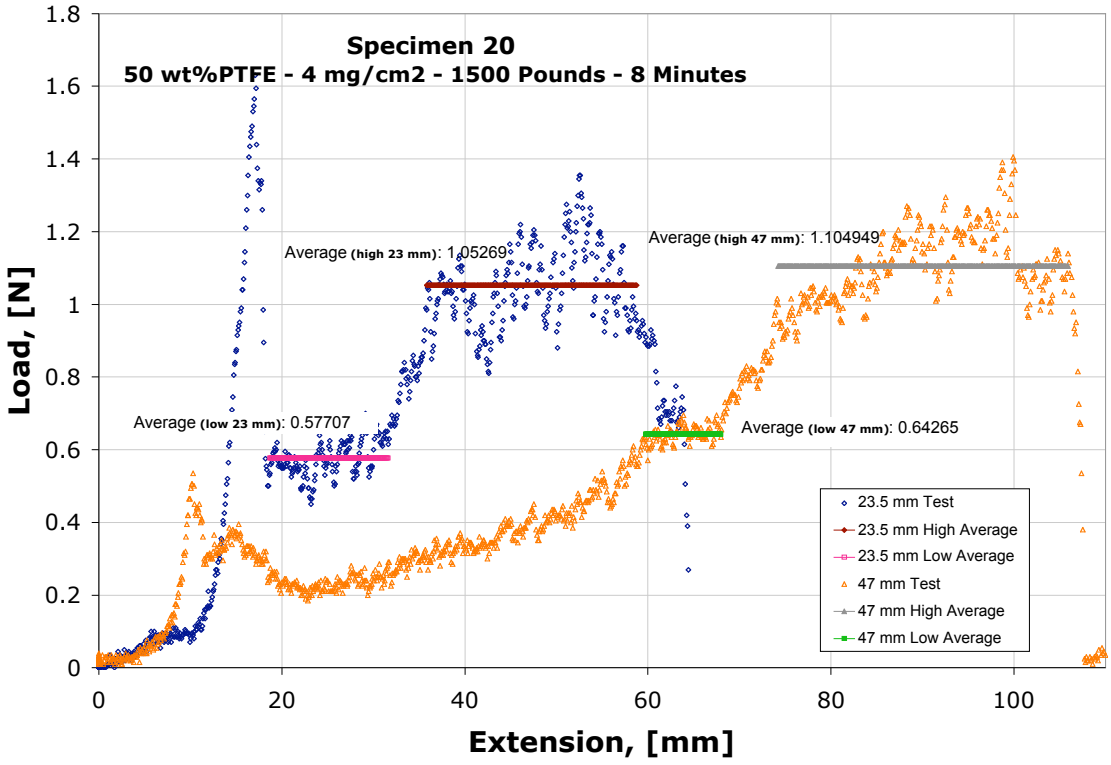

Figure D-20. Adhesion results for design point 20

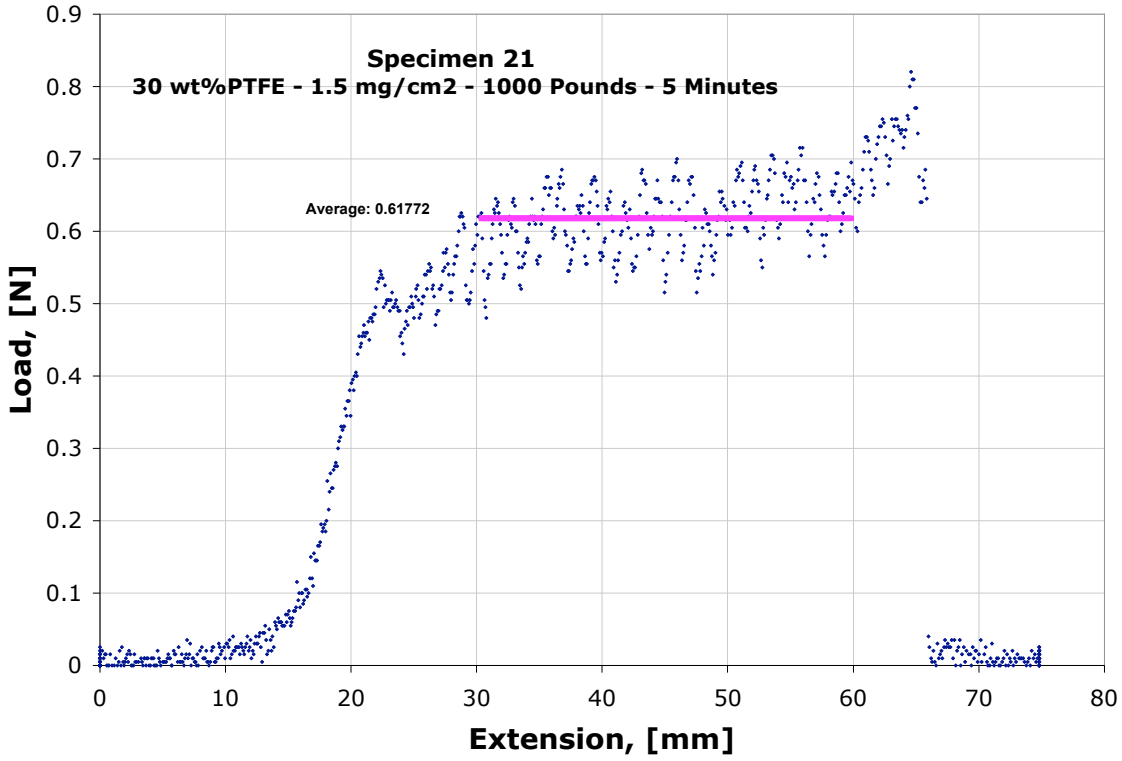

Figure D-21. Adhesion results for design point 21

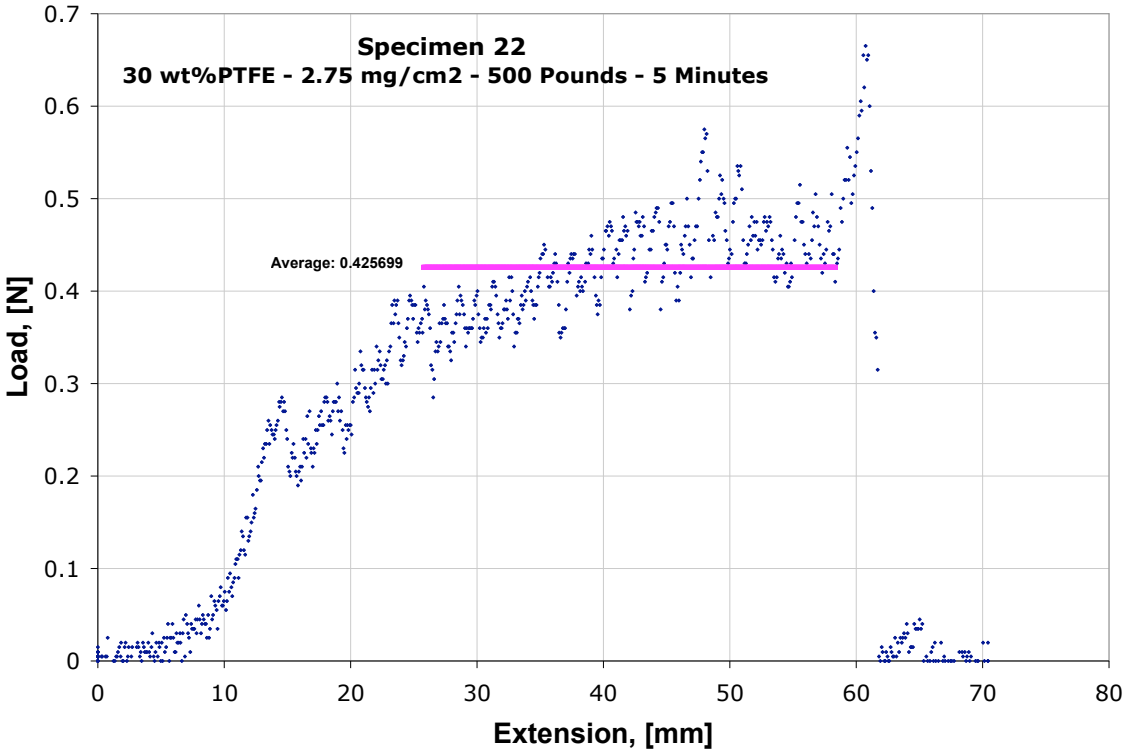

Figure D-22. Adhesion results for design point 22

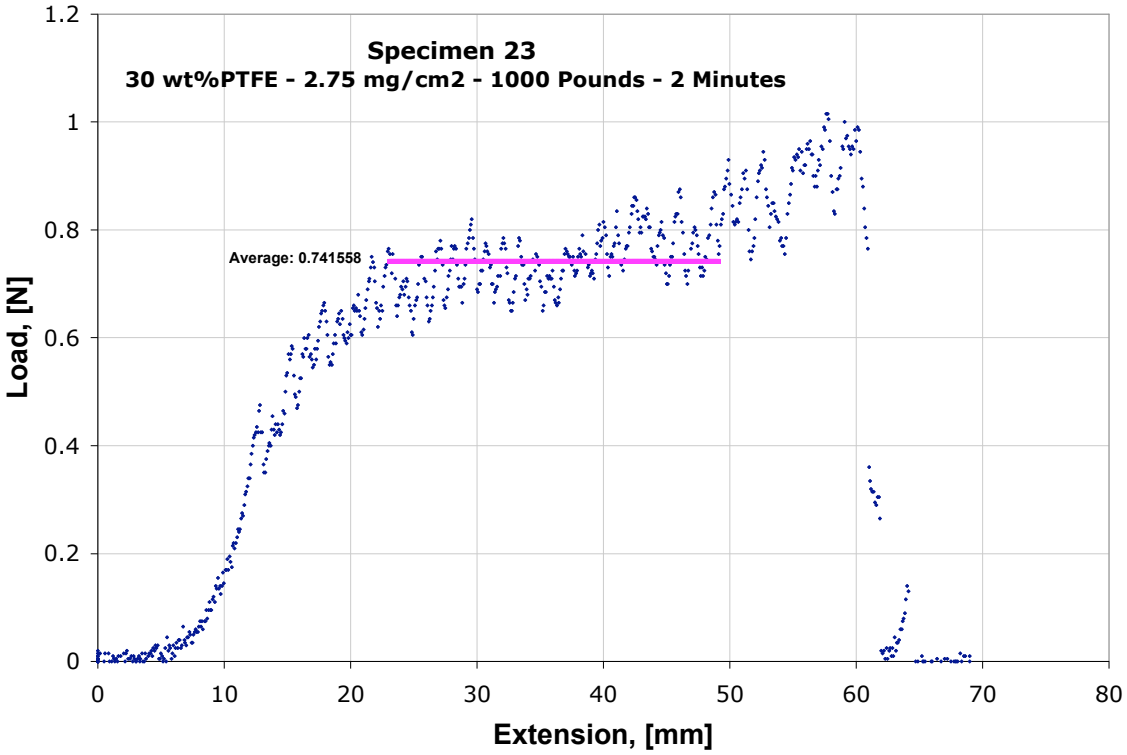

Figure D-23. Adhesion results for design point 23

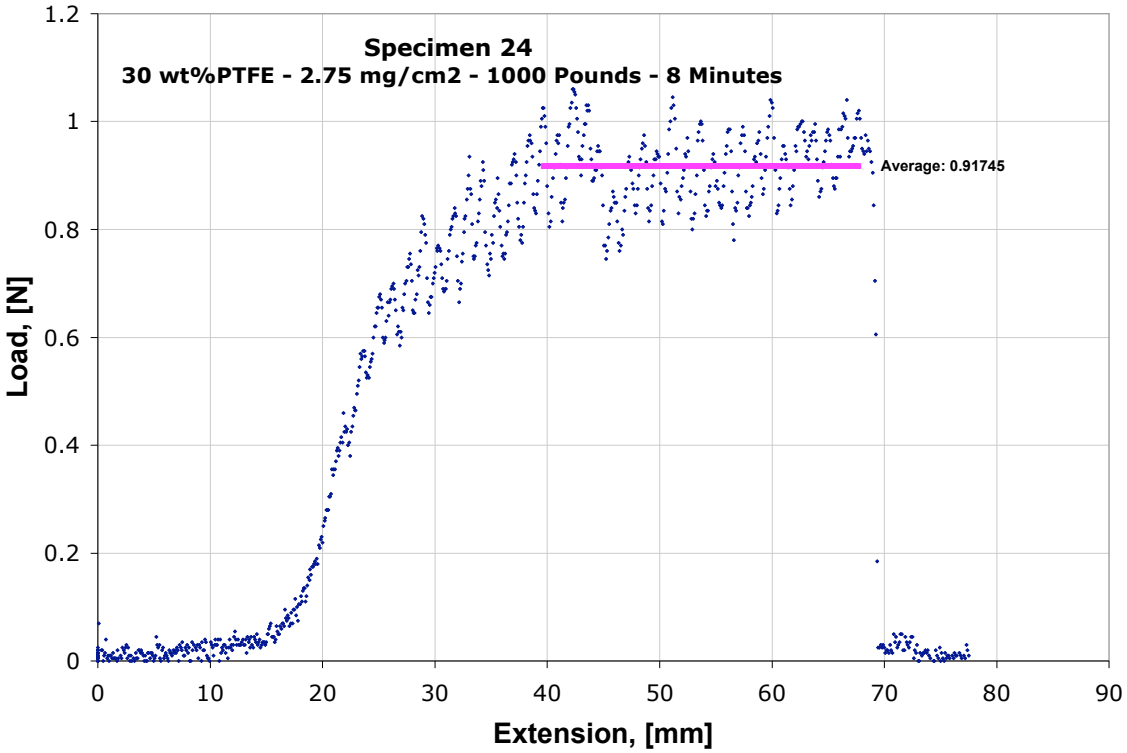

Figure D-24. Adhesion results for design point 24

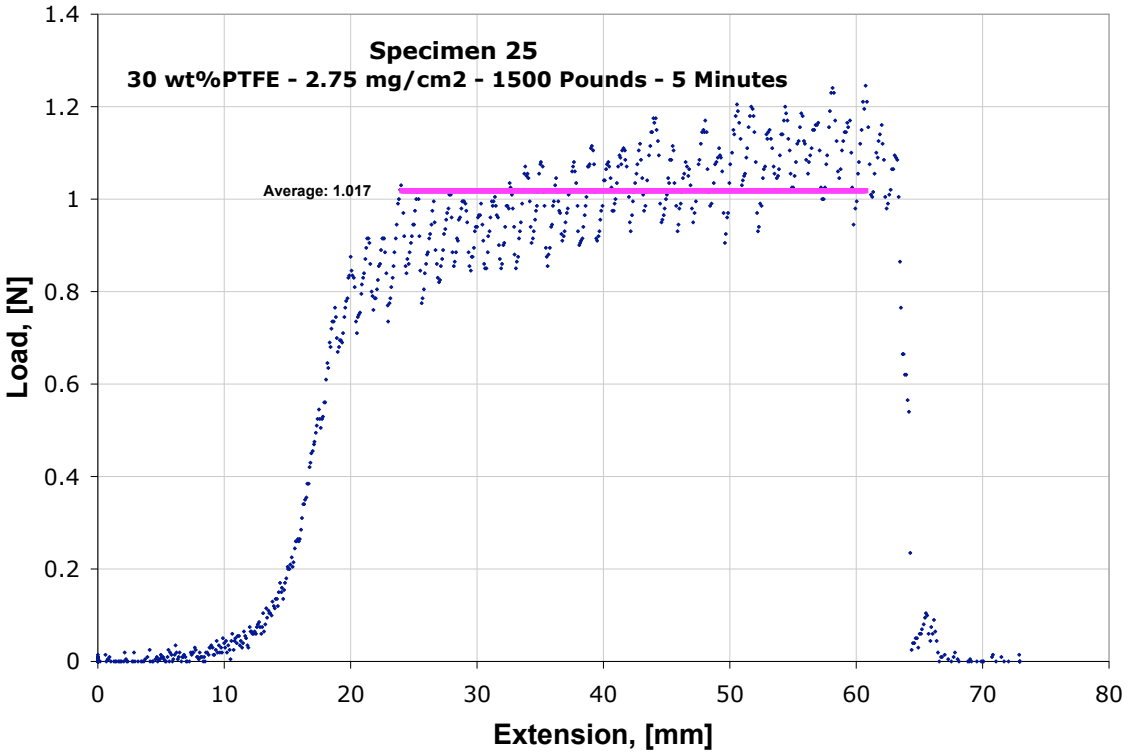

Figure D-25. Adhesion results for design point 25

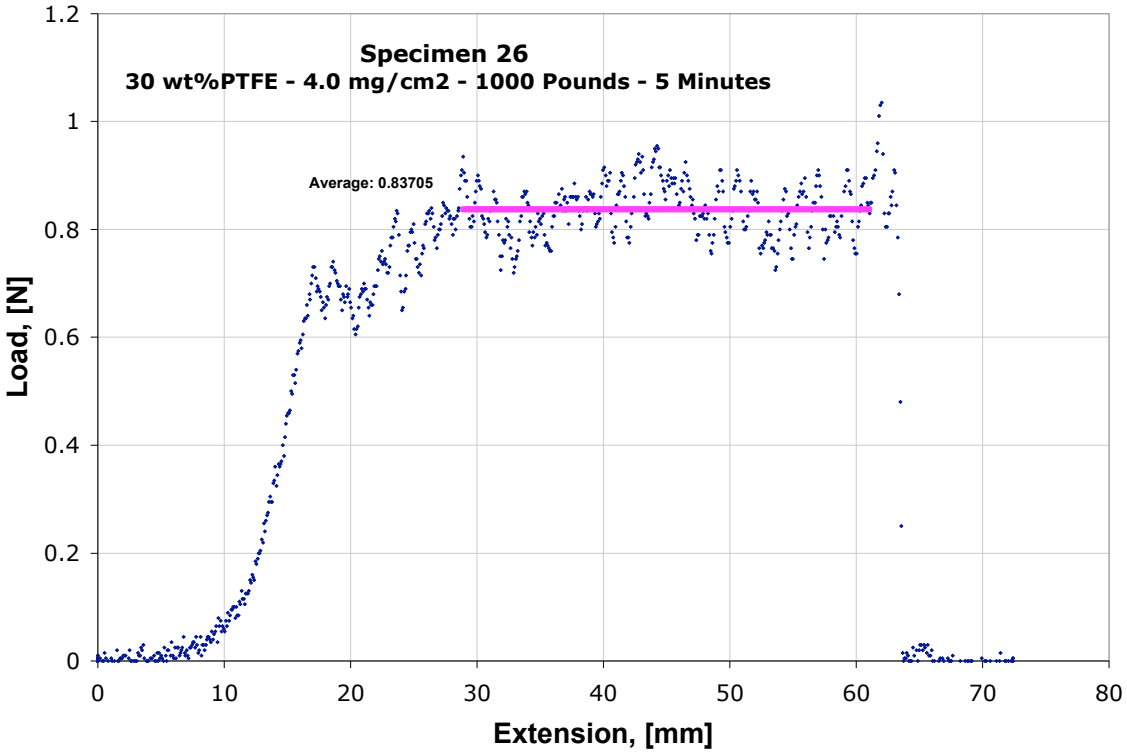

Figure D-26. Adhesion results for design point 26

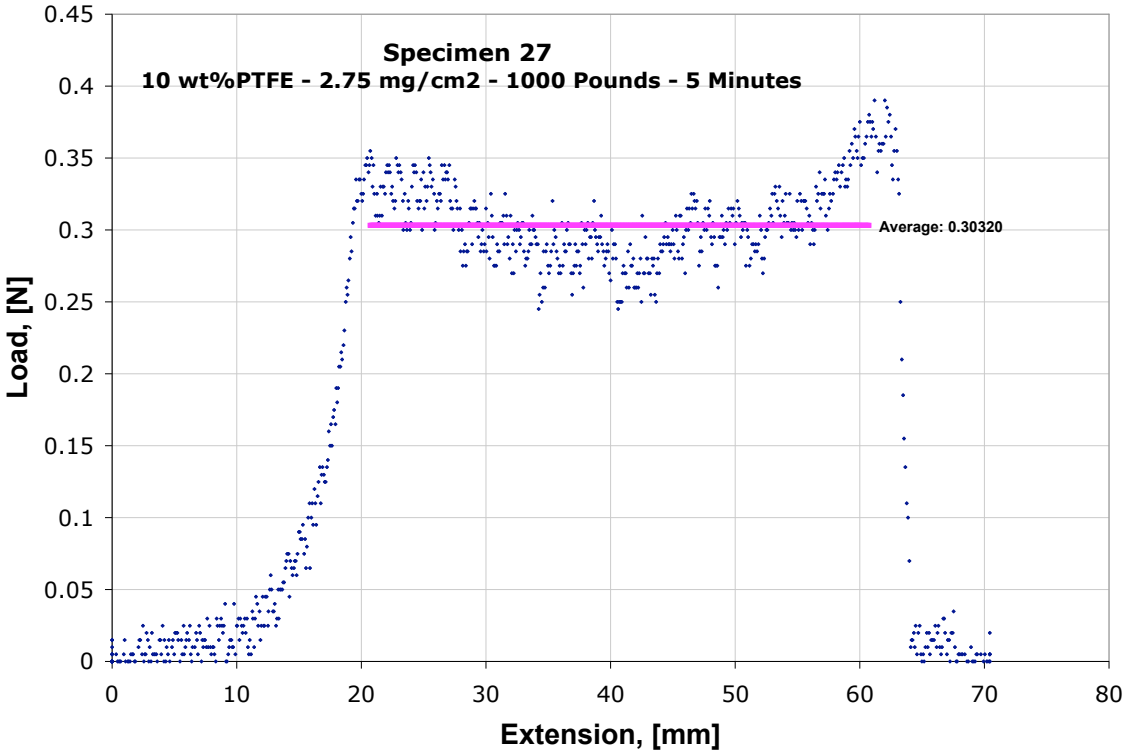

Figure D-27. Adhesion results for design point 27

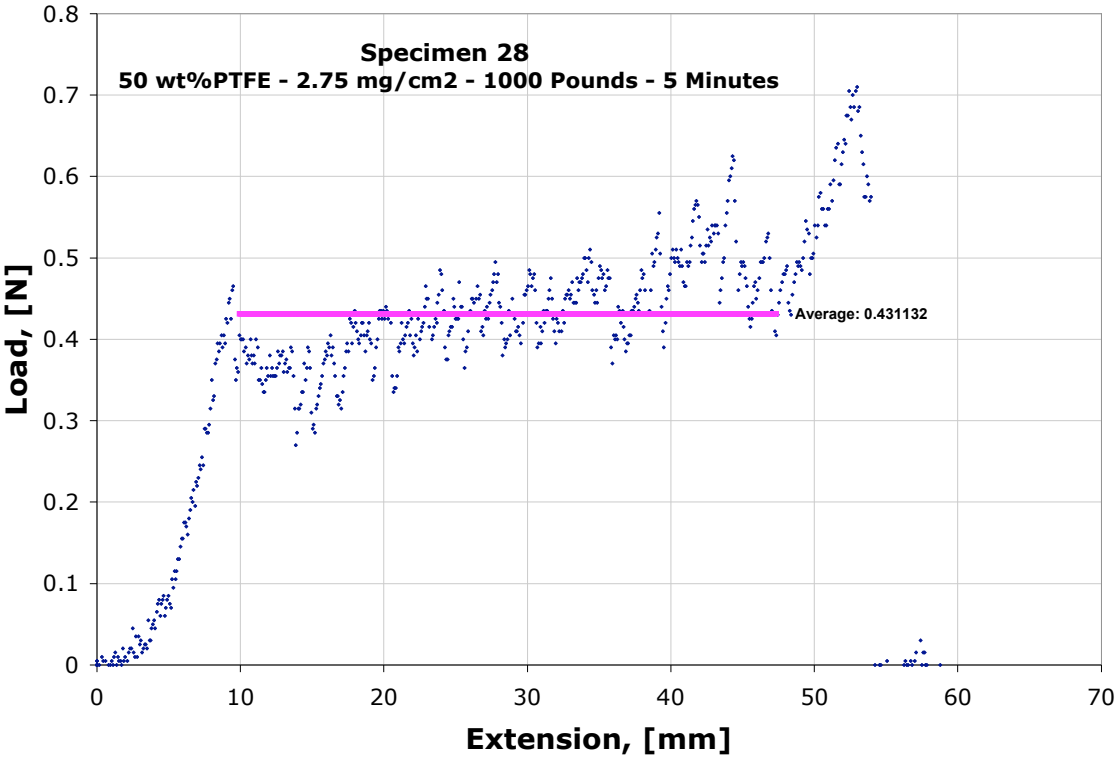

Figure D-28. Adhesion results for design point 28

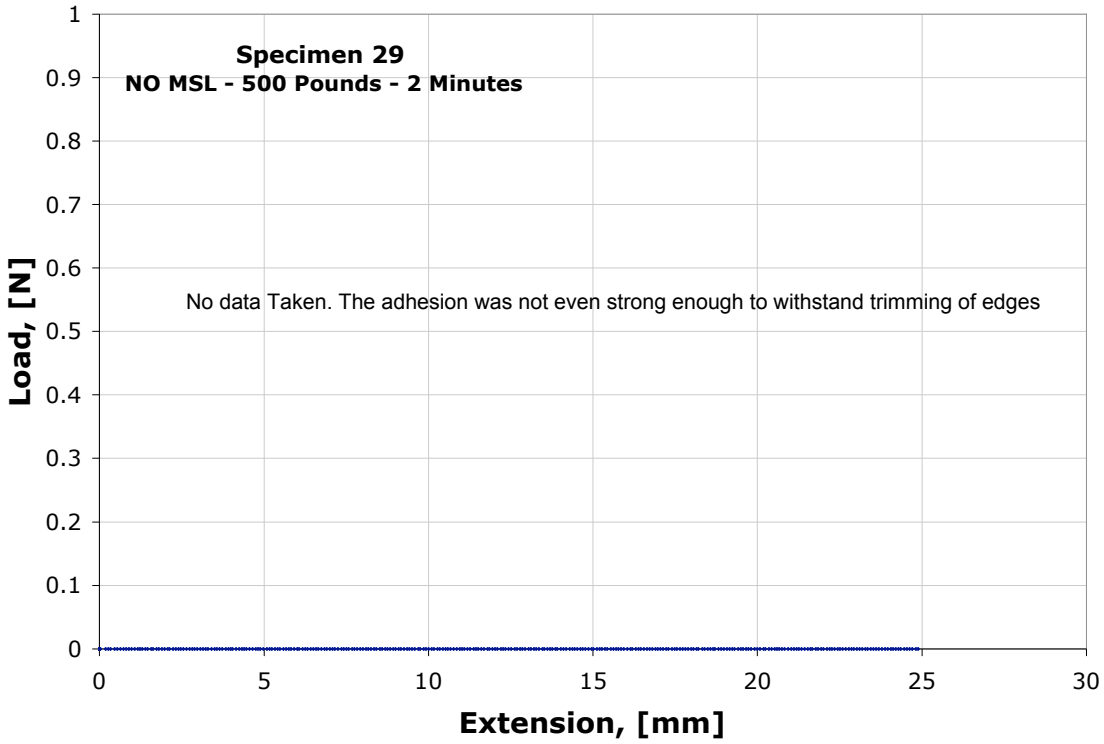

Figure D-29. Adhesion results for design point 29

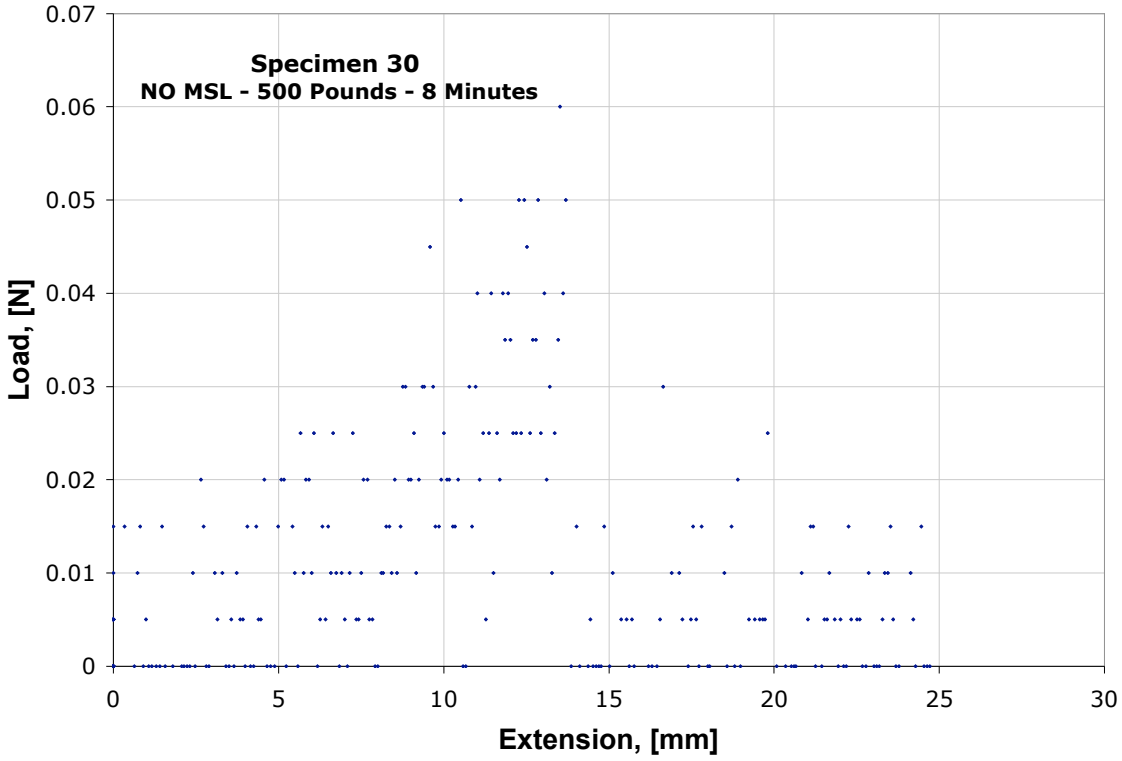

Figure D-30. Adhesion results for design point 30

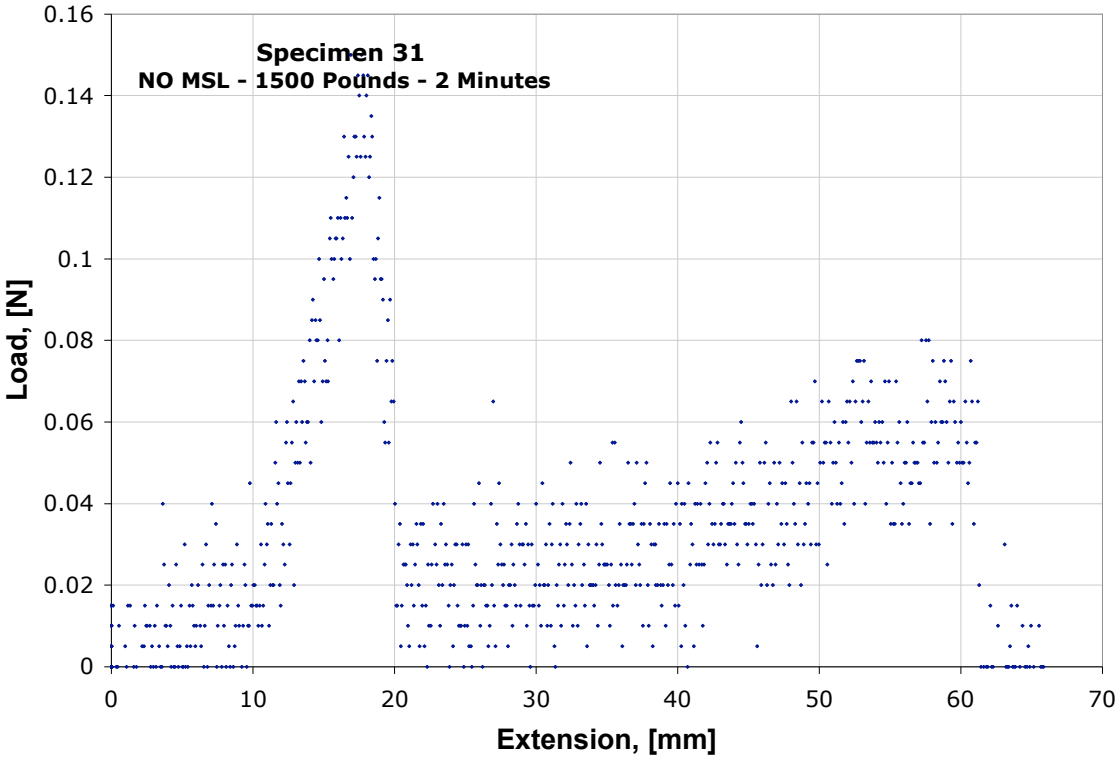

Figure D-31. Adhesion results for design point 31

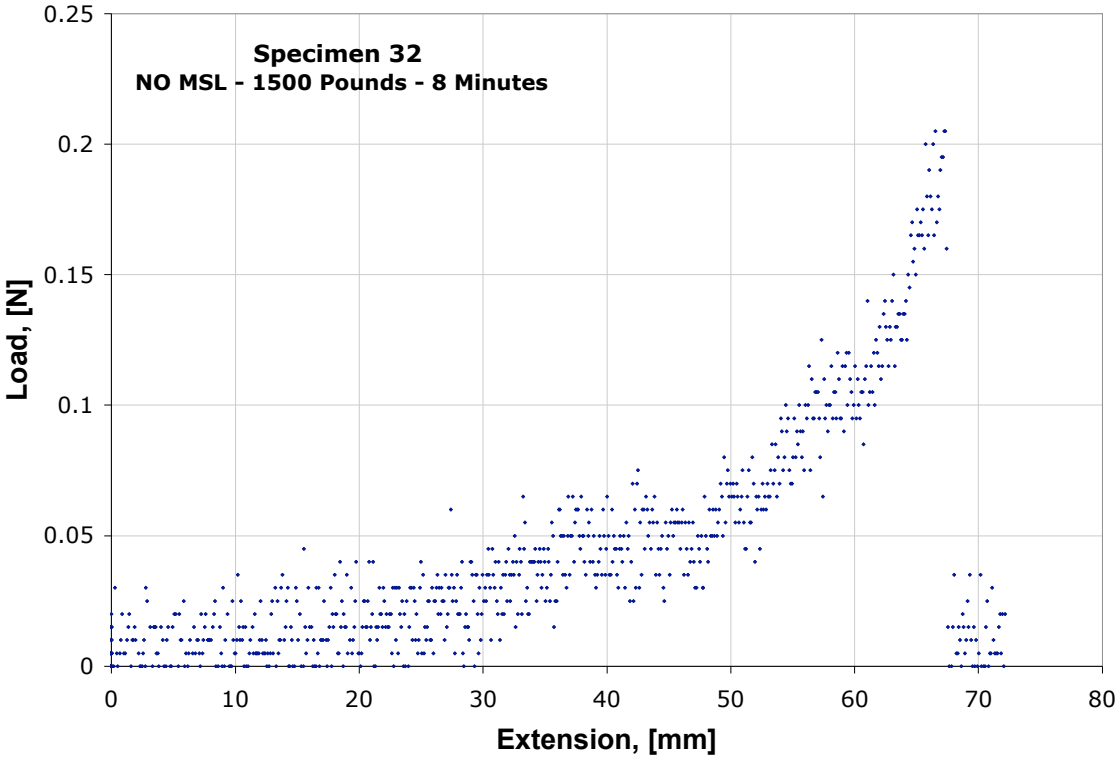

Figure D-32. Adhesion results for design point 32

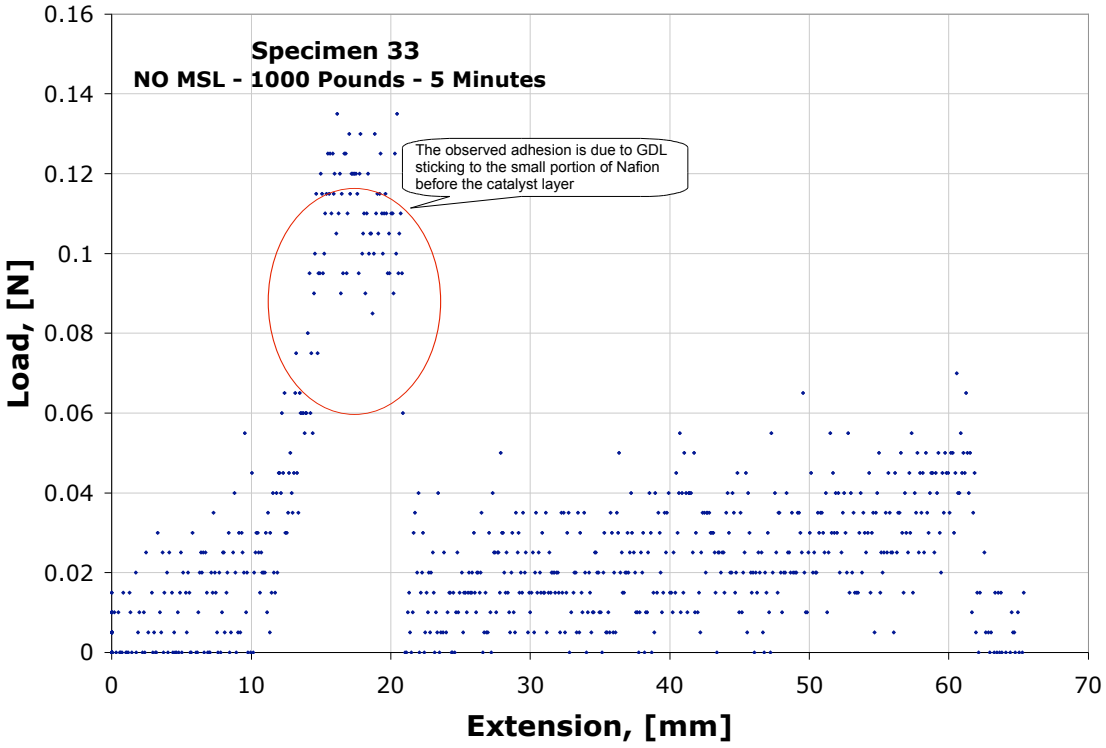

Figure D-33. Adhesion results for design point 33

Appendix E. Design Expert Output

Performance Report:

Use your mouse to right click on individual cells for definitions.
Response: Current Density @ 0.5 Volt
ANOVA for Selected Factorial Model
Analysis of variance table [Partial sum of squares]

Source	Sum of Squares	DF	Mean Square	F Value	Prob > F	
Model	0.18	4	0.045	5.73	0.0069	significant
A	0.030	1	0.030	3.90	0.0699	
B	0.031	1	0.031	3.94	0.0687	
C	0.084	1	0.084	10.81	0.0059	
AB	0.033	1	0.033	4.28	0.0590	
Curvature	0.056	1	0.056	7.21	0.0187	significant
Residual	0.10	13	7.777E-003			
Lack of Fit	0.087	11	7.883E-003	1.10	0.5702	not significant
Pure Error	0.014	2	7.195E-003			
Cor Total	0.34	18				

The Model F-value of 5.73 implies the model is significant. There is only a 0.69% chance that a "Model F-Value" this large could occur due to noise.

Values of "Prob > F" less than 0.0500 indicate model terms are significant.
In this case C are significant model terms.
Values greater than 0.1000 indicate the model terms are not significant.
If there are many insignificant model terms (not counting those required to support hierarchy), model reduction may improve your model.

The "Curvature F-value" of 7.21 implies there is significant curvature (as measured by difference between the average of the center points and the average of the factorial points) in the design space. There is only a 1.87% chance that a "Curvature F-value" this large could occur due to noise.

The "Lack of Fit F-value" of 1.10 implies the Lack of Fit is not significant relative to the pure error. There is a 57.02% chance that a "Lack of Fit F-value" this large could occur due

to noise. Non-significant lack of fit is good -- we want the model to fit.

Std. Dev.	0.088	R-Squared	0.6382
Mean	1.09	Adj R-Squared	0.5269
C.V.	8.12	Pred R-Squared	0.3568
PRESS	0.22	Adeq Precision	6.533

The "Pred R-Squared" of 0.3568 is in reasonable agreement with the "Adj R-Squared" of 0.5269.

"Adeq Precision" measures the signal to noise ratio. A ratio greater than 4 is desirable. Your ratio of 6.533 indicates an adequate signal. This model can be used to navigate the design space.

Factor	Coefficient Estimate	Standard DF	95% CI Error	95% CI Low	High	VIF	
Intercept	1.06	1	0.022	1.01	1.11		
A-Loading	-0.044	1	0.022	-0.091	4.089E-003	1.00	
B-Composition	-0.044	1	0.022	-0.091	3.880E-003	1.00	
C-Pressure	-0.073	1	0.022	-0.12	-0.025	1.00	
AB	0.046	1	0.022	-2.005E-003	0.093	1.00	
Center Point		0.15	1	0.055	0.029	0.27	1.00

Final Equation in Terms of Coded Factors:

Current Density @ 0.5 Volt =
+1.06
-0.044 * A
-0.044 * B
-0.073 * C
+0.046 * A * B

Final Equation in Terms of Actual Factors:
Current Density @ 0.5 Volt =

+1.51906
-0.089583 * Loading
-7.20625E-003 * Composition
-1.45000E-004 * Pressure
+1.82500E-003 * Loading * Composition

Diagnostics Case Statistics

Standard Order	Actual Value	Predicted Value	Residual	Leverage	Student Residual	Cook's Distance	Outlier t	Run Order	
1	1.20	1.27	-0.071	0.313	-0.969	0.071	-0.966	19	
2	1.17	1.09	0.078	0.313	1.060	0.085	1.065	17	
3	1.08	1.09	-8.750E-003		0.313	-0.120	0.001	-0.115	12
4	1.12	1.09	0.027	0.313	0.370	0.010	0.358	9	
5	1.07	1.12	-0.056	0.313	-0.764	0.044	-0.751	6	
6	0.94	0.94	-8.333E-004		0.313	-0.011	0.000	-0.011	3
7	1.03	0.94	0.085	0.313	1.157	0.101	1.173	15	
8	0.89	0.95	-0.058	0.313	-0.792	0.048	-0.780	18	
9	1.23	1.27	-0.041	0.313	-0.558	0.024	-0.543	13	
10	1.00	1.09	-0.093	0.313	-1.265	0.121	-1.298	2	
11	1.14	1.09	0.051	0.313	0.701	0.037	0.686	10	
12	1.15	1.09	0.057	0.313	0.781	0.046	0.768	5	
13	1.29	1.12	0.17	0.313	2.291	0.398	2.850	7	
14	0.96	0.94	0.016	0.313	0.217	0.004	0.208	4	
15	0.82	0.94	-0.13	0.313	-1.738	0.229	-1.906	16	
16	0.92	0.95	-0.026	0.313	-0.359	0.010	-0.347	8	
17	1.25	1.21	0.044	0.333	0.610	0.031	0.594	11	
18	1.26	1.21	0.054	0.333	0.748	0.047	0.735	1	
19	1.11	1.21	-0.098	0.333	-1.358	0.154	-1.408	14	

Note: Predicted values of center points include center point coefficient.

Proceed to Diagnostic Plots (the next icon in progression). Be sure to look at the:
1) Normal probability plot of the studentized residuals to check for normality of residuals.
2) Studentized residuals versus predicted values to check for constant error.
3) Outlier t versus run order to look for outliers, i.e., influential values.
4) Box-Cox plot for power transformations.

If all the model statistics and diagnostic plots are OK, finish up with the Model Graphs icon.

Performance Optimal Solutions:

Constraints

Lower Name	Upper Goal	Lower Limit	Upper Limit	Weight	Weight	Importance	
Loading	is in range		1.5	4	1	1	3
Composition	is in range			10	50	1	1	3
Pressure	is in range		3.447	10.342	1	1	3
Time	is in range		2	8	1	1	3
Current Density @ 0.5 Volt	maximize		1.14	1.35	1	1	3

Solutions

Number	Loading	Composition		Pressure	Time*	Current Density @ 0.5 Volt		Desirability
1	1.50	10.00	3.45	6.35	1.2675	0.607	Selected	
2	1.50	10.00	3.45	7.18	1.2675	0.607		
3	1.50	10.00	3.45	7.05	1.2675	0.607		
4	1.50	10.00	3.45	2.38	1.2675	0.607		
5	1.50	10.00	3.45	4.64	1.26747	0.607		
6	1.50	10.00	3.45	2.34	1.26729	0.606		
7	1.50	10.00	3.49	4.25	1.26654	0.603		
8	1.50	10.00	4.34	2.00	1.24856	0.517		
9	1.50	10.00	5.76	2.00	1.21884	0.375		
10	1.50	10.00	6.21	2.00	1.20949	0.331		

*Has no effect on optimization results.

10 Solutions found

Number of Starting Points 10

Loading	Composition	Pressure	Time
2.30	14.35	8.51	7.74
2.91	26.74	4.59	7.06
2.98	38.29	8.91	4.85

2.92	28.11	7.30	4.56
1.97	21.80	8.74	2.90
2.32	33.10	4.59	3.09
2.67	23.24	4.55	6.75
2.08	20.26	5.09	3.83
1.91	16.24	9.27	3.14
2.13	19.92	5.21	6.96

Adhesion Fit Summary:

Response: Fracture Energy Transform: Square root Constant: 0
*** WARNING: The Cubic Model is Aliased! ***

Sequential Model Sum of Squares

Source	Sum of Squares	DF	Mean Square	F Value	Prob > F	
Mean	1293.23	1	1293.23			
Linear	32.38	4	8.10	2.77	0.0514	
2FI	8.06	6	1.34	0.39	0.8776	
Quadratic	55.63	4	13.91	51.63	< 0.0001	Suggested
Cubic	3.19	8	0.40	6.36	0.0284	Aliased
Residual	0.31	5	0.063			
Total	1392.81	28	49.74			

"Sequential Model Sum of Squares": Select the highest order polynomial where the additional terms are significant.

Lack of Fit Tests

Source	Sum of Squares	DF	Mean Square	F Value	Prob > F	
Linear	66.89	20	3.34	33.17	0.0073	
2FI	58.83	14	4.20	41.68	0.0053	
Quadratic	3.20	10	0.32	3.17	0.1858	Suggested
Cubic	0.011	2	5.546E-003	0.055	0.9474	Aliased
Pure Error	0.30	3	0.10			

"Lack of Fit Tests": Want the selected model to have insignificant lack-of-fit.

Model Summary Statistics

Source	Std. Dev.	Adjusted R-Squared	Predicted R-Squared	PRESS	
Linear	1.71	0.3252	0.2078	0.0333	96.26	
2FI	1.87	0.4062	0.0569	-0.9430	193.47	
Quadratic	0.52	0.9648	0.9270	0.8049	19.43	Suggested
Cubic	0.25	0.9969	0.9830	0.9687	3.11	Aliased

"Model Summary Statistics": Focus on the model maximizing the "Adjusted R-Squared" and the "Predicted R-Squared".

Adhesion Report:

Use your mouse to right click on individual cells for definitions.
Response: Fracture Energy Transform: Square root Constant: 0
Backward Elimination Regression with Alpha to Exit = 0.050
Forced Terms Intercept

Coefficientt for H0

Removed	Estimate	Coeff=0	Prob > |t|	R-Squared	MSE
A	0.012	0.095	0.9260	0.9648	0.25
B	0.023	0.20	0.8466	0.9647	0.23
AC	0.058	0.48	0.6384	0.9642	0.22
BD	0.060	0.51	0.6176	0.9636	0.21
AD	0.081	0.70	0.4938	0.9625	0.21
A2	-0.23	-0.83	0.4182	0.9611	0.20
CD	-0.12	-1.04	0.3123	0.9589	0.20
D2	0.29	1.07	0.2985	0.9566	0.21
C2	-0.38	-1.56	0.1344	0.9516	0.22

Hierarchical Terms Added after StepWise Regression

A, B

ANOVA for Response Surface Reduced Quadratic Model

Analysis of variance table [Partial sum of squares]

Source	Sum of Squares	DF	Mean Square	F Value	Prob > F		
Model	94.76	7	13.54	56.27	< 0.0001	significant	
A	2.416E-003		1	2.416E-003		0.010	0.9212
B	9.722E-003		1	9.722E-003		0.040	0.8427
C	30.38	1	30.38	126.29	< 0.0001		
D	1.98	1	1.98	8.24	0.0094		
B2	54.75	1	54.75	227.57	< 0.0001		
AB	2.75	1	2.75	11.41	0.0030		
BC	4.88	1	4.88	20.30	0.0002		
Residual	4.81	20	0.24				
Lack of Fit	4.51	17	0.27	2.63	0.2314	not significant	
Pure Error	0.30	3	0.10				
Cor Total	99.57	27					

The Model F-value of 56.27 implies the model is significant. There is only a 0.01% chance that a "Model F-Value" this large could occur due to noise.

Values of "Prob > F" less than 0.0500 indicate model terms are significant.
In this case C, D, B□+2□, AB, BC are significant model terms.
Values greater than 0.1000 indicate the model terms are not significant.
If there are many insignificant model terms (not counting those required to support hierarchy), model reduction may improve your model.

The "Lack of Fit F-value" of 2.63 implies the Lack of Fit is not significant relative to the pure error. There is a 23.14% chance that a "Lack of Fit F-value" this large could occur due to noise. Non-significant lack of fit is good -- we want the model to fit.

Std. Dev.	0.49	R-Squared	0.9517
Mean	6.80	Adj R-Squared	0.9348
C.V.	7.22	Pred R-Squared	0.9079
PRESS	9.17	Adeq Precision	25.862

The "Pred R-Squared" of 0.9079 is in reasonable agreement with the "Adj R-Squared" of 0.9348.

"Adeq Precision" measures the signal to noise ratio. A ratio greater than 4 is desirable. Your ratio of 25.862 indicates an adequate signal. This model can be used to navigate the design space.

Factor	Coefficient Estimate	Standard DF	95% CI Error	95% CI Low	High	VIF	
Intercept	8.67	1	0.16	8.35	9.00		
A-Loading	0.012	1	0.12	-0.23	0.25	1.00	
B-Composition		0.023	1	0.12	-0.22	0.26	1.00
C-Pressure	1.30	1	0.12	1.06	1.54	1.00	
D-Time	0.33	1	0.12	0.091	0.57	1.00	
B2	-2.92	1	0.19	-3.32	-2.51	1.00	
AB	-0.41	1	0.12	-0.67	-0.16	1.00	
BC	0.55	1	0.12	0.30	0.81	1.00	

Final Equation in Terms of Coded Factors:

Sqrt(Fracture Energy) =
+8.67
+0.012 * A
+0.023 * B
+1.30 * C
+0.33 * D
-2.92 * B2
-0.41 * A * B
+0.55 * B * C

Final Equation in Terms of Actual Factors:

Sqrt(Fracture Energy) =

-0.81580
+0.50631 * Loading
+0.42925 * Composition
+0.13650 * Pressure
+0.11065 * Time
-7.29607E-003 * Composition2
-0.016568 * Loading * Composition
+8.01223E-003 * Composition * Pressure

Diagnostics Case Statistics

Standard Order	Actual Value	Predicted Value	Residual	Leverage	Student Residual	Cook's Distance	Outlier t	Run Order	
1	4.02	4.23	-0.21	0.403	-0.555	0.026	-0.545	19	
2	5.08	5.08	6.796E-003	0.403	0.018	0.000	0.017	23	
3	4.14	4.00	0.15	0.403	0.389	0.013	0.380	22	
4	2.95	3.19	-0.24	0.403	-0.625	0.033	-0.616	18	
5	6.47	5.72	0.75	0.403	1.992	0.334	2.168	28	
6	6.45	6.57	-0.12	0.403	-0.325	0.009	-0.318	3	
7	7.58	7.70	-0.12	0.403	-0.311	0.008	-0.304	27	
8	6.54	6.89	-0.35	0.403	-0.928	0.073	-0.924	14	
9	5.29	4.89	0.40	0.403	1.059	0.095	1.063	4	
10	5.90	5.74	0.15	0.403	0.408	0.014	0.400	21	
11	4.97	4.66	0.31	0.403	0.817	0.056	0.810	8	
12	3.48	3.85	-0.37	0.403	-0.986	0.082	-0.985	15	
13	5.87	6.38	-0.52	0.403	-1.365	0.157	-1.397	7	
14	6.99	7.24	-0.24	0.403	-0.641	0.035	-0.631	17	
15	7.95	8.36	-0.42	0.403	-1.101	0.102	-1.107	20	
16	7.81	7.56	0.25	0.403	0.663	0.037	0.653	26	
17	7.86	8.66	-0.80	0.156	-1.777	0.073	-1.888	25	
18	9.15	8.68	0.47	0.156	1.032	0.025	1.034	2	
19	5.51	5.73	-0.22	0.111	-0.485	0.004	-0.475	5	
20	6.57	5.78	0.79	0.111	1.706	0.045	1.799	9	
21	6.52	7.37	-0.85	0.156	-1.882	0.082	-2.022	11	
22	10.09	9.97	0.11	0.156	0.254	0.001	0.248	13	
23	8.61	8.34	0.27	0.156	0.601	0.008	0.592	10	
24	9.58	9.00	0.57	0.156	1.274	0.037	1.295	12	
25	8.65	8.67	-0.022	0.100	-0.047	0.000	-0.046	16	
26	9.15	8.67	0.48	0.100	1.025	0.015	1.027	6	
27	8.73	8.67	0.058	0.100	0.125	0.000	0.122	24	
28	8.38	8.67	-0.29	0.100	-0.621	0.005	-0.612	1	

Proceed to Diagnostic Plots (the next icon in progression). Be sure to look at the:
1) Normal probability plot of the studentized residuals to check for normality of residuals.
2) Studentized residuals versus predicted values to check for constant error.
3) Outlier t versus run order to look for outliers, i.e., influential values.
4) Box-Cox plot for power transformations.

If all the model statistics and diagnostic plots are OK, finish up with the Model Graphs icon.

Adhesion Optimal Solutions:

Constraints

Name	Lower Goal	Upper Limit	Lower Limit	Upper Weight	Weight	Importance	
Loading	is in range	1.5	4	1	1	3	
Composition	is in range	10	50	1	1	3	
Pressure	is in range	3.447	10.342	1	1	3	
Time	is in range	2	8	1	1	3	
Fracture Energy	maximize	104	120	1	1	3	

Solutions

Number	Loading	Composition	Pressure	Time	Fracture Energy		Desirability
1	1.50	33.54	10.34	7.99	107.617	0.232	Selected
2	1.50	32.79	10.34	7.80	107.155	0.203	
3	2.10	32.76	10.34	8.00	107.143	0.202	
4	1.50	32.75	10.34	7.78	107.083	0.198	
5	3.89	30.69	10.34	8.00	106.448	0.158	
6	3.97	30.58	10.34	8.00	106.446	0.158	

7	4.00	30.81	10.34	8.00	106.436	0.157
8	4.00	31.51	10.34	7.97	106.244	0.145
9	4.00	30.58	10.34	7.87	106.143	0.138
10	4.00	27.60	10.34	7.95	105.028	0.066

10 Solutions found

Number of Starting Points 10

Loading	Composition		Pressure	Time
3.92	12.15	8.64	6.22	
3.75	30.65	7.04	2.95	
2.60	44.70	5.94	7.22	
2.53	19.40	4.09	3.06	
3.84	37.53	8.05	3.75	
1.73	41.08	9.09	2.40	
3.21	21.72	3.76	5.23	
3.13	42.46	8.33	4.07	
1.97	41.38	7.40	3.64	
3.28	44.37	8.10	4.13	

Appendix F. Vitae

Kenneth R. Henderson Jr.

Current Address:

113 Randolph Hall - VT
Blacksburg, Va. 24060
(443) 629 - 4257
kejr2@vt.edu

Permanent Address:

12225 Heathcliff Ct.
Ellicott City, Md. 21042
(410) 531 - 2647

OBJECTIVE

To obtain a position in the field of mechanical engineering. Specific interests include advanced technology, product development/improvement, and advanced energy systems.

EDUCATION

M.S. Mechanical Engineering: Estimated Fall 2005
Virginia Polytechnic Institute & State University (Virginia Tech), Blacksburg, VA
Overall GPA: 3.8/4.0

B.S. Mechanical Engineering: Completed May 2004
Virginia Polytechnic Institute & State University (Virginia Tech), Blacksburg, VA
Overall GPA: 3.83/4.0 In Major GPA: 3.93/4.0

COMPUTER SKILLS

Software:	**Languages:**	
AutoCAD	LabVIEW	Visual Basic
Turbo-CAD	Mat-Lab	HTML
Microsoft Office	Mathmatica	PHP

EXPERIENCE

Virginia Tech Mechanical Engineering Department
Research Assistant, Fall 2004 - Present

- Performing research related to the materials within the multilayer interfaces found in a membrane electrode assembly of a PEM fuel cell.
- Assisting with the testing and evaluation of next generation fuel cell concepts

National Institute of Standards and Technology (NIST), Gaithersburg, Md.
Engineering Cooperative Education Student, Summer-Fall 2002 & Summer 2003

- Assisted in the construction, instrumentation and evaluation of a state of the art residential fuel cell test facility
- Assisted in the data analysis of a photovoltaic system that was installed on the rooftop of the administration building at NIST
- Co-Authored a paper that was presented during the International Solar Energy Conference that took place in Hawaii during March of 2003 entitled “Measured Performance of a 35 kilowatt Roof Top Photovoltaic System”
- Assisted in the development and implementation of a program to test certain electrical characteristics of photovoltaic panels

Horizon Services Inc., Columbia, Md.
Officer / Technician, Summer Breaks Since 1999

- Performed a large variety of tasks including project supervision, office management and many other critical roles necessary for a small business to operate successfully
- Actively involved in the day-to-day installation of electrical, satellite and integrated voice and data networking systems.
- Performed a variety of executive and administrative functions to support the successful operation of the corporation.
- Directly responsible for the supervision of small work crews.

ACTIVITIES / HONORS

Eagle Scout Rank, 1999
National Society of Collegiate Scholars (NSCS), 2001- Present
Academic Scholarship from the department of engineering (Virginia Tech), 2001- Present
Academic Scholarship from Alfa Laval Thermal, Inc., 2003-2004
National Honor Society, 1999-2000
“Deans List with Distinction” standing, 2000 – Present
Member of American Society of Mechanical Engineers (ASME) as of Spring 2002